Universidad Rey Juan Carlos

TESIS DOCTORAL

CONTRIBUCIÓN AL ESTUDIO DE LA MEZCLA NO LINEAL DE ONDAS ULTRASÓNICAS EN LÍQUIDOS CON BURBUJAS MEDIANTE MODELOS NUMÉRICOS

Autora:

María Teresa Tejedor Sastre

Director:

Christian Vanhille

Programa de Doctorado en Ciencias

Escuela Internacional de Doctorado

2018

Universidad Rey Juan Carlos

TESIS DOCTORAL

CONTRIBUCIÓN AL ESTUDIO DE LA MEZCLA NO LINEAL DE ONDAS ULTRASÓNICAS EN LÍQUIDOS CON BURBUJAS MEDIANTE MODELOS NUMÉRICOS

Autora:

María Teresa Tejedor Sastre

Director:

Christian Vanhille

Programa de Doctorado en Ciencias

Escuela Internacional de Doctorado

2018

Agradecimientos

En primer lugar quiero expresar mi gratitud a Christian por guiarme y ayudarme en todo momento, sin él nada habría sido posible.

También deseo mostrar mi agradecimiento a todos los miembros del tribunal por aceptar la tarea de evaluar la tesis, en especial a Itziar por su interés durante estos años.

De igual modo quiero manifestar mi gratitud a los dos expertos extranjeros, Antoine Lavie y Bertrand Dubus, por aceptar la tarea de revisar la tesis y por el tiempo dedicado durante la estancia en Francia. Asimismo, quiero nombrar a Christian Granger y Alexandre Leblanc por la ayuda durante ese periodo.

También deseo expresar mi agradecimiento a la Universidad Rey Juan Carlos, a la Escuela Superior de Ciencias Experimentales y Tecnología y en especial al Departamento de Matemática Aplicada, Ciencia e Ingeniería de los Materiales y Tecnología Electrónica por acogerme durante este periodo de formación.

De igual modo quiero mostrar mi gratitud a la Comisión Académica del Programa de Doctorado en Ciencias y a la Escuela Internacional de Doctorado por todas las facilidades prestadas durante estos años.

Además, deseo dar las gracias a mis padres, José y Lidi, y a mi hermana, Lidia, por apoyarme, permitirme llegar hasta aquí y por entender todas las ausencias. Gracias también a Jose por su apoyo incondicional en todo momento. Y gracias a todos aquellos que directa o indirectamente han ayudado a que esta tesis tenga forma y fin.

Por último quiero expresar mi gratitud a la Agencia Estatal de Investigación del Ministerio de Economía, Industria y Competitividad de España por el apoyo económico durante el periodo de la tesis: la financiación del contrato predoctoral para la Formación de Personal Investigador (BES-2013-064399), la ayuda para la estancia en Fran-

cia (EEBB-I-15-09737), y las subvenciones a través de los proyectos [DPI2012-34613, DPI2017-84758].

Prefacio

Esta tesis nace como parte del proyecto "Estudio de efectos ultrasónicos no lineales para procesos industriales y medicina: líquidos con burbujas y cavitación" (DPI2012-34613) financiado por el Plan Nacional. Durante los últimos años el equipo de investigación ha estudiado el comportamiento de ondas ultrasónicas no lineales en diversos medios, homogéneos o no. En este proyecto se pretendía aportar nuevos conocimientos utilizables posteriormente en potenciales aplicaciones. Así, el objetivo principal del proyecto era predecir numéricamente los parámetros acústicos de líquidos con burbujas de gas que describen el comportamiento no lineal de los mismos. En particular, se ha detectado la posibilidad de utilizar líquidos con burbujas, acústicamente muy no lineales, para estudiar la mezcla no lineal de frecuencias. Se ha analizado la posibilidad de generar bajas frecuencias a partir de varias señales ultrasónicas de distintas frecuencias.

Por tanto, el propósito de esta tesis doctoral es estudiar en profundidad los fenómenos no lineales que ocurren cuando un campo acústico se propaga a través de un líquido con burbujas oscilantes de gas. Principalmente, el objetivo se centra en el análisis de la mezcla no lineal de frecuencias (generación de armónicos, frecuencias diferencia y suma), y primordialmente, en la frecuencia diferencia por sus interesantes características de alta directividad y baja atenuación.

En la introducción, Capítulo 1, se da un resumen de los principales modelos matemáticos que se usan en acústica no lineal, antes de plantear el modelo matemático con el que se trabaja en esta tesis. A continuación, se dan algunas soluciones aproximadas al modelo mediante métodos perturbativos. Seguidamente, se presentan las técnicas numéricas en las que se basan los modelos desarrollados en esta tesis. Además, se dan ejemplos de los distintos enfoques de trabajos hechos en esta temática. Los Capítulos 2, 3, 4 y 5 recogen los artículos científicos escritos durante el desarrollo de la tesis

doctoral.[1] Cabe mencionar aquí que otras comunicaciones científicas en formato de comunicaciones presentadas en congresos nacionales e internacionales han sido realizadas.[2] Después, se exponen la discusión general y las conclusiones generales derivadas de este trabajo. Por último, se incluyen unos anexos sobre el análisis del comportamiento numérico de los métodos desarrollados y sobre la Transformada Rápida de Fourier. En cada capítulo se incluye una sección de referencias.

---

[1]M. T. Tejedor Sastre, C. Vanhille, A numerical model for the study of the difference frequency generated from nonlinear mixing of standing ultrasonic waves in bubbly liquids, Ultrason. Sonochem. 34 (2017) 881-888.

M.T. Tejedor Sastre, C. Vanhille, Numerical models for the study of the nonlinear frequency mixing in two and three-dimensional resonant cavities filled with a bubbly liquid, Ultrason. Sonochem. 39 (2017) 597-610.

M.T. Tejedor Sastre, C. Vanhille, Nonlinear resonance of cavities filled with bubbly liquids: A numerical study, Shock Vib. (2018) Enviado.

M.T. Tejedor Sastre, C. Vanhille, Numerical study of frequency mixing in a focused ultrasonic field in bubbly liquids from a dual-frequency spherical source, Results Phys. (2018) Enviado.

[2]M.T. Tejedor Sastre, C. Vanhille, Un modelo numérico para el análisis no lineal de ondas ultrasńicas estacionarias en líquidos con burbujas, 45° Congreso Español de Acústica, 8° Congreso Ibérico de Acústica y Simposio Europeo sobre Ciudades Inteligentes y Acústica Ambiental, Murcia (2014) 1414-1419.

M.T. Tejedor Sastre, C. Vanhille, A numerical model for the simulation of standing ultrasonic waves in bubbly liquids: analysis of some nonlinear effects, The 22nd International Congress on Sound and Vibration ICSV22, Florence, Italy (2015) 3055-3061.

C. Vanhille , M.T. Tejedor Sastre, Une étude des phénomènes physiques non-linéaires en milieu bulleux par la modélisation numérique, Journées Scientifiques Ultrasons et Procédés - 4ième édition, Actes des Journées Scientifiques Ultrasons et Procédés - 4ième édition, Toulouse, (2017).

M.T. Tejedor Sastre, C. Vanhille, Mezcla no lineal de señales ultrasónicas en líquidos con burbujas: simulación numérica en cavidades esféricas, 48° Congreso Español de Acústica, Encuentro Ibérico de Acústica, European Symposium on Underwater Acoustics Applications y European Symposium on Sustainable Acoustics -TECNIACUSTICA 2017-, A Coruña (2017) 1408-1414.

M.T. Tejedor Sastre, C. Vanhille, Estudio numérico de ultrasonidos de baja frecuencia generados no linealmente en líquidos con burbujas a partir de un campo focalizado, 48° Congreso Español de Acústica, Encuentro Ibérico de Acústica, European Symposium on Underwater Acoustics Applications y European Symposium on Sustainable Acoustics -TECNIACUSTICA 2017-, A Coruña (2017) 1432-1439.

Resumen

Los líquidos con burbujas son medios con gran potencial en distintos tipos de aplicaciones médicas e industriales. Las características que presentan son de gran interés ya que una cantidad muy pequeña de aire en forma de burbujas (del orden del 0.001 % en volumen) puede modificar completamente el comportamiento acústico del líquido. Propiedades acústicas tan importantes como la velocidad, atenuación, compresibilidad o no linealidad se ven modificadas incluso en varios órdenes de magnitud. Cuando un campo acústico excita un líquido con burbujas tienen lugar fenómenos no lineales muy interesantes, como por ejemplo la aparición de nuevas frecuencias.

El estudio experimental de los líquidos con burbujas es complejo ya que controlar la cantidad, la densidad, la distribución espacial y el tamaño de las burbujas no es tarea fácil. Esto lleva a buscar alternativas que permitan analizarlos mediante modelos matemáticos que describan el comportamiento de este tipo de medios cuando un campo acústico se propaga a través de ellos. La interacción no lineal mutua entre la presión acústica y las vibraciones de las burbujas viene descrita mediante el sistema de ecuaciones diferenciales acopladas formado por la ecuación de ondas y una ecuación de Rayleigh-Plesset. Además, este sistema diferencial, por su complejidad, no admite soluciones analíticas exactas, por lo que se requiere el desarrollo de modelos numéricos para obtener soluciones aproximadas.

El propósito de esta tesis doctoral es desarrollar modelos numéricos que permitan el estudio de los fenómenos no lineales que tienen lugar cuando un campo acústico se propaga a través de un líquido con burbujas de gas. Principalmente, el objetivo de este trabajo se centra en el análisis de nuevas frecuencias producidas durante este proceso no lineal, como son los armónicos cuando se trabaja con fuentes mono-frecuenciales y las frecuencias suma y diferencia cuando se trabaja con fuentes de dos frecuencias.

Para conseguir este objetivo se sigue el siguiente proceso. En primer lugar se proponen diferentes modelos físicos (en una y varias dimensiones). Después se modelan matemáticamente con los correspondientes sistemas de ecuaciones diferenciales y condiciones auxiliares (de contorno e iniciales). A continuación se desarrollan los modelos numéricos que resuelven los sistemas diferenciales, basados en técnicas por volúmenes finitos y diferencias finitas en las coordenadas espaciales y en el dominio temporal respectivamente, antes de implementar los diferentes códigos informáticos. Por último, se hacen las correspondientes simulaciones para analizar y estudiar los comportamientos no lineales y proponer leyes físicas que los describen. Este proceso permite, a partir de un problema complejo, obtener conclusiones físicas que simplifican su comprensión.

Los resultados presentados en esta tesis doctoral muestran la utilidad y versatilidad de los modelos numéricos desarrollados, que permiten estudiar en profundidad el comportamiento de este tipo de medios al ser excitados por ondas ultrasónicas de amplitud finita en muchas configuraciones: i) unidimensionales, ii) bidimensionales, iii) tridimensionales (con simetría axial), tanto en resonadores como en dominios espaciales abiertos. El comportamiento no lineal de producción de armónicos y de mezcla de frecuencias se analiza en detalle atendiendo a los principales elementos que influyen en su generación (tamaño y densidad de burbujas, amplitud de onda) para definir cómo potenciarlos. Además, el estudio proporciona la observación de efectos que sugieren un cambio en la velocidad de propagación del medio global en función de la amplitud de presión acústica.

Abstract

Bubbly liquids are media with important potential in different kinds of medical and industrial applications. They present very interesting characteristics since a very small amount of gas bubbles (of the order of 0.001% in volume) is able to modify the acoustic behavior of the liquid drastically. Important acoustic properties such as sound speed, attenuation, compressibility or nonlinearity are modified up to several orders of magnitude. Very interesting nonlinear phenomena take place when an acoustic field excites a bubbly liquid, like, for instance, the production of new frequencies.

The experimental study of bubbly liquids is complex since it is not an easy task to control the amount, density, spatial distribution, and size of bubbles. This difficulties lead to look for alternatives that allow us to analyze them by means of mathematical models able to describe the propagation of acoustic waves through this kind of media. The mutual nonlinear interaction between acoustic pressure and bubble vibrations is described by the coupled differential system of equations formed by the wave equation and a Rayleigh-Plesset equation. Moreover, since this differential system, due to its complexity, does not admit exact analytical solutions, the development of numerical models is necessary to obtain approximate solutions.

The goal of this doctoral thesis is to develop numerical models that allow us to study the nonlinear phenomena occurring when an acoustic wave travels through a liquid with gas bubbles. Mainly, the objective of this work is the analysis of new frequencies produced during this nonlinear process, harmonic components when we work with a mono-frequency source and both sum and difference frequency components when we work with a dual-frequency source.

The following procedure is followed to achieve this objective. First, different physical models are proposed (in one and several dimensions). Then, their mathematical

modelization is carried out through the corresponding systems of differential equations and auxiliary conditions (boundary and initial conditions). Afterwards, we develop the numerical models that solve the differential systems, based on finite-volume and finite-difference techniques for the spatial coordinates and time domain respectively, before performing the implementation of the different computational codes. Finally, the corresponding simulations are carried out to analyze and study the nonlinear behaviors and to propose physical laws that describe them. This procedure allows us, from a complex problem, to obtain physical conclusions that simplify its comprehension.

The results presented in this doctoral thesis show the usefulness and versatility of the numerical models we have developed. These models allow us to study thoroughly the behavior of this kind of media when they are excited by ultrasonic waves of finite amplitude in many configurations: i) one dimension, ii) two dimensions, iii) three dimensions (axial symmetry), for both resonators and open-field problems. The nonlinear behavior of harmonic production and frequency mixing is analyzed in detail according to the main elements that influence its generation (bubble size and density, wave amplitude) to define how to enhance them. Moreover, the study provides us with the observation of effects that suggest a sound speed change of the medium as a function of the amplitude of acoustic pressure.

Índice general

Capítulo 1

Introducción general

1.1. Ecuaciones fundamentales de la acústica no lineal

Las ecuaciones de la acústica lineal describen adecuadamente el modelado de ciertos problemas físicos concretos, en los que las ondas son de amplitud infinitesimal. Para aplicaciones donde las amplitudes son finitas, estas ecuaciones no describen con fidelidad los fenómenos observados experimentalmente. Es por ello que se han desarrollado modelos para la descripción de los fenómenos no lineales. Se obtienen a partir de las ecuaciones fundamentales de la dinámica de fluidos que están asociadas a la conservación de distintas magnitudes físicas (masa y momento en este caso) y a una ecuación de estado que permite cerrar el sistema.

Sean $\vec{v} = \vec{v_0} + \vec{v'}$ la velocidad, $\rho = \rho_0 + \rho'$ la densidad y $p = p_0 + p'$ la presión, donde el subíndice 0 indica los valores de las variables en el estado de equilibrio.

1.1.1. Ecuación de continuidad

La ecuación de continuidad expresa la conservación de la masa, se escribe [1]

$$\frac{\partial \rho}{\partial t} + \vec{\nabla} \cdot (\rho \vec{v}) = 0. \tag{1.1}$$

donde t es el tiempo y el símbolo $\vec{\nabla}$ es el gradiente. Si se toma la velocidad en el estado de equilibrio como nula se tiene

$$\frac{\partial \rho'}{\partial t} + \vec{\nabla} \cdot (\rho_0 \vec{v'} + \rho' \vec{v'}) = 0 \tag{1.2}$$

y operando se obtiene

$$\frac{\partial \rho'}{\partial t} + \rho_0 \vec{\nabla} \cdot \vec{v'} = -\rho' \vec{\nabla} \cdot \vec{v'} - \vec{v'} \cdot \vec{\nabla} \rho'. \tag{1.3}$$

El término de la izquierda representa la aproximación de la ecuación de continuidad de primer orden y el término de la derecha representa la ecuación de continuidad de segundo orden.

1.1.2. Ecuación de movimiento

La ecuación de movimiento expresa la conservación del momento, se escribe [1]

$$\rho \frac{D\vec{v}}{Dt} = -\vec{\nabla} p, \tag{1.4}$$

$$(\rho_0 + \rho') \frac{D\vec{v'}}{Dt} = -\vec{\nabla} p'. \tag{1.5}$$

La derivada material $\frac{D\vec{v'}}{Dt}$ se puede expresar como $\frac{\partial \vec{v'}}{\partial t} + (\vec{v'}\vec{\nabla})\vec{v'}$ luego la Eq. (1.5) se puede poner [2]

$$(\rho_0 + \rho') \left(\frac{\partial \vec{v'}}{\partial t} + \vec{v'} \vec{\nabla} \vec{v'} \right) = -\vec{\nabla} p', \tag{1.6}$$

$$\rho_0 \frac{\partial \vec{v'}}{\partial t} + \vec{\nabla} p' = -\rho' \frac{\partial \vec{v'}}{\partial t} - \rho_0 \vec{v'} \vec{\nabla} \vec{v'} - \rho' \vec{v'} \vec{\nabla} \vec{v'}. \tag{1.7}$$

Despreciando el tercer término de la derecha por ser de tercer orden se obtiene

$$\rho_0 \frac{\partial \vec{v'}}{\partial t} + \vec{\nabla} p' = -\rho' \frac{\partial \vec{v'}}{\partial t} - \rho_0 \vec{v'} \vec{\nabla} \vec{v'}. \tag{1.8}$$

El término de la izquierda representa la aproximación de la ecuación de movimiento de primer orden y el término de la derecha representa la aproximación de segundo orden. Además, si se usa la densidad de energía Lagrangiana, $L = E_c - E_p$, que es la diferencia entre la energía cinética, E_c, y la energía potencial, E_p, y utilizando las relaciones de onda plana se tiene

$$L = E_c - E_p = \frac{1}{2}\rho_0 \vec{v'}^2 - \frac{p'^2}{2\rho_0 c_0^2}, \tag{1.9}$$

$$\rho' \frac{\partial \vec{v'}}{\partial t} = -\vec{\nabla}\left(\frac{p'^2}{2\rho_0 c_0^2}\right) = -\vec{\nabla} E_p, \tag{1.10}$$

$$\rho_0 (\vec{v'}\vec{\nabla})\vec{v'} = \vec{\nabla}\left(\frac{\rho_0 \vec{v'}^2}{2}\right) = \vec{\nabla} E_c. \tag{1.11}$$

donce c_0 es la velocidad de propagación en el estado de equilibrio, entonces la ecuación de movimiento queda

$$\rho_0 \frac{\partial \vec{v'}}{\partial t} + \vec{\nabla} p' = -\vec{\nabla} L. \tag{1.12}$$

Para tener en cuenta la viscosidad del fluido se puede escribir la ecuación de movimiento añadiendo un término que dé cuenta de su contribución [1]

$$\rho_0 \frac{\partial \vec{v'}}{\partial t} + \vec{\nabla} p' - \left(\zeta + \frac{4}{3}\eta\right) \vec{\nabla}^2 \vec{v'} = -\vec{\nabla} L, \tag{1.13}$$

donde η y ζ son los coeficientes de viscosidad de cizalla y de volumen respectivamente.

1.1.3. Ecuación de estado

Para cerrar el sistema es necesario añadir una ecuación que describa el estado termodinámico del fluido. Una manera de hacerlo es expresar la presión en función de la densidad y la entropía por unidad de masa $p = p(\rho, s)$. Para ello se desarrolla en serie de Taylor la presión en torno a ρ_0 considerando la entropía como constante,

$$p = p_0 + \left(\frac{\partial p}{\partial \rho}\right)_{\rho_0, s} \rho' + \frac{1}{2}\left(\frac{\partial^2 p}{\partial \rho^2}\right)_{\rho_0, s} \rho'^2 + ... \tag{1.14}$$

Se definen los coeficientes de no linealidad A y B, siendo c la velocidad del sonido variable con la densidad del fluido $c = \sqrt{\frac{\partial p}{\partial \rho}}$,

$$A = \rho_0 \left(\frac{\partial p}{\partial \rho}\right)_{\rho_0, s} = \rho_0 c_0^2, \tag{1.15}$$

$$B = \rho_0^2 \left(\frac{\partial^2 p}{\partial \rho^2}\right)_{\rho_0, s} = 2\rho_0^2 c_0^3 \left(\frac{\partial c}{\partial p}\right)_{\rho_0, s}. \tag{1.16}$$

Luego la densidad quedaría

$$\rho' \approx \frac{p'}{c_0^2} - \frac{B}{2A}\frac{p'^2}{\rho_0 c_0^4}. \tag{1.17}$$

Cuando los efectos disipativos no son despreciables se han de tener en cuenta las posibles variaciones de entropía en la ecuación de estado. Para ello se desarrolla en serie de Taylor la presión en torno a (ρ_0, s_0) hasta primer orden en la entropía,

$$p = p_0 + \left(\frac{\partial p}{\partial \rho}\right)_{\rho_0,s} \rho' + \frac{1}{2}\left(\frac{\partial^2 p}{\partial \rho^2}\right)_{\rho_0,s} \rho'^2 + \left(\frac{\partial p}{\partial s}\right)_{\rho,s_0} s' + ... \tag{1.18}$$

La densidad quedaría

$$\rho' \approx \frac{p'}{c_0^2} - \frac{B}{2A}\frac{p'^2}{\rho_0 c_0^4} + \frac{k}{\rho_0 c_0^4}\left(\frac{1}{C_V} - \frac{1}{C_P}\right)\frac{\partial p'}{\partial t}. \tag{1.19}$$

donde k es la conductividad térmica, C_V y C_P son los calores específicos a volumen y presión contante respectivamente [1].

1.1.4. Ecuación de Westervelt

La ecuación de Westervelt tiene en cuenta la no linealidad y la disipación. Si se sustituye la Eq. (1.19) en la ecuación de continuidad, Eq. (1.3), y se deriva parcialmente respecto al tiempo y se le aplica el gradiente a la ecuación de movimiento, Eq. (1.13), y se restan ambas ecuaciones se tiene [1]

$$\vec{\nabla}^2 p' - \frac{1}{c_0^2}\frac{\partial^2 p'}{\partial t^2} + \frac{b}{c_0^2}\frac{\partial^3 p'}{\partial t^3} = -\frac{\beta}{\rho_0 c_0^4}\frac{\partial^2 p'^2}{\partial t^2} - \left(\vec{\nabla}^2 + \frac{1}{c_0^2}\frac{\partial^2}{\partial t^2}\right) L, \tag{1.20}$$

donde $\beta = 1 + \frac{B}{2A}$ es el parámetro de no linealidad del medio y $b = \frac{1}{\rho_0 c_0^2}\left(\zeta + \frac{4}{3}\eta\right) + \frac{k}{\rho_0 c_0^4}\left(\frac{1}{C_V} - \frac{1}{C_P}\right)$ representa la disipación. El segundo término de la derecha se puede eliminar debido a que para ondas planas de primer orden $v' = \frac{p'}{\rho_0 c_0}$ y por tanto $L = 0$, entonces se obtiene lo que se conoce como ecuación Westervelt [1],

$$\vec{\nabla}^2 p' - \frac{1}{c_0^2}\frac{\partial^2 p'}{\partial t^2} + \frac{b}{c_0^2}\frac{\partial^3 p'}{\partial t^3} = -\frac{\beta}{\rho_0 c_0^4}\frac{\partial^2 p'^2}{\partial t^2}. \tag{1.21}$$

1.1.5. Ecuación de Burgers

La ecuación de Westervelt se puede simplificar para tomarla como una ecuación de propagación en forma unidimensional en la dirección z, así, si se factoriza la Eq. (1.21) se tiene

$$\left(\frac{\partial}{\partial z} - \frac{1}{c_0}\frac{\partial}{\partial t} + \frac{b}{2c_0}\frac{\partial^2}{\partial t^2} + \frac{\beta p'}{\rho_0 c_0^3}\frac{\partial}{\partial t}\right)\left(\frac{\partial}{\partial z} + \frac{1}{c_0}\frac{\partial}{\partial t} - \frac{b}{2c_0}\frac{\partial^2}{\partial t^2} - \frac{\beta p'}{\rho_0 c_0^3}\frac{\partial}{\partial t}\right) p' = 0, \tag{1.22}$$

donde el primer término se corresponde con la propagación hacia atrás y el segundo término se corresponde con la propagación hacia delante. Si nos quedamos sólo con el término hacia delante se obtiene la ecuación de Burgers, Eq. (1.23), que al igual que la ecuación de Westervelt tiene en cuenta la no linealidad y la disipación [1],

$$\frac{\partial p'}{\partial z} + \frac{1}{c_0}\frac{\partial p'}{\partial t} - \frac{b}{2c_0}\frac{\partial^2 p'}{\partial t^2} - \frac{\beta p'}{\rho_0 c_0^3}\frac{\partial p'}{\partial t} = 0. \tag{1.23}$$

Reorganizando la ecuación se puede poner

$$\frac{\partial p'}{\partial z} + \frac{1}{c'}\frac{\partial p'}{\partial t} - \frac{b}{2c_0}\frac{\partial^2 p'}{\partial t^2} = 0, \tag{1.24}$$

siendo $c' \approx c_0 \left(1 + \frac{\beta p'}{\rho_0 c_0^2}\right)$ la velocidad de propagación de la onda.

1.1.6. Ecuación de Khokhlov - Zabolotskaya - Kuznetov (KZK)

Cuando las ondas no pueden considerarse como planas y sea necesario tener en cuenta el efecto de difracción, considerando que éste puede ser interpretado como una difusión transversal del campo, la ecuación KZK se puede obtener introduciendo el tiempo de retardo $\tau = t - \frac{z}{c_0}$ y cambiando el sistema de coordenadas a uno en tres dimensiones (x, y, z) sobre la Eq. (1.21) [1],

$$\frac{\partial p'}{\partial \tau \partial z} = \frac{c_0}{2}\nabla_\perp^2 + \frac{b}{2c_0}\frac{\partial^3 p'}{\partial \tau^3} + \frac{\beta}{2\rho_0 c_0^3}\frac{\partial^2 p'^2}{\partial \tau^2}, \tag{1.25}$$

donde $\nabla_\perp^2 = \frac{\partial}{\partial x^2} + \frac{\partial}{\partial y^2}$ es el laplaciano en dirección perpendicular a la dirección de propagación z.

1.2. Líquidos con burbujas

La presencia de burbujas en un líquido (incluso en muy pequeñas concentraciones del orden de 0,001 % en volumen) modifica completamente las propiedades acústicas del líquido. La compresibilidad y la nolinealidad aumentan, la velocidad del sonido disminuye y aparecen fenómenos dispersivos.

1.2.1. Ecuación de ondas

En el modelo físico considerado en esta tesis se considera un líquido que contiene una distribución espacialmente uniforme de burbujas esféricas e iguales, suponemos que son pequeñas comparando con la longitud de onda de la perturbación [3]. Sea $\rho = \rho_0 + \rho'$ la densidad de la mezcla del líquido con burbujas, $\rho_l = \rho_{0l} + \rho'_l$ la densidad del líquido y $\rho_g = \rho_{0g} + \rho'_g$ la del gas. El volumen de cada burbuja es $V = v_{0g} + v$ donde el subíndice 0 indica los valores en el equilibrio. El número de burbujas por unidad de volumen es N_g, entonces la densidad de la mezcla en el estado del equilibrio es

$$\rho_0 = N_g v_{0g} \rho_{0g} + (1 - N_g v_{0g}) \rho_{0l}. \tag{1.26}$$

Fuera del equilibrio la densidad viene dada por

$$\frac{\rho_0}{\rho} = N_g V + (1 - N_g v_{0g}) \frac{\rho_{0l}}{\rho_l}. \tag{1.27}$$

Cuando la fracción de gas es pequeña ($N_g V \ll 1$) se tiene que $\rho_0 \approx \rho_{0l} \gg \rho_{0g}$, lo que permite hacer una aproximación de la Eq. (1.27) a

$$\frac{\rho'}{\rho_0} = \frac{p}{\rho_0 c_{0l}^2} - N_g v, \tag{1.28}$$

donde p es la presión sonora y c_{0l} es la velocidad del sonido en el líquido. Combinando la Eq. (1.28) con las ecuaciones de continuidad Eq. (1.3) y de movimiento Eq. (1.8) linealizadas se obtiene la ecuación inhomogénea de ondas [3,4]

$$\bigtriangledown^2 p - \frac{1}{c_{0l}^2} \frac{\partial^2 p}{\partial t^2} = -\rho_0 N_g \frac{\partial^2 v}{\partial t^2}. \tag{1.29}$$

1.2.2. Ecuación de Rayleigh-Plesset

Se considera una burbuja vacía de radio $R(t)$ en un líquido incompresible de dimensión infinita. $\dot{R}$ es la velocidad radial y r es la distancia de cualquier punto respecto al origen (centro de la burbuja). Suponiendo un flujo irrotacional entonces el campo de velocidades se puede poner en términos de un potencial

$$\dot{r} = - \bigtriangledown \phi. \tag{1.30}$$

Debido a la simetría esférica el potencial se puede poner como $\phi = \phi(r)$ y satisfacerá la ecuación de Laplace $\bigtriangledown^2\phi(r) = 0$ que escrita en coordenades esféricas queda

$$\frac{1}{r^2}\frac{d}{dr}\left(r^2\frac{d\phi}{dr}\right) = 0, \tag{1.31}$$

si se integra la Eq. (1.31) se obtiene

$$\phi(r) = -\frac{k_1}{r} + c_1, \tag{1.32}$$

donde k_1 y c_1 son constantes. Reemplazando la Eq. (1.32) en la Eq. (1.30)

$$\dot{r} = -\frac{d\phi}{dr} = -\frac{k_1}{r^2}, \tag{1.33}$$

y aplicando las condiciones de contorno en la superficie de la burbuja donde $r = R$ en la Eq. (1.33), se puede obtener el valor de k_1

$$\dot{R} = \frac{k_1}{R^2}. \tag{1.34}$$

Como $k_1 = R^2\dot{R}$, se obtiene la ecuación del potencial

$$\phi(r) = -\frac{R^2\dot{R}}{r}. \tag{1.35}$$

Si P es la presión a la distancia r de la burbuja, ρ_{0l} es la densidad del líquido, P_∞ es la presión en el infinito, entonces se puede aplicar el teorema de Bernoulli para describir el movimiento del líquido [5,6]

$$-\frac{\partial\phi}{\partial t} - \frac{1}{2}\dot{r}^2 = \frac{P - P_\infty}{\rho_{0l}}, \tag{1.36}$$

$$-\frac{2R\dot{R}^2 + R^2\ddot{R}}{r} - \frac{1}{2}\frac{R^4\dot{R}^2}{r^4} = \frac{P - P_\infty}{\rho_{0l}}. \tag{1.37}$$

Si se sustituye el radio de la burbuja en la Eq. (1.37) se puede describir el movimiento de la burbuja

$$R\ddot{R} + \frac{3}{2}\dot{R}^2 = \frac{P_L - P_\infty}{\rho_{0l}}, \tag{1.38}$$

donde P_L es la presión en la pared de la burbuja. Si ahora en vez de considerar la burbuja vacía suponemos que esta llena de un gas ideal, obedecerá por tanto la ecuación de los gases ideales

$$p_g\left(\frac{4\pi R^3}{3}\right) = R_g T, \tag{1.39}$$

donde p_g es la presión del gas y R_g es la contante de los gases ideales y T es la temperatura. Asumiendo transformaciones adiabáticas se cumple

$$p_g \left(\frac{4\pi R^3}{3}\right)^{\gamma_g} = c_2, \tag{1.40}$$

donde γ_g es el cociente de los calores específicos y c_2 es una constante. Para tener el cuenta la viscosidad se añade un término que dé cuenta de ella. Y asumiendo que la presión del gas es la presión en la pared de la burbuja, $P_\infty = P$ es la presión total en la mezcla y que la densidad es ahora la densidad de la mezcla

$$R\ddot{R} + \frac{3}{2}\dot{R}^2 + \frac{4\nu_l \dot{R}}{R} = \frac{p_g - P}{\rho_0}, \tag{1.41}$$

donde ν_l es la viscosidad cinemática, p_g es la presión del gas, $p_g = p_{0g}\left(\frac{v_{0g}}{V}\right)^{\gamma_g}$, que es la Eq. (1.40) en términos de volumen, y como:

$$V = \frac{4}{3}\pi R^3, \tag{1.42}$$

$$\dot{V} = 4\pi R^2 \dot{R}, \tag{1.43}$$

$$\ddot{V} = 8\pi R\dot{R}^2 + 4\pi R^2 \ddot{R}. \tag{1.44}$$

Sustituyendo en la Eq. (1.41) se obtiene:

$$\frac{1}{4\pi}\left(\frac{4\pi}{3V}\right)^{\frac{1}{3}}\left(\ddot{V} - \frac{1}{6}\frac{\dot{V}^2}{V}\right) + \frac{4\nu_l}{3}\frac{\dot{V}}{V} = \frac{p_{0g}\left(\frac{v_{0g}}{V}\right)^{\gamma_g} - P}{\rho_0}. \tag{1.45}$$

La presión de la mezcla es $P = p_{0g} + p$ y el volumen se pone como $V = v_{0g} + v$. Usando las siguientes aproximaciones cuando $v \ll v_{0g}$:

$$\left(\frac{v_{0g}}{v_{0g} + v}\right)^{\gamma_g} \approx 1 - \frac{\gamma_g}{v_{0g}}v + \frac{\gamma_g(\gamma_g + 1)}{2{v_{0g}}^2}v^2, \tag{1.46}$$

$$\frac{1}{(v_{0g} + v)^{\frac{1}{3}}} \approx \frac{1}{v_{0g}^{\frac{1}{3}}} - \frac{1}{3v_{0g}^{\frac{4}{3}}}v, \tag{1.47}$$

$$V \approx v_{0g}. \tag{1.48}$$

Y sustituyendo en la Eq. (1.45) se obtiene

$$\ddot{v} - \frac{1}{6v_{0g}}(\dot{v}^2 - 2v\ddot{v}) + \frac{1}{18}\frac{v\dot{v}^2}{v_{0g}^2} = -\frac{3p_{0g}\gamma_g}{\rho_0 R_{0g}^2}v + \frac{3\gamma_g(\gamma_g + 1)p_{0g}}{2v_{0g}R_{0g}^2} - \frac{4\pi R_{0g}}{\rho_0}p - \frac{4\nu_l \dot{v}}{R_{0g}}, \tag{1.49}$$

Despreciando el tercer término del lado izquierdo por ser de tercer orden se obtiene una ecuación de Rayleigh-Plesset [3]

$$\ddot{v} + \delta\omega_{0g}\dot{v} + \omega_{0g}^2 v + \eta p = av^2 + b\left(2v\ddot{v} + \dot{v}^2\right), \tag{1.50}$$

donde $\delta = 4\nu_l/\omega_{0g}R_{0g}^2$ es el coeficiente de viscosidad, $\omega_{0g} = \sqrt{3\gamma_g p_{0g}/\rho_0 R_{0g}^2}$ es la frecuencia de resonancia de las burbujas, en la cual γ_g es el cociente entre los calores específicos del gas , $p_{0g} = \rho_{0g}c_{0g}^2/\gamma_g$ es la presión atmosférica del gas, ρ_{0g} y c_{0g} son la densidad y la velocidad del sonido en el estado de equilibrio para el gas . El parámetro $\eta = 4\pi R_{0g}/\rho_0$, y los coeficientes no lineales $a = (\gamma_g + 1)\omega_{0g}^2/2v_{0g}$ y $b = 1/6v_{0g}$. El término av^2 está asociado con la ley adiabática y el término $b(2v\ddot{v} + \dot{v}^2)$ está asociado con la respuesta dinámica de la burbuja. El sistema de ecuaciones diferenciales en derivadas parciales formado por Eqs. (1.29)(1.50) se debe resolver simultáneamente para obtener cómo es la presión acústica y las variaciones de volumen sufridas por las burbujas. Este sistema supone que las burbujas son la única fuente de no linealidad, y no tiene en cuenta la tensión superficial ni la fuerza de empuje.

1.2.3. Algunas aproximaciones a la solución del sistema

1.2.3.1. Solución aproximada de Zabolotskaya

Una propuesta de solución aproximada de este sistema de ecuaciones es presentada en [7,8]. Para la solución del segundo armónico se asume que la presión fuera de burbuja varía según la ecuación $p = Acos(\omega t + \phi)$. Cuando la amplitud es suficientemente intensa, la burbuja ejecutará oscilaciones a las frecuencias ω y 2ω debido a la no linealidad, entonces, la amplitud de las variaciones de volumen de la burbuja para la frecuencia 2ω es

$$V_{2\omega} = \frac{\eta^2(a - 3b\omega^2)A^2}{2\left((\omega_{0g}^2 - \omega^2)^2 + \omega^4\delta^2\right)\left((\omega_{0g}^2 - 4\omega^2)^2 + 16\omega^4\delta^2\right)^{\frac{1}{2}}}. \tag{1.51}$$

Si ahora se asume que la presión fuera de la burbuja varía según la ecuación $p = A_1cos(\omega_1 t + \phi_1) + A_2cos(\omega_2 t + \phi_2)$ con $\omega_2 > \omega_1$, y si la amplitud es suficientemente intensa, la burbuja ejecutará oscilaciones a las frecuencias ω_1, ω_2 y, debido a la no linealidad, a la frecuencia diferencia $\Omega = \omega_2 - \omega_1$. La amplitud de las variaciones de

volumen de la burbuja para la frecuencia Ω es

$$v_\Omega = \frac{\eta^2(a - b(\omega_1^2 + \omega_2^2 - \omega_1\omega_2))A_1A_2}{\left(\left((\omega_{0g}^2 - \omega_1^2)^2 + \omega_1^4\delta^2\right)\left((\omega_{0g}^2 - \omega_2^2)^2 + \omega_2^4\delta^2\right)\left((\omega_{0g}^2 - \Omega^2)^2 + \Omega^4\delta^2\right)\right)^{\frac{1}{2}}}. \tag{1.52}$$

Si las frecuencias fuera de la burbuja son cercanas, la frecuencia diferencia obtenida será baja, entonces la amplitud de la presión se puede poner siempre que las distancia r sea mucho mayor la longitud de onda como

$$p_\Omega = \frac{\Omega^2\rho_0 v_\Omega}{4\pi r}. \tag{1.53}$$

1.2.3.2. Solución aproximada de Hamilton

Otra forma de llevar a cabo esta tarea es mediante un método de sucesivas aproximaciones como propone [3]. Se considera el problema de la generación del segundo armónico para ilustrar el procedimiento. Sea

$$p = \frac{1}{2}(p_1 e^{j\omega t} + p_2 e^{j2\omega t} + c.c.) \tag{1.54}$$

$$v = \frac{1}{2}(v_1 e^{j\omega t} + v_2 e^{j2\omega t} + c.c.) \tag{1.55}$$

Sustituyendo Eq. (1.54) y Eq. (1.55) hasta el primer orden en las ecuaciones Eq. (1.29) y Eq. (1.50) se obtiene.

$$\left(\nabla^2 + \frac{\omega^2}{c_{0l}^2}\right) p_1 = \rho_0 N_g \omega^2 v_1, \tag{1.56}$$

$$(\omega_{0g}^2 - \omega^2 + j\delta\omega_{0g}\omega)v_1 = -\eta p_1. \tag{1.57}$$

Sustituyendo v_1 de la Eq. (1.57) y sustituyendo en Eq. (1.56), se tiene

$$\left(\nabla^2 + \frac{\omega^2}{\tilde{c}_1^2}\right) p_1 = 0, \tag{1.58}$$

donde $\tilde{c}_1$ es definido al establecer $n = 1$ en la siguiente ecuación

$$\frac{c_{0l}^2}{\tilde{c}_n^2} = 1 + \frac{\mu C}{1 - n^2\omega^2/\omega_{0g}^2 + j\delta n\omega/\omega_{0g}}, \tag{1.59}$$

donde $\mu = N_g v_{0g}$ es la fracción de volumen en el estado de equilibrio y $C = \rho_0 c_{0l}^2/\gamma_g p_{0g}$. La solución para onda plana de la Eq. (1.58) es $e^{-j\frac{\omega}{\tilde{c}_1}x}$ luego la velocidad de propagación y atenuación se pueden obtener a partir de la Eq. (1.59)

$$c_n(\omega) = \frac{1}{\mathrm{Re}\,(\tilde{c}_n^{-1})}, \tag{1.60}$$

$$\alpha_n(\omega) = -n\omega \mathrm{Im}\,(\tilde{c}_n^{-1}). \tag{1.61}$$

Si ahora se desarrollan las ecuaciones para el segundo armónico sustituyendo Eq. (1.54) y Eq. (1.55) en las ecuaciones (1.29) y (1.50) hasta el orden 2 se obtiene

$$\left(\nabla^2 + \frac{4\omega^2}{c_{0l}^2}\right) p_2 = 4\rho_0 N_g \omega^2 v_2, \tag{1.62}$$

$$(\omega_{0g}^2 - 4\omega^2 + j2\delta\omega_{0g}\omega)v_2 = -\eta p_2 + \frac{1}{2}\left(a - 3b\omega^2\right) v_1^2. \tag{1.63}$$

La Eq. (1.57) es usada para expresar v_1^2 en términos de p_1^2. Las Eqs. (1.62) y (1.63) se pueden combinar para obtener la presión para el segundo armónico

$$\left(\nabla^2 + \frac{4\omega^2}{\tilde{c}_2^2}\right) p_2 = \beta_2(\omega)\frac{2\omega^2}{\rho_0 c_{0l}^4} p_1^2. \tag{1.64}$$

El valor de $\tilde{c}_2$ se obtiene de Eq. (1.59) con $n = 2$ y $\beta_2(\omega)$ es el coeficiente de no linealidad que viene dado por

$$\beta_2(\omega) = \frac{\mu C^2(\gamma + 1 - \frac{\omega^2}{\omega_{0g}^2})}{2(1 - 4\frac{\omega^2}{\omega_{0g}^2} + j2\delta\omega_{0g}\omega)(1 - \frac{\omega^2}{\omega_{0g}^2} + j\delta\omega_{0g}\omega)^2}. \tag{1.65}$$

Para obtener la solución del segundo armónico, se deben imponer condiciones de contorno sobre Eqs. (1.58) y (1.64). Se asume la propagación de onda plana en dirección $+x$ y $p_1 = P_0$ y $p_2 = 0$ en $x = 0$, para simplificar se supone $\delta = 0$. La Eq. (1.58) conduce a $p_1 = P_0 e^{-jk_1 x}$ con $(k_n = n\omega/c_n, n = 1, 2)$ y sustituyendo en Eq. (1.64) se obtiene la solución para el segundo armónico

$$p_2 = \frac{jP_0^2\left((\gamma_g + 1)\frac{\omega_{0g}^2}{\omega^2} - 1\right)}{6\gamma_g p_{0g}(1 - \frac{\omega^2}{\omega_0^2})} sin\left((k_2 - 2k_1)\frac{x}{2}\right) e^{-j(k_2+2k_1)\frac{x}{2}} \tag{1.66}$$

1.3. Métodos numéricos

La alta complejidad del sistema no lineal de ecuaciones diferenciales formado por la ecuación inhomogénea de ondas y la ecuación de Rayleigh-Plesset, Eqs. (1.29)(1.50), la falta de soluciones analíticas exactas, la dificultad y el elevado coste de tomar medidas experimentales nos lleva directamente a la necesidad de desarrollar modelos numéricos para obtener soluciones que nos permitan acercarnos a la realidad del problema físico considerado en esta tesis doctoral. Los técnicas numéricas en las que se basan los modelos numéricos desarrollados en esta tesis son el método de los volúmenes finitos en las dimensiones espaciales y el método de las diferencias finitas en el dominio temporal.

1.3.1. Aproximaciones en el dominio temporal

El método de las diferencias finitas se basa en la aproximación numérica de las derivadas. Esta técnica consiste en discretizar, en este caso, el dominio temporal total T_t en $R-1$ intervalos de duración τ. Se denota cada instante temporal t_k con el subíndice k. El esquema de discretización se puede ver en el Capítulo 3, en la Fig. 2a. A continuación, se escriben cómo son las aproximaciones de la variable p para ilustrar el método. En este caso las aproximaciones se basan en desarrollar en serie de Taylor la variable a aproximar p en los tiempos $p(t_k+\tau)$ y $p(t_k-\tau)$ alrededor del tiempo t_k, como se observa en las siguientes aproximaciones [9,10],

$$p(t_k+\tau) = p(t_k) + \tau\frac{dp(t_k)}{d\tau} + \frac{\tau^2}{2!}\frac{d^2p(t_k)}{d\tau^2} + \frac{\tau^3}{3!}\frac{d^3p(t_k)}{d\tau^3} + O(\tau^4), \tag{1.67}$$

$$p(t_k-\tau) = p(t_k) - \tau\frac{dp(t_k)}{d\tau} + \frac{\tau^2}{2!}\frac{d^2p(t_k)}{d\tau^2} - \frac{\tau^3}{3!}\frac{d^3p(t_k)}{d\tau^3} + O(\tau^4). \tag{1.68}$$

De este modo se puede obtener la aproximación de la derivada de orden dos en el instante t_k al sumar las Eqs. (1.67) y (1.68),

$$p(t_k+\tau) + p(t_k-\tau) = 2p(t_k) + 2\frac{\tau^2}{2!}\frac{d^2p(t_k)}{d\tau^2} + O(\tau^4), \tag{1.69}$$

$$\frac{d^2p(t_k)}{d\tau^2} = \frac{p(t_k+\tau) - 2p(t_k) + p(t_k-\tau)}{\tau^2} + O(\tau^2), \tag{1.70}$$

siendo el error de truncamiento $O(\tau^2)$. En el esquema de discretización quedaría

$$\frac{d^2p_k}{dt^2} \approx \frac{p_{k+1} - 2p_k + p_{k-1}}{\tau^2}. \tag{1.71}$$

La aproximación de la derivada de orden uno en t_k se puede obtener haciendo la diferencia entre la Eq. (1.67) y la Eq.(1.68), entre $p(t_k)$ y la Eq. (1.68) o entre la Eq. (1.67) y $p(t_k)$:

$$p(t_k+\tau)-p(t_k-\tau)=2\tau\frac{dp(t_k)}{d\tau}+O(\tau^3), \tag{1.72}$$

$$p(t_k)-p(t_k-\tau)=\tau\frac{dp(t_k)}{d\tau}+O(\tau^2), \tag{1.73}$$

$$p(t_k+\tau)-p(t_k)=\tau\frac{dp(t_k)}{d\tau}+O(\tau^2). \tag{1.74}$$

Luego se tiene

$$\frac{dp(t_k)}{d\tau}=\frac{p(t_k+\tau)-p(t_k-\tau)}{2\tau}+O(\tau^2), \tag{1.75}$$

$$\frac{dp(t_k)}{d\tau}=\frac{p(t_k)-p(t_k-\tau)}{\tau}+O(\tau), \tag{1.76}$$

$$\frac{dp(t_k)}{d\tau}=\frac{p(t_k+\tau)-p(t_k)}{\tau}+O(\tau). \tag{1.77}$$

Los errores de truncamiento en estas aproximaciones son de orden $O(\tau^2)$, $O(\tau)$ y $O(\tau)$ respectivamente. En los modelos desarrollados en esta tesis se usa la Eq. (1.76) a fin de tener un sistema explícito que dé agilidad a la hora de resolver el sistema. En el sistema discretizado quedaría

$$\frac{dp_k}{dt}\approx\frac{p_k-p_{k-1}}{\tau}. \tag{1.78}$$

1.3.2. Aproximaciones en las dimensiones espaciales

El método los volúmenes finitos se basa en la integración de las ecuaciones diferenciales en volúmenes de control que discretizan el dominio de estudio. Esta técnica numérica resulta muy efectiva cuando se modelan problemas para los cuales el flujo es de importancia, como en mecánica de fluidos, en transferencia de calor o masa. El método tiene la propiedad de conservar localmente el flujo numérico, es decir, de un volumen de control al volumen vecino [11]. Este método numérico resulta muy efectivo para desarrollar los modelos implementados en esta tesis debido a la versatilidad que tiene a la hora de simular cualquier tipo de geometría en problemas de varias dimensiones [12]. Además, las condiciones de contorno se implementan de una manera razonablemente sencilla. El método consiste en considerar una discretización del dominio del problema y para cada punto de esa partición construir a su alrededor un

volumen de control que no se solape con los volúmenes adyacentes. De esta forma el volumen total del dominio resulta ser la unión de todos los volúmenes de control. Las ecuaciones diferenciales que se pretenden resolver se integran sobre cada uno de los volúmenes dando lugar a una versión discretizada antes de obtener la solución aproximada. Para realizar la integración se requiere especificar cómo es la variación de las variables entre volúmenes adyacentes y así evaluar las integrales resultantes. En este trabajo se considera una variación lineal entre volúmenes contiguos [13]. Una de las ventajas del método de los volúmenes finitos es que sólo tiene que evaluar las variables en los límites de los volúmenes. Esto también es válido para problemas no lineales, lo que hace que sea un método muy poderoso para el manejo de leyes no lineales de conservación [14,15]. A continuación se hacen las aproximaciones de la variable p a fin de ilustrar este método en dos dimensiones para coordenadas cartesianas primero, y en tres dimensiones para coordenadas cilíndricas después. El esquema de discretización se puede ver en el Capítulo 3, en la Fig. 2b.

1.3.2.1. Coordenadas cartesianas

Se divide el dominio total $L_x \times L_y$ en las coordenadas (x, y) en $N \times M$ volúmenes de control de tamaño $h \times s$ y se integra las ecuaciones en cada uno de esos volúmenes. Se denota cada volumen de control con los subíndices (i, j). Así las aproximaciones para las integrales de las derivadas de orden dos que son las que aparecen en la ecuación no lineal de ondas, Eq. (1.29), en coordenadas cartesianas serán:

$$\begin{aligned}\int_{V_c} \frac{d^2 p_{i,j}}{dx^2} dv = \int_{So}^{No} dy \int_{We}^{Ea} \frac{d^2 p_{i,j}}{dx^2} dx = s\left(\frac{dp_{i,j}}{dx}|_{Ea} - \frac{dp_{i,j}}{dx}|_{We}\right) \\ \approx s\left(\frac{p_{i+1,j} - p_{i,j}}{h} - \frac{p_{i,j} - p_{i-1,j}}{h}\right) = s\left(\frac{p_{i+1,j} - 2p_{i,j} + p_{i-1,j}}{h}\right),\end{aligned} \tag{1.79}$$

$$\begin{aligned}\int_{V_c} \frac{d^2 p_{i,j}}{dy^2} dv = \int_{We}^{Ea} dx \int_{So}^{No} \frac{d^2 p_{i,j}}{dy^2} dy = h\left(\frac{dp_{i,j}}{dy}|_{No} - \frac{dp_{i,j}}{dy}|_{So}\right) \approx \\ h\left(\frac{p_{i,j+1} - p_{i,j}}{s} - \frac{p_{i,j} - p_{i,j-1}}{s}\right) = h\left(\frac{p_{i,j+1} - 2p_{i,j} + p_{i,j-1}}{s}\right).\end{aligned} \tag{1.80}$$

La integral para una constante k será:

$$\int_{V_c} k dv = \int_{So}^{No} dy \int_{We}^{Ea} k dx = khs. \tag{1.81}$$

Cuando se tienen condiciones de contorno tipo Dirichlet por ejemplo, $p = P_{x0}$ si $x = 0$, $p = P_{y0}$ si $y = 0$, $p = P_{L_x}$ si $x = L_x$ y $p = P_{L_y}$ si $y = L_y$. Para los volúmenes cuyo contorno coincide con $x = 0$ se tendrá la aproximación para la integral de las derivadas de orden dos en x:

$$\begin{aligned}\int_{V_c} \frac{d^2 p_{i,j}}{dx^2} dv &= \int_{So}^{No} dy \int_{We}^{Ea} \frac{d^2 p_{i,j}}{dx^2} dx = s\left(\frac{dp_{i,j}}{dx}|_{Ea} - \frac{dp_{i,j}}{dx}|_{We}\right) \\ &\approx s\left(\frac{p_{i+1,j} - p_{i,j}}{h} - \frac{p_{i,j} - P_{x0}}{h/2}\right) = s\left(\frac{p_{i+1,j} - 3p_{i,j} + 2P_{x0}}{h}\right),\end{aligned} \tag{1.82}$$

y para volúmenes cuyo contorno coincide con $x = L_x$:

$$\begin{aligned}\int_{V_c} \frac{d^2 p_{i,j}}{dx^2} dv &= \int_{So}^{No} dy \int_{We}^{Ea} \frac{d^2 p_{i,j}}{dx^2} dx = s\left(\frac{dp_{i,j}}{dx}|_{Ea} - \frac{dp_{i,j}}{dx}|_{We}\right) \\ &\approx s\left(\frac{P_{L_x} - p_{i,j}}{h/2} - \frac{p_{i,j} - p_{i-1,j}}{h}\right) = s\left(\frac{2P_{L_x} - 3p_{i,j} + p_{i-1,j}}{h}\right).\end{aligned} \tag{1.83}$$

Si el volumen tiene un contorno en $y = 0$ se tendrá la siguiente aproximación para la integral de las derivadas de orden dos en y:

$$\begin{aligned}\int_{V_c} \frac{d^2 p_{i,j}}{dy^2} dv &= \int_{We}^{Ea} dx \int_{So}^{No} \frac{d^2 p_{i,j}}{dy^2} dy = h\left(\frac{dp_{i,j}}{dy}|_{No} - \frac{dp_{i,j}}{dy}|_{So}\right) \\ &\approx h\left(\frac{p_{i,j+1} - p_{i,j}}{s} - \frac{p_{i,j} - 2P_{y0}}{s/2}\right) = h\left(\frac{p_{i,j+1} - 3p_{i,j} + 2P_{y0}}{s}\right),\end{aligned} \tag{1.84}$$

y si lo tiene en $y = L_y$:

$$\begin{aligned}\int_{V_c} \frac{d^2 p_{i,j}}{dy^2} dv &= \int_{We}^{Ea} dx \int_{So}^{No} \frac{d^2 p_{i,j}}{dy^2} dy = h\left(\frac{dp_{i,j}}{dy}|_{No} - \frac{dp_{i,j}}{dy}|_{So}\right) \\ &\approx h\left(\frac{P_{L_y} - p_{i,j}}{s/2} - \frac{p_{i,j} - p_{i,j-1}}{s}\right) = h\left(\frac{2P_{L_y} - 3p_{i,j} + p_{i,j-1}}{s}\right).\end{aligned} \tag{1.85}$$

Cuando se tienen condiciones de contorno tipo Neumann por ejemplo, $\frac{dp}{dx} = D_{x0}$ si $x = 0$, $\frac{dp}{dy} = D_{y0}$ si $y = 0$, $\frac{dp}{dx} = D_{L_x}$ si $x = L_x$ y $\frac{dp}{dy} = D_{L_y}$ si $y = L_y$. Para los volúmenes cuyo contorno coincide con $x = 0$ se tendrá la siguiente aproximación para la integral de la derivadas de orden dos en x:

$$\begin{aligned}\int_{V_c} \frac{d^2 p_{i,j}}{dx^2} dv &= \int_{So}^{No} dy \int_{We}^{Ea} \frac{d^2 p_{i,j}}{dx^2} dx = s\left(\frac{dp_{i,j}}{dx}|_{Ea} - \frac{dp_{i,j}}{dx}|_{We}\right) \\ &\approx s\left(\frac{p_{i+1,j} - p_{i,j}}{h} - D_{x0}\right) = s\left(\frac{p_{i+1,j} - p_{i,j} - hD_{x0}}{h}\right),\end{aligned} \tag{1.86}$$

y para volúmenes cuyo contorno coincide con $x = L_x$:

$$\begin{aligned}\int_{V_c} \frac{d^2 p_{i,j}}{dx^2} dv &= \int_{So}^{No} dy \int_{We}^{Ea} \frac{d^2 p_{i,j}}{dx^2} dx = s\left(\frac{dp_{i,j}}{dx}|_{Ea} - \frac{dp_{i,j}}{dx}|_{We}\right) \\ &\approx s\left(D_{L_x} - \frac{p_{i,j} - p_{i-1,j}}{h}\right) = s\left(\frac{hD_{L_x} - p_{i,j} + p_{i-1,j}}{h}\right).\end{aligned} \tag{1.87}$$

Si el volumen tiene un contorno en $y = 0$ se tendrá la siguiente aproximación para la integral de las derivadas de orden dos en y:

$$\begin{aligned}\int_{V_c} \frac{d^2 p_{i,j}}{dy^2} dv = \int_{We}^{Ea} dx \int_{So}^{No} \frac{d^2 p_{i,j}}{dy^2} dy = h \left(\frac{dp_{i,j}}{dy}|_{No} - \frac{dp_{i,j}}{dy}|_{So} \right) \\ \approx h \left(\frac{p_{i,j+1} - p_{i,j}}{s} - D_{y0} \right) = h \left(\frac{p_{i,j+1} - p_{i,j} + sD_{y0}}{s} \right),\end{aligned} \tag{1.88}$$

y si lo tiene en $y = L_y$:

$$\begin{aligned}\int_{V_c} \frac{d^2 p_{i,j}}{dy^2} dv = \int_{We}^{Ea} dx \int_{So}^{No} \frac{d^2 p_{i,j}}{dy^2} dy = h \left(\frac{dp_{i,j}}{dy}|_{No} - \frac{dp_{i,j}}{dy}|_{So} \right) \\ \approx h \left(D_{L_y} - \frac{p_{i,j} - p_{i,j-1}}{s} \right) = h \left(\frac{sD_{L_y} - p_{i,j} + p_{i,j-1}}{s} \right).\end{aligned} \tag{1.89}$$

Otra de las condiciones de contorno que se usan en los desarrollos numéricos de la tesis es la condición de campo abierto donde aparece el tiempo, luego se hace uso de la Eq. (1.78). Por ello se ha de poner también el subíndice k. Por ejemplo, si se tuvieran condiciones de campo abierto $\frac{dp}{dx} = -\frac{1}{c_0^2}\frac{dp}{dt}$ si $x = 0$, $\frac{dp}{dy} = -\frac{1}{c_0^2}\frac{dp}{dt}$ si $y = 0$, $\frac{dp}{dx} = -\frac{1}{c_0^2}\frac{dp}{dt}$ si $x = L_x$ y $\frac{dp}{dy} = -\frac{1}{c_0^2}\frac{dp}{dt}$ si $y = L_y$. Para los volúmenes cuyo contorno coincide con $x = 0$ se tendrá la aproximación para la integral de las derivadas de orden dos en x:

$$\begin{aligned}\int_{V_c} \frac{d^2 p_{i,j,k}}{dx^2} dv = \int_{So}^{No} dy \int_{We}^{Ea} \frac{d^2 p_{i,j,k}}{dx^2} dx = s \left(\frac{dp_{i,j,k}}{dx}|_{Ea} - \frac{dp_{i,j,k}}{dx}|_{We} \right) \\ \approx s \left(\frac{p_{i+1,j,k} - p_{i,j,k}}{h} + \frac{1}{c_0^2}\frac{dp}{dt} \right) \approx s \left(\frac{p_{i+1,j,k} - p_{i,j,k}}{h} + \frac{1}{c_0^2}\frac{p_{i,j,k} - p_{i,j,k-1}}{\tau} \right) \\ = s \left(\frac{1}{h} p_{i+1,j,k} + \left(-\frac{1}{h} + \frac{1}{c_0^2 \tau} \right) p_{i,j,k} - \frac{1}{c_0^2 \tau} p_{i,j,k-1} \right),\end{aligned} \tag{1.90}$$

y para volúmenes cuyo contorno coincide con $x = L_x$:

$$\begin{aligned}\int_{V_c} \frac{d^2 p_{i,j,k}}{dx^2} dv = \int_{So}^{No} dy \int_{We}^{Ea} \frac{d^2 p_{i,j,k}}{dx^2} dx = s \left(\frac{dp_{i,j,k}}{dx}|_{Ea} - \frac{dp_{i,j,k}}{dx}|_{We} \right) \\ \approx s \left(-\frac{1}{c_0^2}\frac{dp}{dt} - \frac{p_{i,j,k} - p_{i-1,j,k}}{h} \right) \approx s \left(-\frac{1}{c_0^2}\frac{p_{i,j,k} - p_{i,j,k-1}}{\tau} - \frac{p_{i-1,j,k} - p_{i,j,k}}{h} \right) \\ = s \left(\left(-\frac{1}{c_0^2 \tau} + \frac{1}{h} \right) p_{i,j,k} + \frac{1}{c_0^2 \tau} p_{i,j,k-1} - \frac{1}{h} p_{i-1,j,k} \right).\end{aligned} \tag{1.91}$$

Si el volumen tiene un contorno en $y = 0$ se tendrá la siguiente aproximación para la

integral de las derivadas de orden dos en y:

$$\begin{aligned}\int_{V_c}\frac{d^2p_{i,j,k}}{dy^2}dv &= \int_{We}^{Ea}dx\int_{So}^{No}\frac{d^2p_{i,j,k}}{dy^2}dy = h\left(\frac{dp_{i,j,k}}{dy}|_{No}-\frac{dp_{i,j,k}}{dy}|_{So}\right)\\ \approx h\left(\frac{p_{i,j+1,k}-p_{i,j,k}}{s}+\frac{1}{c_0^2}\frac{dp}{dt}\right) &\approx h\left(\frac{p_{i,j+1,k}-p_{i,j,k}}{s}+\frac{1}{c_0^2}\frac{p_{i,j,k}-p_{i,j,k-1}}{\tau}\right)\\ &= h\left(\frac{1}{s}p_{i,j+1,k}+\left(-\frac{1}{s}+\frac{1}{c_0^2\tau}\right)p_{i,j,k}-\frac{1}{c_0^2\tau}p_{i,j,k-1}\right),\end{aligned} \tag{1.92}$$

y si lo tiene en $y = L_y$:

$$\begin{aligned}\int_{V_c}\frac{d^2p_{i,j,k}}{dy^2}dv &= \int_{We}^{Ea}dx\int_{So}^{No}\frac{d^2p_{i,j,k}}{dy^2}dy = h\left(\frac{dp_{i,j,k}}{dy}|_{No}-\frac{dp_{i,j,k}}{dx}|_{So}\right)\\ \approx h\left(-\frac{1}{c_0^2}\frac{dp}{dt}-\frac{p_{i,j,k}-p_{i,j-1,k}}{s}\right) &\approx h\left(-\frac{1}{c_0^2}\frac{p_{i,j,k}-p_{i,j,k-1}}{\tau}-\frac{p_{i,j,k}-p_{i,j-1,k}}{s}\right)\\ &= h\left(\left(-\frac{1}{c_0^2\tau}-\frac{1}{s}\right)p_{i,j,k}+\frac{1}{c_0^2\tau}p_{i,j,k-1}+\frac{1}{s}p_{i,j-1,k}\right).\end{aligned} \tag{1.93}$$

El error en todas estas aproximaciones es de orden $O(h, s)$.

1.3.2.2. Coordenadas cilíndricas

Se divide dominio total $L_r \times L_z$ en las coordenadas (r, z) en $N \times M$ en volúmenes de control de tamaño $h \times s$ y se integran las ecuaciones en cada volumen de control. Se denota cada volumen de control con los subíndices (i, j). Así las aproximaciones para las integrales que aparecen en la ecuación no lineal de ondas, Eq. (1.29), en coordenadas cilíndricas serán:

$$\begin{aligned}\int_{V_c}r\frac{d^2p_{i,j}}{dr^2}dv+\int_{V_c}r\frac{1}{r}\frac{dp_{i,j}}{dr}dv &= \int_{So}^{No}dz\int_{We}^{Ea}r\frac{d^2p_{i,j}}{dr^2}dr\\ +\int_{So}^{No}dz\int_{We}^{Ea}r\frac{1}{r}\frac{dp_{i,j}}{dr}dr &= sr\frac{dp_{i,j}}{dr}|_{Ea}-sr\frac{dp_{i,j}}{dr}|_{We}-s\int_{We}^{Ea}\frac{dp_{i,j}}{dr}dr\\ +s\int_{We}^{Ea}\frac{dp_{i,j}}{dr}dr &\approx shi\left(\frac{p_{i+1,j}-p_{i,j}}{h}\right)-sh(i-1)\left(\frac{p_{i,j}-p_{i-1,j}}{h}\right)\\ &= s(ip_{i+1,j}+(1-2i)p_{i,j}+(i-1)p_{i-1,j}),\end{aligned} \tag{1.94}$$

$$\begin{aligned}\int_{V_c} r\frac{d^2p_{i,j}}{dz^2}dv &= \int_{We}^{Ea} rdr\int_{So}^{No}\frac{d^2p_{i,j}}{dz^2}dz = \int_{We}^{Ea} rdr\left(\frac{dp_{i,j}}{z}|_{No}-\frac{dp_{i,j}}{z}|_{So}\right)\\ &\approx\left(\frac{r^2}{2}|_{Ea}-\frac{r^2}{2}|_{We}\right)\left(\frac{p_{i,j+1}-p_{i,j}}{s}-\frac{p_{i,j}-p_{i,j-1}}{s}\right)\\ &\approx\left(\frac{(hi)^2}{2}-\frac{(h(i-1))^2}{2}\right)\left(\frac{p_{i,j+1}-2p_{i,j}+p_{i,j-1}}{s}\right)\\ &= \frac{h^2}{2}(2i-1)\left(\frac{p_{i,j+1}-2p_{i,j}+-p_{i,j-1}}{s}\right).\end{aligned} \tag{1.95}$$

La integral para una constante k será:

$$\int_{V_c} kdv = \int_{So}^{No} dz\int_{We}^{Ea} rkdr \approx \frac{ksh^2}{2}(2i-1). \tag{1.96}$$

Cuando se tienen condiciones de simetría por ejemplo respecto al eje z, se tiene la condición $\frac{dp}{dr}=0$ en $r=0$, la aproximaciones para las integrales para las derivadas que aparecen en la ecuación de ondas, Eq. (1.29), en coordenadas cilíndricas serán:

$$\begin{aligned}\int_{V_c} r\frac{d^2p_{i,j}}{dr^2}dv + \int_{V_c} r\frac{1}{r}\frac{dp_{i,j}}{dr}dv &= \int_{So}^{No} dz\int_{We}^{Ea} r\frac{d^2p_{i,j}}{dr^2}dr\\ +\int_{So}^{No} dz\int_{We}^{Ea} r\frac{1}{r}\frac{dp_{i,j}}{dr}dr &= s\left(r\frac{dp_{i,j}}{dr}|_{Ea}-r\frac{dp_{i,j}}{dr}|_{We}\right)\\ &\approx ish\left(\frac{p_{i+1,j}-p_{i,j}}{h}-0\right) = is(p_{i+1,j}-p_{i,j}),\end{aligned} \tag{1.97}$$

$$\begin{aligned}\int_{V_c} r\frac{d^2p_{i,j}}{dz^2}dv &= \int_{We}^{Ea} rdr\int_{So}^{No}\frac{d^2p_{i,j}}{dz^2}dz = \int_{We}^{Ea} rdr\left(\frac{dp_{i,j}}{dz}|_{No}-\frac{dp_{i,j}}{dz}|_{So}\right)\\ &\approx\left(\frac{r^2}{2}|_{Ea}-\frac{r^2}{2}|_{We}\right)\left(\frac{p_{i,j+1}-p_{i,j}}{s}-\frac{p_{i,j}-p_{i,j-1}}{s}\right)\\ \approx\left(\frac{(hi)^2}{2}-0\right)\left(\frac{p_{i,j+1}-2p_{i,j}+p_{i,j-1}}{s}\right) &= \frac{(hi)^2}{2}\left(\frac{p_{i,j+1}-2p_{i,j}+-p_{i,j-1}}{s}\right).\end{aligned} \tag{1.98}$$

Cuando se tienen condiciones de contorno tipo Dirichlet por ejemplo, $p=P_{z0}$ si $z=0$, $p=P_{L_r}$ si $r=L_r$ y $p=P_{L_z}$ si $z=L_z$. Para los volúmenes cuyo contorno coincide con $r=L_r$ se tendrá la siguiente aproximación para la integral de las derivadas en r :

$$\begin{aligned}\int_{V_c} r\frac{d^2p_{i,j}}{dr^2}dv + \int_{V_c} r\frac{1}{r}\frac{dp_{i,j}}{dr}dv &= \int_{So}^{No} dz\int_{We}^{Ea} r\frac{d^2p_{i,j}}{dr^2}dr\\ +\int_{So}^{No} dz\int_{We}^{Ea} r\frac{1}{r}\frac{dp_{i,j}}{dr}dr &= s\left(r\frac{dp_{i,j}}{dr}|_{Ea}-r\frac{dp_{i,j}}{dr}|_{We}\right)\approx ish\left(\frac{P_{L_r}-p_{i,j}}{h/2}\right)\\ -(i-1)sh\frac{p_{i,j}-p_{i-1,j}}{h} &= s(2iP_{L_r}+(1-3i)p_{i,j}+(i-1)p_{i-1,j}).\end{aligned} \tag{1.99}$$

Para los volúmenes cuyo contorno coincide con $z = 0$ se tendrá la aproximación para la integral las derivadas de orden dos en z:

$$\begin{aligned}\int_{V_c} r\frac{d^2p_{i,j}}{dz^2}dv &= \int_{We}^{Ea} rdr \int_{So}^{No} \frac{d^2p_{i,j}}{dz^2}dz = \int_{We}^{Ea} rdr \left(\frac{dp_{i,j}}{z}|_{No} - \frac{dp_{i,j}}{z}|_{So}\right) \\ &\approx \left(\frac{r^2}{2}|_{Ea} - \frac{r^2}{2}|_{We}\right)\left(\frac{p_{i,j+1} - p_{i,j}}{s} - \frac{p_{i,j} - P_{z0}}{s/2}\right) \\ &= \frac{h^2}{2}(2i-1)\left(\frac{p_{i,j+1} - 3p_{i,j} + 2P_{z0}}{s}\right),\end{aligned} \tag{1.100}$$

y para volúmenes cuyo contorno coincide con $z = L_z$:

$$\begin{aligned}\int_{V_c} r\frac{d^2p_{i,j}}{dz^2}dv &= \int_{We}^{Ea} rdr \int_{So}^{No} \frac{d^2p_{i,j}}{dz^2}dz = \int_{We}^{Ea} rdr \left(\frac{dp_{i,j}}{z}|_{No} - \frac{dp_{i,j}}{z}|_{So}\right) \\ &\approx \left(\frac{r^2}{2}|_{Ea} - \frac{r^2}{2}|_{We}\right)\left(\frac{P_{L_z} - p_{i,j}}{s/2} - \frac{p_{i,j} - p_{i,j-1}}{s}\right) \\ &= \frac{h^2}{2}(2i-1)\left(\frac{2P_{L_z} - 3p_{i,j} + p_{i,j-1}}{s}\right).\end{aligned} \tag{1.101}$$

Cuando se tienen condiciones de contorno tipo Neumann por ejemplo, $\frac{dp}{dz} = D_{z0}$ si $z = 0$, $\frac{dp}{dr} = D_{L_r}$ si $r = L_r$ y $\frac{dp}{dz} = D_{L_z}$ si $z = L_z$. Para los volúmenes cuyo contorno coincide con $r = L_r$ se tendrá la siguiente aproximación para la integral de las derivadas en r:

$$\begin{aligned}&\int_{V_c} r\frac{d^2p_{i,j}}{dr^2}dv + \int_{V_c} r\frac{1}{r}\frac{dp_{i,j}}{dr}dv = \int_{So}^{No} dz \int_{We}^{Ea} r\frac{d^2p_{i,j}}{dr^2}dr \\ &+ \int_{So}^{No} dz \int_{We}^{Ea} r\frac{1}{r}\frac{dp_{i,j}}{dr}dr = s\left(r\frac{dp_{i,j}}{dr}|_{Ea} - r\frac{dp_{i,j}}{dr}|_{We}\right) \\ \approx\ & ishD_{L_r} - (i-1)sh\frac{p_{i,j} - p_{i,j-1}}{h} = s(ihD_{L_r} + (1-i)p_{i,j} + (i-1)p_{i-1,j}).\end{aligned} \tag{1.102}$$

Para los volúmenes cuyo contorno coincide con $z = 0$ se tendrá la aproximación para la integral de las derivadas de orden dos en z:

$$\begin{aligned}&\int_{V_c} r\frac{d^2p_{i,j}}{dz^2}dv = \int_{We}^{Ea} rdr \int_{So}^{No} \frac{d^2p_{i,j}}{dz^2}dz = \int_{We}^{Ea} rdr \left(\frac{dp_{i,j}}{z}|_{No} - \frac{dp_{i,j}}{z}|_{So}\right) \\ \approx\ & \left(\frac{r^2}{2}|_{Ea} - \frac{r^2}{2}|_{We}\right)\left(\frac{p_{i,j+1} - p_{i,j}}{s} - D_{z0}\right) = \frac{h^2}{2}(2i-1)\left(\frac{p_{i,j+1} - p_{i,j} + sD_{z0}}{s}\right),\end{aligned} \tag{1.103}$$

y para volúmenes cuyo contorno coincide con $z = L_z$:

$$\int_{V_c} r\frac{d^2p_{i,j}}{dz^2}dv = \int_{We}^{Ea} rdr \int_{So}^{No} \frac{d^2p_{i,j}}{dz^2}dz = \int_{We}^{Ea} rdr \left(\frac{dp_{i,j}}{z}|_{No} - \frac{dp_{i,j}}{z}|_{So}\right)$$
$$\approx \left(\frac{r^2}{2}|_{Ea} - \frac{r^2}{2}|_{We}\right)\left(D_{L_z} - \frac{p_{i,j} - p_{i,j-1}}{s}\right) = \frac{h^2}{2}(2i-1)\left(\frac{sD_{L_z} - p_{i,j} + p_{i,j-1}}{s}\right). \tag{1.104}$$

Otras de las condiciones de contorno que se usan en los desarrollos numéricos de la tesis es la condición de campo abierto donde aparece el tiempo, luego se hace uso de la Eq. (1.78). Por ello ha de aparecer también el subíndice k. Por ejemplo, si se tuvieran condiciones de campo abierto $\frac{dp}{dz} = -\frac{1}{c_0^2}\frac{dp}{dt}$ si $z = 0$, $\frac{dp}{dr} = -\frac{1}{c_0^2}\frac{dp}{dt}$ si $r = L_r$ y $\frac{dp}{dz} = -\frac{1}{c_0^2}\frac{dp}{dt}$ si $z = L_z$. Para los volúmenes cuyo contorno coincide con $r = L_r$ se tendrá las siguiente aproximación para la integral de las derivadas en r:

$$\begin{aligned}
&\int_{V_c} r\frac{d^2p_{i,j,k}}{dr^2}dv + \int_{V_c} r\frac{1}{r}\frac{dp_{i,j,k}}{dr}dv = \int_{So}^{No} dz \int_{We}^{Ea} r\frac{d^2p_{i,j,k}}{dr^2}dr \\
&+ \int_{So}^{No} dz \int_{We}^{Ea} r\frac{1}{r}\frac{dp_{i,j,k}}{dr}dr = s\left(r\frac{dp_{i,j,k}}{dr}|_{Ea} - r\frac{dp_{i,j,k}}{dr}|_{We}\right) \approx -\frac{shi}{c_0^2}\frac{dp}{dt} - \\
&hs(i-1)\frac{p_{i,j,k} - p_{i-1,j,k}}{h} \approx s\left(-\frac{hi}{c_0^2}\frac{p_{i,j,k} - p_{i,j,k-1}}{\tau} - (i-1)(p_{i,j,k} - p_{i-1,j,k})\right) \\
&= s\left(\left(-\frac{hi}{c_0^2\tau} - (i-1)\right)p_{i,j,k} + \frac{hi}{c_0^2\tau}p_{i,j,k-1} + (i-1)p_{i-1,j,k}\right).
\end{aligned} \tag{1.105}$$

Para los volúmenes cuyo contorno coincide con $z = 0$ se tendrá la aproximación para la integral de las derivadas de orden dos en z:

$$\begin{aligned}
\int_{V_c} r\frac{d^2p_{i,j,k}}{dz^2}dv &= \int_{We}^{Ea} rdr \int_{So}^{No} \frac{d^2p_{i,j,k}}{dz^2}dz = \int_{We}^{Ea} rdr \left(\frac{dp_{i,j,k}}{z}|_{No} - \frac{dp_{i,j,k}}{z}|_{So}\right) \\
&\approx \left(\frac{r^2}{2}|_{Ea} - \frac{r^2}{2}|_{We}\right)\left(\frac{p_{i,j+1,k} - p_{i,j,k}}{s} + \frac{1}{c_0^2}\frac{dp}{dt}\right) \\
&= \frac{h^2}{2}(2i-1)\left(\frac{p_{i,j+1,k} - p_{i,j,k}}{s} + \frac{1}{c_0^2}\frac{p_{i,j,k} - p_{i,j,k-1}}{\tau}\right) \\
&= \frac{h^2}{2}(2i-1)\left(\frac{1}{s}p_{i,j+1,k} + \left(-\frac{1}{s} + \frac{1}{c_0^2\tau}\right)p_{i,j,k} - \frac{1}{c_0^2\tau}p_{i,j,k-1}\right),
\end{aligned} \tag{1.106}$$

y para volúmenes cuyo contorno coincide con $z = L_z$:

$$\begin{aligned}
\int_{V_c} r\frac{d^2p_{i,j,k}}{dz^2}dv = \int_{We}^{Ea} rdr \int_{So}^{No} \frac{d^2p_{i,j,k}}{dz^2}dz &= \int_{We}^{Ea} rdr \left(\frac{dp_{i,j,k}}{z}|_{No} - \frac{dp_{i,j,k}}{z}|_{So}\right) \\
&\approx \left(\frac{r^2}{2}|_{Ea} - \frac{r^2}{2}|_{We}\right)\left(-\frac{1}{c_0^2}\frac{dp}{dt} - \frac{p_{i,j,k} - p_{i,j-1,k}}{s}\right) \\
&= \frac{h^2}{2}(2i-1)\left(-\frac{1}{c_0^2}\frac{p_{i,j,k} - p_{i,j,k-1}}{\tau} - \frac{p_{i,j,k} - p_{i,j-1,k}}{s}\right) \\
&= \frac{h^2}{2}(2i-1)\left(\left(-\frac{1}{c_0^2\tau} - \frac{1}{s}\right)p_{i,j,k} + \frac{1}{c_0^2\tau}p_{i,j,k-1} + \frac{1}{s}p_{i,j-1,k}\right).
\end{aligned} \tag{1.107}$$

El error en todas estas aproximaciones es de orden $O(h, s)$.

1.4. Métodos numéricos aplicados a la propagación ultrasónica en líquidos con burbujas: precedentes

Últimamente se ha llevado a cabo un intenso esfuerzo para crear herramientas numéricas capaces de simular la propagación ultrasónica en distintos tipos de cavidades con fluidos en los que intervienen burbujas [16]. Muchos de estos trabajos se basan en la resolución de ecuaciones lineales que describen la propagación ultrasónica en líquidos homogéneos. Ejemplo de ello podrían ser los trabajos presentados en [17,18], donde se caracteriza y optimiza, respectivamente, la propagación del campo ultrasónico en un sonoreactor de 20 kHz usando el método de los elementos finitos para resolver la ecuación de ondas lineal.

Algunos modelos tienen en cuenta el efecto de la viscosidad del líquido y del amortiguamiento que sufren los ultrasonidos al propagarse. Estos estudios se basan en la resolución de la ecuación de ondas lineal pero teniendo en cuenta una velocidad y densidad compleja que dan cuenta de la contribución de estos efectos. Entre otros están los trabajos desarrollados en [19,20], donde se estudia la distribución del campo de presión usando el método de los elementos finitos para frecuencias de 20 kHz y 490 kHz respectivamente.

Cuando los ultrasonidos son lo suficientemente intensos aparecen fenómenos no lineales, dispersivos y disipativos, debido a la presencia de burbujas, por lo que el empleo de ecuaciones lineales deja de ser suficiente. La propagación acústica teniendo en cuenta estos efectos ha sido estudiada teóricamente. Muchos de estos trabajos están basados en el conjunto de ecuaciones no lineales propuestas en [21,22] que describen el movimiento de las mezclas de líquidos y burbujas de gas. Este conjunto de ecuaciones fue derivado en [23] usando un método de scattering múltiple [24]. A estas ecuaciones se las denomina ecuaciones de Caflisch. Posteriormente en [25] se desarrolla un modelo linealizado de las ecuaciones de Caflish para poblaciones de burbujas mono y polidispersas. Este sistema lineal es de un gran interés pues da cuenta en cierta medida de los efectos de las burbujas con la incorporación de la atenuación en la ecuación de ondas lineal empleando

un número de onda complejo que depende de la cantidad de burbujas. Ejemplos de este enfoque son entre otros los trabajos [26-28], donde se simula un campo acústico lineal en un líquido conteniendo una distribución uniforme y no uniforme (distribución Gaussiana de tamaños) de burbujas usando la técnica de las diferencias finitas. También se hacen comparaciones experimentales en [29]. Otro estudio del mismo tipo se hace en [30] donde se analiza la propagación ultrasónica con una distribución inhomogénea de burbujas. En este caso las simulaciones están basadas en la técnica de los elementos finitos. Otro ejemplo sería el trabajo presentado en [31] donde se simula la interacción del campo ultrasónico con las burbujas de cavitación con modelos basados en el método de los volúmenes finitos.

Además de tener en cuenta las burbujas hay algunos aspectos respecto a las paredes de los recipientes donde se hacen los experimentos que deben ser tenidos en cuenta. En algunos modelos se toman paredes como rígidas sin tener en cuenta las deformaciones que tienen lugar cuando el campo acústico interactúa con ellas. El método de los elementos finitos, debido a sus propiedades, resulta muy útil para este tipo de enfoques. Ejemplo de este tipo de estudios puede ser entre otros [32], donde se analiza el campo acústico a través de la posición de ciertos objetos en el recipiente dando cuenta así de los modos de vibración y de su dependencia en función de las condiciones de contorno. Otro trabajo donde se calcula el campo de presión considerando la vibración de las paredes del reactor y la atenuación de las burbujas es el presentado en [33]. Algunas tendencias van en la dirección de tener en cuenta también la interacción del campo con las deformaciones del transductor. Ejemplo de este enfoque es el trabajo [34], donde se investiga teóricamente los fundamentos de la transformación de energía entre el líquido y el transductor asumiendo una vibración lineal de las burbujas.

Cuando los modelos lineales no son suficientes para describir la interación entre el campo acústico y las vibraciones de la burbujas se hace necesario trabajar con modelos que tengan en cuentan fenómenos no lineales. Un ejemplo es el trabajo presentado en [35], donde se representa la propagación del campo ultrasónico en líquidos con burbujas mediante la resolución de la ecuación no lineal de ondas. Este modelo tiene en cuenta la dinámica y la disipación de energía de la burbuja, la conservación de energía en el líquido y la atenuación no lineal de los ultrasonidos. Las simulaciones se obtienen

mediante el método de los elementos finitos. Otro de los enfoques más usados es el modelo presentado en [7] en el cual se sostiene que las burbujas son la única fuente de no linealidad. Se resuelven la ecuación no homogénea de ondas acoplada con una ecuación de Rayleigh-Plesset que representa las oscilaciones de la burbujas. Ejemplos de este enfoque son los trabajos [36-39], donde se utilizan modelos numéricos (principalmente basados en el método de las diferencias finitas) para obtener la solución de la presión y las variaciones de volumen de la burbujas. Es en este enfoque donde entran los trabajos desarrollados en esta tesis.

Referencias

[1] K. Naugolnykh, L. Ostrovsky, Nonlinear Wave Processes in Acoustics, Cambridge University Press, New York, 1998.

[2] P.M. Morse, K.U. Ingard, Theoretical acoustics, McGraw-Hill, New York, 1968.

[3] M.F. Hamilton, D.T. Blackstock (Eds.), Nonlinear Acoustics, Academic Press, San Diego, 1998.

[4] F. Grieser, P.K. Choi, N. Enomoto, H. Harada, K. Okitsu, K. Yasui (Eds.), Sonochemistry and the Acoustic Bubble, Elsevier, Amsterdam, 2015.

[5] F.R. Young, Cavitation, McGraw-Hill, London, 1989.

[6] T.G. Leighton, The Acoustic Bubble, Academic Press, London, 1997.

[7] E.A. Zabolotskaya, S.I. Soluyan, Emission of harmonic and combination-frequency waves by air bubbles. Sov. Phys. Acoust. 18 (1973) 396-398.

[8] E.A. Zabolotskaya, Acoustic second-harmonic generation in a liquid containing uniformly distributed air bubbles, Sov. Phys. Acoust. 21 (1974) 569-571.

[9] G.D. Smith, Numerical Solution of Partial Differential Equations, Finite Difference Methods, Clarendon Press, Oxford, 1985.

[10] C. Vanhille, A. Lavie, C. Campos-Pozuelo, Modélisation numérique en mécanique: introduction et mise en pratique, Hermes Science Publications, Lavoisier, París, 2007.

[11] R. Eymard, T. Galloüet, R. Herbin, P.G. Ciarlet, J.L. Lions (Eds.), Finite volume methods, Handbook of numerical analysis, vol. VII, North-Holland, Amsterdam,

2000.

[12] H. Ji, X. Xu, X. Guo, S. Ye, J. Chen, X. Yang, Direct FVM simulation for sound propagation in an ideal wedge, Shock Vib. 2016 (2016) 1-9.

[13] H.K. Versteeg, W. Malalasekera, An introduction to computational fluid dynamics: the finite volume method, John Wiley y Sons Inc., New York, 1995.

[14] R.J. LeVEque, Finite Volume Methods for Hyperbolic Problems, Cambridge University Press, Cambridge, 2002.

[15] A.M. Alakashi, B. Basuno, H.T.M. Elkamel, Comparison between Finite Volume Method (FVM) Based on Inviscid and Viscous Flow with Experimental and Fluent Results, Appl. Comput. Math. 4 (2015) 12-17.

[16] I. Tudela, V. Sáez, M.D. Esclapez, M.I. Díez-García, P. Bonete, J. González-García, Simulation of the spatial distribution of the acoustic pressure in sonochemical reactors with numerical methods: a review, Ultrason. Sonochem. 21 (2014) 909-919.

[17] V. Sáez, J. Frías-Ferrer, J. Iniesta, J. González-García, A. Aldaz, E. Riera, Characterization of a 20 kHz sonoreactor: part I: analysis of mechanical effects by classical and numerical methods, Ultrason. Sonochem. 12 (2005) 59-65.

[18] J. Klíma, J. Frías-Ferrer, J. González-García, J. Ludvík, V. Saéz, J. Iniesta, Optimisation of 20 kHz sonoreactor geometry on the basis of numerical simulation of local ultrasonic intensity and qualitative comparison with experimental results, Ultrason. Sonochem. 14 (2007) 19-28.

[19] V.S. Sutkar, P.R. Gogate, L. Csoka, Theoretical prediction of cavitational activity distribution in sonochemical reactors, Chem. Eng. J. 158 (2010) 290-295.

[20] Z. Xu, K. Yasuda, S. Koda, Numerical simulation of liquid velocity distribution in a sonochemical reactor, Ultrason. Sonochem. 20 (2013) 452-459.

[21] L. Van Wijngaarden, On equations of motion for mixtures of liquid and gas bubbles, J. Fluid Mech. 33 (1968) 465-474.

[22] L. Van Wijngaarden, One-dimensional flow of liquids containing small gas-bubbles, Ann. Rev. Fluid Mech. 4 (1972) 369-394.

[23] R.E. Caflisch, M.J. Miksis, G.C. Papanicolaou, L. Ting, Effective equations for wave propagation in bubbly liquids, J. Fluid Mech. 153 (1985) 259-273.

[24] L.L. Foldy, The multiple scattering of waves, Phys. Rev. 67 (1944) 107-119.

[25] K.W. Commander, A. Prosperetti, Linear pressure waves in bubbly liquids: comparison between theory and experiments, J. Acoust. Soc. Am. 85 (1989) 732-746.

[26] S. Dähnke, F.J. Keil, Modeling of three-dimensional linear pressure fields in sonochemical reactors with homogeneous and inhomogeneous density distributions of cavitation bubbles, Ind. Eng. Chem. Res. 37 (1998) 848-864.

[27] S. Dähnke, F.J. Keil, Modeling of linear pressure fields in sonochemical reactors considering an inhomogeneous density distribution of cavitation bubbles, Chem. Eng. Sci. 54 (1999) 2865-2872.

[28] S. Dähnke, K.M. Swamy, F.J. Keil, Modeling of three-dimensional pressure fields in sonochemical reactors with an inhomogeneous density distribution of cavitation bubbles. Comparison of theoretical and experimental results, Ultrason. Sonochem. 6 (1999) 31-41.

[29] S. Dähnke, K.M. Swamy, F.J. Keil, A comparative study on the modeling of sound pressure field distributions in a sonoreactor with experimental investigation, Ultrason. Sonochem. 6 (1999) 221-226.

[30] R. Jamshidi, B. Pohl, U.A. Peuker, G. Brenner, Numerical investigation of sonochemical reactors considering the effect of inhomogeneous bubble clouds on ultrasonic wave propagation, Chem. Eng. J. 189-190 (2012) 364-375.

[31] G. Servant, J. P. Caltaginone, A. Gérad, J.L. Laborde , A. Hita, Numerical simulation of the cavitation bubble dinamics induced by ultrasound waves in a high frequency reactor, Ultrason. Sonochem. 7 (2000) 217-227.

[32] Y. Liu, T. Yamabuchi, T. Yoshizawa, S. Hirobayashi, Finite element simlation of coupled vibration modes in an ultrasonic cleaning tub: Effect of the presence of a washing object, Acoust. Sci. Technol. 25 (2004) 173-176.

[33] K. Yasui, T. Kozuka, T. Tuziuti, A. Towata, Y. Iida, J. King, P. Macey, FEM calculation of an acoustic field in a sonochemical reactor, Ultrason. Sonochem. 14 (2007) 605-614.

[34] C. Horst, Y.-S. Chen, U. Kunz, U. Hoffmann, Design, modeling and performance of a novel sonochemical reactor for heterogeneous reactions, Chem. Eng. Sci. 51 (1996) 1837-1846.

[35] O. Louisnard, A simple model of propagation in a cavitating liquid. Part I:

Theory, nonlinear attenuation and traveling wave generation, Ultrason. Sonochem. 19 (2012) 56-65.

[36] C. Vanhille, C. Campos-Pozuelo, Numerical simulation of nonlinear ultrasonic standing waves in bubbly liquids, Int. J. Nonlinear Sci. Numer. Simul. 10 (2009) 751-757.

[37] C. Vanhille, C. Campos-Pozuelo, Nonlinear ultrasonic standing waves: two dimensional simulations in bubbly liquids, Ultrason. Sonochem. 18 (2011) 679-682.

[38] C. Vanhille, C. Campos-Pozuelo, Numerical simulations of three-dimensional nonlinear acoustic waves in bubbly liquids, Ultrason. Sonochem. 20 (2013) 963-969.

[39] C. Vanhille, C. Campos-Pozuelo, D.N. Sinha, Nonlinear frequency mixing in a resonant cavity: numerical simulations in a bubbly liquid, Ultrasonics 54 (2014) 2051-2054.

Capítulo 2

Modelo numérico para el estudio de la frecuencia diferencia producida a partir de la mezcla no lineal de ondas ultrasónicas estacionarias en líquidos con burbujas

En este capítulo se estudia el comportamiento de ondas ultrasónicas estacionarias en líquidos con burbujas en cavidades unidimensionales. Para este fin se desarrolla un modelo numérico basado en el método de volúmenes finitos y el método de las diferencias finitas. En este modelo se resuelve el sistema diferencial que acopla la presión acústica con las vibraciones de la burbujas que viene descrito mediante la ecuación de ondas y una ecuación de Rayleigh-Plesset.

Los resultados obtenidos permiten validar el nuevo modelo propuesto además de observar los efectos físicos debidos a la presencia de burbujas. Se estudia con detalle la generación de armónicos (cuando se trabaja con fuentes mono-frecuenciales) como función de las principales fuentes de no linealidad, amplitud de la fuente y cantidad de burbujas presentes proponiendo leyes que rigen su generación. Además se examina qué tamaños de resonadores son más eficientes a la hora de generar nuevas frecuencias

dando como resultado longitudes proporcionales a media longitud de onda. Cuando se trabaja con fuentes de dos frecuencias se investiga la frecuencia diferencia como función de la amplitud de la fuente proponiendo una ley para su generación. También se estudia su producción como función de las frecuencias fuente. Los resultados sugieren una mejor respuesta para las frecuencias primarias situadas por debajo de la frecuencia de resonancia de las burbujas. Este trabajo podría ser útil para algunas aplicaciones prácticas.

Se incluye la publicación en revista científica (Factor de impacto JCR-ISI: 6,012) cuya referencia es:

M.T. Tejedor Sastre, C. Vanhille, A numerical model for the study of the difference frequency generated from nonlinear mixing of standing ultrasonic waves in bubbly liquids, Ultrason. Sonochem. 34 (2017) 881-888.

Ultrasonics Sonochemistry

Jones, Jennifer (ELS-OXF)<J.Jones@elsevier.com>

vie 13/07/2018 10:54

Para:Christian Vanhille . <christian.vanhille@urjc.es>;

ELSEVIER

Dear Dr Christian Vanhille
We hereby grant María Teresa Tejedor Sastre permission to reproduce the material detailed below at no charge in her thesis, in print and on OpenDOAR and subject to the following conditions:

1. If any part of the material to be used (for example, figures) has appeared in our publication with credit or acknowledgement to another source, permission must also be sought from that source. If such permission is not obtained then that material may not be included in your publication/copies.

2. Suitable acknowledgment to the source must be made, either as a footnote or in a reference list at the end of your publication, as follows:

   "This article was published in Publication title, Vol number, Author(s), Title of article, Page Nos, Copyright Elsevier (or appropriate Society name) (Year)."

3. Her thesis may be submitted to her institution in either print or electronic form.

4. Reproduction of this material is confined to the purpose for which permission is hereby given.

5. This permission is granted for non-exclusive world **English** rights only. For other languages please reapply separately for each one required. Permission excludes use in an electronic form other than as specified above. Should she have a specific electronic project in mind please reapply for permission.

6. Should her thesis be published commercially, please reapply for permission.

Yours sincerely

Jennifer Jones
Permissions Specialist

Elsevier Limited, a company registered in England and Wales with company number 1982084, whose registered office is The Boulevard, Langford Lane, Kidlington, Oxford, OX5 1GB, United Kingdom.

03 Jul 2018 4:09pm
Question Answer

Question	Answer
Title	Dr.
First name	Christian
Last name	Vanhille
Institute/company	Universidad Rey Juan Carlos
Address	Tulipán, s/n
Post/Zip Code	28933
City	Móstoles
State/Territory	Madrid
Country	Spain
Telephone	+34 916647482
Email	christian.vanhille@urjc.es
Please select the type of publication	Journal
Journal - Title	Ultrasonics Sonochemistry
Journal - ISSN	1350-4177
Journal - Volume	34
Journal - Issue	1
Journal - Year	2017
Journal - Pages from	881
Journal - Pages to	888
Journal - Author	María Teresa Tejedor Sastre, Christian Vanhille
Journal - Article Title	A numerical model for the study of the difference frequency generated from nonlinear mixing of standing ultrasonic waves in bubbly liquids
I would like to use (please select one of the following options)	Full article/chapter
If using figures/tables or illustrations please specify the quantity	
If using excerpts please provide a total word count	
Are you the author of the Elsevier material?	Yes
If not, is the Elsevier author involved with your project?	Yes
If yes, please provide details of how the Elsevier author is involved	
In what format will you use the material?	Print and Electronic
Will you be translating the material?	No
If yes, please specify the languages	
Information about your proposed use	Reuse in a thesis/dissertation
Proposed use text	Posting in a repository.
AdditionalComments/Information	I would need this permission as soon as possible since the dissertation of María Teresa Tejedor Sastre must be submitted next week (I am the doctoral thesis director). Thank you.

Ultrasonics Sonochemistry 34 (2017) 881–888

Contents lists available at ScienceDirect

Ultrasonics Sonochemistry

journal homepage: www.elsevier.com/locate/ultson

A numerical model for the study of the difference frequency generated from nonlinear mixing of standing ultrasonic waves in bubbly liquids

María Teresa Tejedor Sastre, Christian Vanhille *

Universidad Rey Juan Carlos, Tulipán, s/n, 28933 Móstoles, Madrid, Spain

ARTICLE INFO

Article history:
Received 29 April 2016
Received in revised form 15 July 2016
Accepted 26 July 2016
Available online 27 July 2016

Keywords:
Ultrasound
Nonlinear acoustics
Bubbly liquids
Frequency mixing
Standing waves
Numerical simulations

ABSTRACT

The aim of this paper is the study of the behavior of nonlinear standing ultrasonic waves in bubbly liquids and the generation of the difference frequency by nonlinear mixing of several signals. To this end we present a new numerical model based on the finite-volume method and the finite-difference method. This model solves the differential system formed by the wave equation and a Rayleigh-Plesset equation coupling the acoustic pressure field with the bubble vibrations. We consider a resonator filled with a bubbly liquid excited by an ultrasonic pressure source. The numerical experiments presented here are performed by modifying the source amplitude and frequency, the void fraction in the liquid, as well as the length of the resonator. The results allow us to observe the physical effects due to the presence of the bubbles in the liquid: nonlinearity, dispersion, attenuation. The nonlinear frequency mixing performed in the resonator is also evidenced. The amplitude of the generated difference frequency is studied as a function of the pressure amplitude and for several primary frequencies. Our results suggest that a better response is obtained for primary frequencies situated below the bubble resonance. They show a very high difference-frequency amplitude response for a cavity resonant at one wavelength of the difference frequency in the bubbly medium. This analyze could be useful for some practical applications.

1. Introduction

Industrial and medical applications of ultrasound can be divided into two categories. Low intensity applications are employed to obtain information about the medium in which the wave travels. Nondestructive testing and diagnostic ultrasound belong to this class. High intensity applications are employed to produce permanent effects in the medium [1]. This group is used in the framework of food industry (processing, preservation, extraction) [2], medicine (ablation, therapy) [3], particle filtration (agglomeration) [4], and chemical industry [5,6]. Acoustic waves in this category are of high amplitudes and the propagation of ultrasound is nonlinear in most fluids and solids [7]. The nonlinearity of a medium is measured by evaluating its nonlinear parameter [7]. A higher value of this parameter implies that lower intensity is required to produce nonlinear propagation, i.e., to create nonlinear distortion of the acoustic signal (existence of harmonics) and shock waves.

A particular use of high power ultrasound is the nonlinear frequency mixing [8,9]. This nonlinear effect has multiple applications. It can be used in medicine in the context of medical imaging [10], in industrial applications, such as the bubble detection and characterization [11–13], in underwater communication [14] and in parametric arrays for generating a penetrating low ultrasonic-frequency signal from two high frequency waves (end-fire arrays) [8].

Bubbly liquids are very interesting media because a small concentration of bubbles changes their acoustic properties. In particular, the nonlinear parameter of the liquid is drastically increased [6,15,16]. The propagation of ultrasonic waves produces oscillations of the bubbles that become nonlinear at finite amplitude and at the same time the oscillations of the bubbles produce nonlinear effects of the acoustic field. These nonlinear effects are associated to other phenomena due to the presence of the bubbles in the liquid: dissipation and dispersion. This situation gives rise to complex waves [6,16].

The production of a stable population of gas bubbles in a liquid in which acoustic waves are propagating is not an easy task. It is thus extremely difficult to obtain stable experimental measures in bubbly liquids. Therefore, an intense endeavor has been carried out lately in order to create numerical tools able to simulate the ultrasonic propagation in such media [17]. Sáez et al. characterize the ultrasonic field propagation in a 20 kHz sonoreactor [18]. They

* Corresponding author.
E-mail address: christian.vanhille@urjc.es (C. Vanhille).

http://dx.doi.org/10.1016/j.ultsonch.2016.07.020
1350-4177/

use the finite element method to solve the linear equation wave. Klíma et al. study the geometric optimization of a 20 kHz sonoreactor by using the element finite method [19]. They show that an appropriate geometry can compensate the decrease in intensity of the acoustic signal when the distance from the source is increased. Sutkar et al. predict the cavitation activity in terms of pressure field [20]. They solve the wave equation by taking into account the damping effects (reflection, refraction and scattering), modifying the density and sound speed in the medium. They use a software based on the finite element method. Prosperetti develop a linear model based on the Caflisch equations [21,22]. They take into account the attenuation in the wave number. Dänke et al. simulate the three-dimensional distribution of a linear acoustic field in a liquid with an inhomogeneous distribution of bubbles by using a finite difference approach [23,24]. They assume a Gaussian distribution of bubble sizes and a wave number that considers attenuation. Nomura and Nakagawa analyze the pressure field inside an ultrasonic cleaning vessel [25]. They use a boundary element method to solve the wave equation considering the dissipation of the bubbles. Yasui et al. use the finite element method to calculate the pressure field by considering the vibration of the reactor walls and the attenuation of the bubbles [26]. Vanhille and Campos-Pozuelo characterize the acoustic field in a bubbly liquid by taking into account the nonlinearity, dispersion, and dissipation in one, two, and three dimensions [27–29].

Since the presence of bubbles in a liquid enhances the nonlinear behavior of ultrasound, bubbly liquids are interesting media for all the applications that require the nonlinear frequency mixing technique. Several studies have been carried out about this method in a bubbly liquid. Zabolotskaya and Soluyan [30] study the generation of harmonics and the creation of the sum and difference frequencies theoretically. Kobelev and Sutin [31] perform a theoretical and experimental study about the difference-frequency generation with a continuous size distribution of bubbles. Druzhinin et al. [32] analyze the low-frequency generation from two high-frequency waves in a resonant bubble layer analytically and numerically. Vanhille et al. [33] study the nonlinear frequency mixing in a resonant cavity numerically.

New developments are necessary to progress in this field and to get rid of the restrictions associate to the existing methods. In this paper we develop a new numerical tool based on the finite-volume method [34,35] and on the finite-difference method [35,36]. We consider a system that couples the acoustic pressure with the volume variation of the bubbles. We solve a set of differential equations formed by the wave equation and a Rayleigh-Plesset equation.

The objective of this work is to study the propagation of nonlinear ultrasonic waves in bubbly liquids by means of a new numerical tool able to describe the particular effects due to the oscillating bubbles on the acoustic field, and to analyze some aspects of the nonlinear frequency mixing. After describing the physical model and the development of the numerical model in Section 2, some numerical experiments are presented in Section 3. The results shown make it possible to validate the new model. A comparison between linear and nonlinear data obtained at infinitesimal and finite amplitudes, respectively, allows us to highlight the nonlinear effects due to the presence of the bubbles in the liquid and to study the distribution of the harmonic components of the pressure wave in the cavity. A law is proposed for the description of the second and third harmonics as a function of the source amplitude and the bubble density. A study is carried out by modifying the resonator length. The nonlinear mixing of two frequencies in the cavity shows the generation of the difference frequency component. The amplitude of this created frequency is studied versus the amplitude and the range of the two driving frequencies.

2. Material and methods

2.1. Physical problem and mathematical model

We consider a resonator of length L filled with a bubbly liquid. We suppose a homogeneous distribution of spherical gas bubbles of the same size in the liquid. We study the nonlinear interaction between the acoustic waves and the bubble oscillations. This interaction is described by a differential system that couples the acoustic pressure $p(x,t)$ and the bubble volume variation $v(x,t) = V(x,t) - v_{0g}$, where $V(x,t)$ is the current bubble volume, $v_{0g} = 4\pi R_{0g}^3/3$ is the initial bubble volume, R_{0g} is its initial radius, x is the one-dimensional space coordinate, and t is the time coordinate [6,16,30]. The resonator is excited by a pressure source placed at $x = 0$ from time $t = 0$ to $t = T_t$. The differential system is formed by the wave equation, Eq. (1), and the Rayleigh-Plesset equation, Eq. (2):

$$\frac{\partial^2 p}{\partial x^2} - \frac{1}{c_{0l}^2}\frac{\partial^2 p}{\partial t^2} = -\rho_{0l} N_g \frac{\partial^2 v}{\partial t^2}, \quad 0 < x < L, \quad 0 < t < T_t, \tag{1}$$

$$\frac{\partial^2 v}{\partial t^2} + \delta\omega_{0g}\frac{\partial v}{\partial t} + \omega_{0g}^2 v + \eta p = av^2 + b\left(2v\frac{\partial^2 v}{\partial t^2} + \left(\frac{\partial v}{\partial t}\right)^2\right), \quad 0 \leqslant x \leqslant L, \quad 0 < t < T_t. \tag{2}$$

In these equations c_{0l} is the sound speed in the liquid, ρ_{0l} is the density of the liquid at the equilibrium state, and N_g is the density of the bubbles. $\delta = 4\nu_l/(\omega_{0g}R_{0g}^2)$ is the viscous damping coefficient, where ν_l is the cinematic viscosity of the liquid, $\omega_{0g} = \sqrt{3\gamma_g p_{0g}/\rho_{0l}R_{0g}^2}$ is the resonance frequency of the bubbles, where γ_g is the specific heat ratio of the gas, $p_{0g} = \rho_{0g}c_{0g}^2/\gamma_g$ is its atmospheric pressure, ρ_{0g} is its density at the equilibrium state, and c_{0g} is the sound speed in the gas. $\eta = 4\pi R_{0g}/\rho_{0l}$, $a = (\gamma_g + 1)\omega_{0g}^2/(2v_{0g})$, and $b = 1/(6v_{0g})$ are constants. We assume that p and v are at rest at the outset by imposing the following initial conditions:

$$p(x\neq 0,0) = 0, \quad v(x,0) = 0, \quad \frac{\partial p}{\partial t}(x\neq 0,0) = 0, \quad \frac{\partial v}{\partial t}(x,0) = 0, \quad 0 \leqslant x \leqslant L. \tag{3}$$

Furthermore, we impose two boundary conditions that set the free-reflector condition at $x = L$:

$$p(L,t) = 0, \quad 0 \leqslant t \leqslant T_t, \tag{4}$$

and the excitation of the system by a time-dependent pressure source at $x = 0$:

$$p(0,t) = s(t), \quad 0 \leqslant t \leqslant T_t. \tag{5}$$

This model considers that attenuation, dispersion, and nonlinear phenomena are due to the bubbles only, and also assumes the following physical restrictions [6,16,30]: bubbles are monopole and have the same size, they are spherical and oscillate at their first radial mode, their surface tension is neglected, they pulsate at finite but moderate amplitude (collapse is not modeled), they do not radiate sound themselves, the adiabatic gas law is used, and their thermal damping is considered negligible. In addition, the void fraction in the liquid must be much lower than one, and the buoyancy, Bjerknes and viscous drag forces are not considered.

2.2. Numerical model

The numerical model developed to solve the differential system is a combination of the finite-difference method in the time domain and the finite-volume method in the space dimension.

2.2.1. Approximation in the time domain (finite-difference method)

The time domain T_t is divided into $M-1$ constant intervals of duration τ. Each time discretization point is denoted by t_j ($j = 2,\ldots,M-1$). The following equations are used to approximate the time derivatives that appear in Eqs. (1)–(3) (Fig. 1a):

$$\frac{\partial^2 p_j}{\partial t^2} \approx \frac{p_{j+1} - 2p_j + p_{j-1}}{\tau^2}, \quad \frac{\partial^2 v_j}{\partial t^2} \approx \frac{v_{j+1} - 2v_j + v_{j-1}}{\tau^2}, \quad \frac{\partial v_j}{\partial t} \approx \frac{v_j - v_{j-1}}{\tau}, \quad \frac{\partial p_j}{\partial t} \approx \frac{p_j - p_{j-1}}{\tau}. \tag{6}$$

The error in these approximations is $O(\tau^2)$ for the second-order derivatives and $O(\tau)$ for the first-order derivative [35,36].

2.2.2. Approximation in the space dimension (finite-volume method)

The resonator length L is divided into N control volumes V_C of length h. The central point of each V_C is denoted by x_i ($i = 1,\ldots,N$). The differential equations are integrated in each V_C. The following equations are used to approximate the integrals that come from Eq. (1), where E and W indicate the east and west sides of V_C, respectively, and K is a generic constant (Fig. 1b):

$$\int_{V_C} \frac{\partial^2 p_i}{\partial x^2} dv = \int_W^E \frac{\partial^2 p_i}{\partial x^2} dx = \left.\frac{\partial p}{\partial x}\right|_E - \left.\frac{\partial p}{\partial x}\right|_W \approx \frac{p_{i+1} - p_i}{h} - \frac{p_i - p_{i-1}}{h} = \frac{p_{i+1} - 2p_i + p_{i-1}}{h}, \tag{7a}$$

$$\int_{V_C} K dv = \int_W^E K dx = Kh. \tag{7b}$$

The error in the approximation used in Eq. (7a) is $O(h)$ [34,35].

The application of Eqs. (6) and (7) to Eqs. (1) and (2) is described below. The first and last V_C must consider specific applications of Eq. (7a) to Eq. (1).

2.2.2.1. Generic volume. For any t_j ($j = 2,\ldots,M-1$) and any V_C ($i = 2,\ldots,N-1$) Eq. (1) yields, after multiplying by $h\tau^2$:

$$\frac{h^2}{c_{0l}^2} p_{i,j+1} - \rho_{0l} N_g h^2 v_{i,j+1} = \tau^2 p_{i+1,j} + \tau^2 p_{i-1,j} + 2\left(\frac{h^2}{c_{0l}^2} - \tau^2\right) p_{i,j} - \frac{h^2}{c_{0l}^2} p_{i,j-1} - 2\rho_{0l} N_g h^2 v_{i,j} + \rho_{0l} N_g h^2 v_{i,j-1} \quad j = 2,\ldots,M-1, \quad i = 2,\ldots,N-1. \tag{8}$$

After multiplying by τ^2, Eq. (2) yields:

$$(2bv_{i,j} - 1)v_{i,j+1} = (1 - \delta\omega_{0g}\tau - bv_{i,j-1})v_{i,j-1} + \left(-2 + \delta\omega_{0g}\tau + \omega_{0g}^2\tau^2\right)v_{i,j} + \eta\tau^2 p_{i,j} + (-a\tau^2 + 3b)v_{i,j}^2 \quad j = 2,\ldots,M-1, \quad i = 2,\ldots,N-1 \tag{9}$$

2.2.2.2. First volume. The approximation for $i = 1$ is (Fig. 1b):

$$\int_{V_C} \frac{\partial^2 p_1}{\partial x^2} dv = \int_W^E \frac{\partial^2 p_1}{\partial x^2} dx = \left.\frac{\partial p}{\partial x}\right|_E - \left.\frac{\partial p}{\partial x}\right|_W \approx \frac{p_2 - p_1}{h} - \frac{p_1 - P_0}{h/2} = \frac{p_2 - 3p_1 + 2P_0}{h}, \tag{10}$$

where P_0 is the pressure at $x = 0$ (see Eq. (5)). Thus, Eq. (1) for the first volume yields, after multiplying by $h\tau^2$:

$$\frac{h^2}{c_{0l}^2} p_{1,j+1} - \rho_{0l} N_g h^2 v_{1,j+1} = \tau^2 p_{2,j} + 2\tau^2 P_0 + \left(2\frac{h^2}{c_{0l}^2} - 3\tau^2\right) p_{1,j} - \frac{h^2}{c_{0l}^2} p_{1,j-1} - 2\rho_{0l} N_g h^2 v_{1,j} + \rho_{0l} N_g h^2 v_{1,j-1} \quad i = 1, \quad j = 2,\ldots,M-1 \tag{11}$$

2.2.2.3. Last volume. The approximation for $i = N$ is (Fig. 1b):

$$\int_{V_C} \frac{\partial^2 p_N}{\partial x^2} dv = \int_W^E \frac{\partial^2 p_N}{\partial x^2} dx = \left.\frac{\partial p}{\partial x}\right|_E - \left.\frac{\partial p}{\partial x}\right|_W \approx \frac{P_L - p_N}{h/2} - \frac{p_N - p_{N-1}}{h} = \frac{2P_L - 3p_N + p_{N-1}}{h}, \tag{12}$$

where P_L is the pressure at $x = L$ (see Eq. (4)). Thus, Eq. (1) for the last volume yields, after multiplying by $h\tau^2$:

$$\frac{h^2}{c_{0l}^2} p_{N,j+1} - \rho_{0l} N_g h^2 v_{N,j+1} = 2\tau^2 P_L + \tau^2 p_{N-1,j} + (2\frac{h^2}{c_{0l}^2} - 3\tau^2) p_{N,j} - \frac{h^2}{c_{0l}^2} p_{N,j-1} - 2\rho_{0l} N_g h^2 v_{N,j} + \rho_{0l} N_g h^2 v_{N,j-1} \quad i = N, \quad j = 2,\ldots,M-1. \tag{13}$$

Therefore, Eqs. (8), (9), (11), and (13) form a system valid for all i and $j > 1$. These equations are solved in the entire space domain at each time step. At the end we obtain the acoustic pressure and bubble volume variation values in the entire cavity at any time.

3. Results

This section shows several numerical experiments performed by the model developed in Section 2 assuming the bubbly liquid made of water and air bubbles: $c_{0l} = 1500$ m/s, $c_{0g} = 340$ m/s,

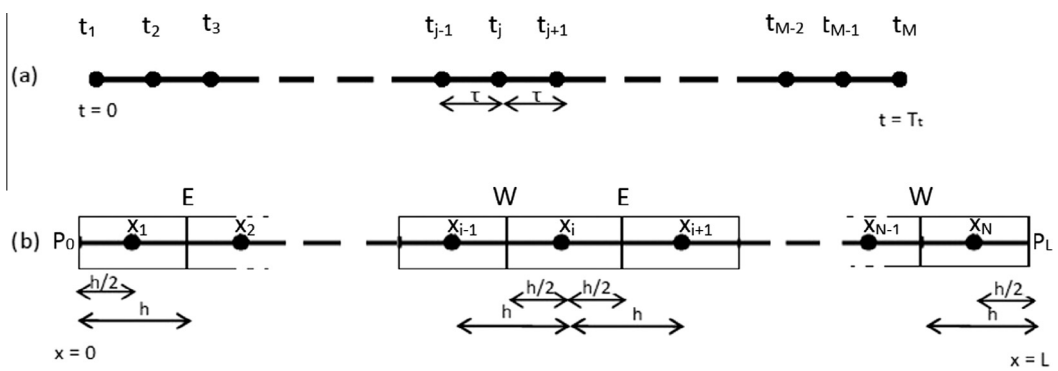

Fig. 1. (a) Finite-difference discretization of the time domain (subscript j). (b) Finite-volume discretization of the space domain (subscript i, control volume of center x_i).

$\rho_{0l} = 1000\ \mathrm{kg/m^3}$, $\rho_{0g} = 1.29\ \mathrm{kg/m^3}$, and $\nu_l = 1.43 \times 10^{-6}\ \mathrm{m^2/s}$. Section 3.1 presents results obtained by exciting the bubbly liquid with a single frequency source. Only one resonator length is considered in Section 3.1.1. We show a comparison between the data given in Ref. [27] and our results that allows us to validate our new numerical model in Section 3.1.1.1. A comparison between linear and nonlinear results is given in Section 3.1.1.2. This study allows us to highlight the nonlinear effects due to the bubbles in the liquid. Sections 3.1.1.3 and 3.1.1.4 analyze the effect of the amplitude at the source and the bubble density on the generation of harmonics. A physical law is proposed in each case for the second and the third harmonics in the resonator. Different resonator lengths are assumed in Section 3.1.2 to localize which of them allows the enhancement of the second harmonic component. Section 3.2 presents results obtained by exciting the bubbly liquid with a two-frequency source. We show the difference frequency generation in Section 3.2.1. Sections 3.2.2 and 3.2.3 study the effect of the amplitude and frequencies at the source on the generation of the difference frequency. Note that the steady state is reached inside the resonator in all the cases presented in this paper. It must also be noted that the situation assumed in the numerical simulations corresponds to the presence of stable oscillating bubbles that could be obtained with a microbubble generator based on the introduction of gas into the liquid through a porous material, or could be a ultrasound contrast agent microbubble suspension.

3.1. One frequency experiment

Air bubbles of radius $R_{0g} = 4.5 \times 10^{-6}$ m are used. Their density in the water is $N_g = 2 \times 10^{11}\ \mathrm{m^{-3}}$ (except in Section 3.1.1.4). The time-dependent function $s(t) = p_0 \sin(\omega_f t)$ of amplitude p_0 and frequency f is used at the source in Eq. (5), where $\omega = 2\pi f$. The driving frequency is set to f = 200 kHz. The sound speed in the bubbly liquid at f is $c_f = 1002.2$ m/s [16]. We consider $T_t = 200\,T$, where $T = 1/f$ is the acoustic period. In this section we use $\tau = 1.25 \times 10^{-8}$ s, corresponding to 400 points per period, and $h = 1.96 \times 10^{-5}$ m, corresponding to 256 control volumes per wavelength. These values ensure the convergence of the numerical solution.

3.1.1. Resonator length L = λ / 4

The length of the resonant cavity is set to $L = \lambda/4$, where $\lambda = c_f/f$ is the wavelength at frequency f in the bubbly liquid.

3.1.1.1. Validation of the model. We use our model with the parameter values employed in Ref. [27]. Qualitatively (pressure and bubble volume variation field, waveforms) and quantitatively (peak-to-peak pressure and bubble volume variation, rms pressure), similar results are obtained with both models. For $p_0 = 25$ kPa, nonlinear behaviors are found, the maximum and minimum pressure values obtained are respectively $p_{max} = 25.325$ kPa and $p_{min} = -13.285$ kPa. These values match the data observed in Fig. 4(a) shown in Ref. [27]. This qualitative and quantitative agreement validates our new model.

3.1.1.2. Comparison of linear and nonlinear regimes. We compare the results obtained for two source amplitudes, $p_0 = 1$ Pa and $p_0 = 28.7$ kPa, corresponding respectively to the linear and nonlinear regimes [37].

The normalized pressure waveform at L/2 during two periods is displayed in Fig. 2 for both driving amplitudes. The wave has symmetric compression and rarefaction pressures in the linear case. However, in the nonlinear regime this symmetry does not exist. Affected by the nonlinearity and the dispersion of the bubbly liquid, the wave is sharpened for positive pressures and smoothed

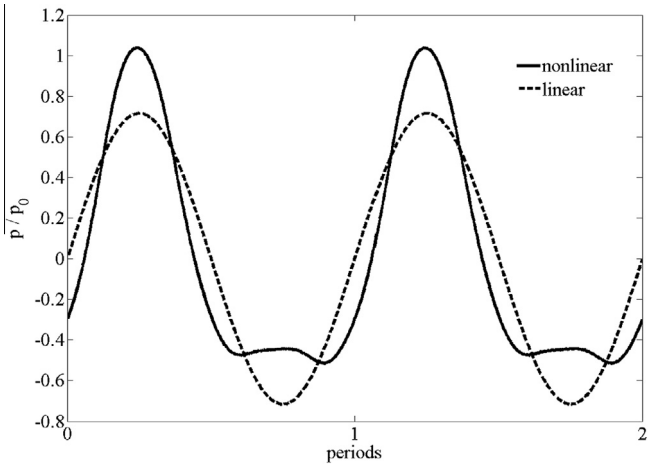

Fig. 2. Waveform at L/2 during two periods. Linear ($p_0 = 1$ Pa) and nonlinear ($p_0 = 28.7$ kPa) regimes. $R_{0g} = 4.5 \times 10^{-6}$ m, $N_g = 2 \times 10^{11}\ \mathrm{m^{-3}}$, f = 200 kHz, $L = \lambda/4$.

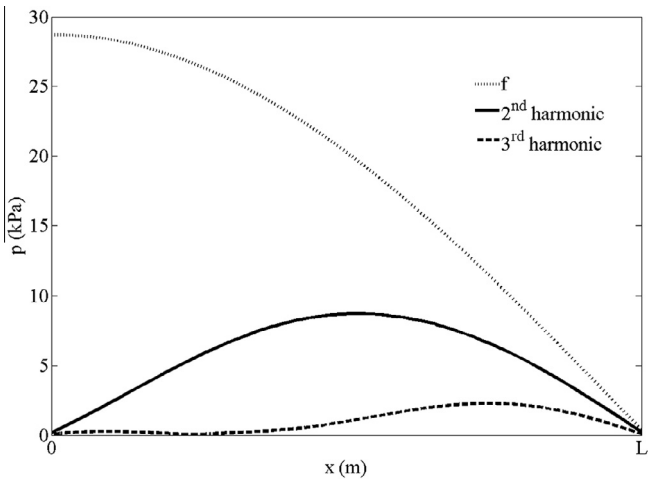

Fig. 3. Distribution of harmonics. $R_{0g} = 4.5 \times 10^{-6}$ m, $N_g = 2 \times 10^{11}\ \mathrm{m^{-3}}$, f = 200 kHz, $L = \lambda/4$, $p_0 = 28.7$ kPa.

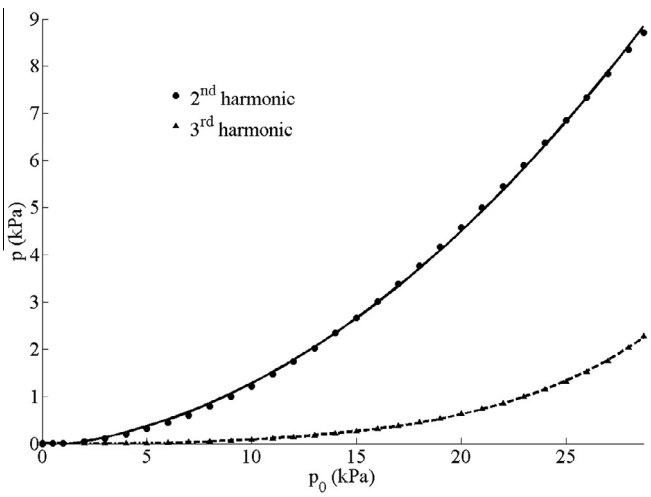

Fig. 4. Second (at L/2) and third (at 2L/3) harmonic amplitudes vs. source amplitude. $R_{0g} = 4.5 \times 10^{-6}$ m, $N_g = 2 \times 10^{11}\ \mathrm{m^{-3}}$, $f = 200$ kHz, $L = \lambda/4$.

for negative pressure values. Amplitudes reach values slightly higher than the source amplitude. There are not rarefaction values below the minimum value at the source. The root mean square pressure at L/2 is $p_{rms} = 0.51$ Pa in the linear regime and $p_{rms} = 15.755$ kPa in the nonlinear regime.

Fig. 3 represents the frequency decomposition in the entire resonator in the highest amplitude case ($p_0 = 28.7$ kPa) obtained after applying a Fast Fourier Transform. Different shapes are observed for each frequency. The fundamental frequency distribution is a quarter wavelength. The second harmonic distribution almost fits a half-wavelength form. The third harmonic distribution almost matches the shape of a three-quarter wavelengths. The shapes of the second and third harmonics are not exactly equal to half and three-quarter wavelengths because sound speed is dispersive in the bubbly liquid. The second harmonic reaches its maximum amplitude near L/2. The third harmonic reaches its maximum amplitude near 2L/3. This displacement of maxima at each different harmonic component explains the slightly higher amplitudes than the source amplitude observed in the previous paragraph. Note that the generation of harmonic components only occurs at high amplitude, i.e., the amplitude at the source is high enough to excite the nonlinear behavior of the pressure signal through the presence of the nonlinearly oscillating bubbles.

Note that, in relation to the model described in Ref. [27], the code developed here permits the use of higher pressure amplitudes at the source. This advantage is due to the use of the finite-volume method and allows us lower CPU costs. This benefit should lead to a better observation of nonlinear effects.

3.1.1.3. Influence of source amplitude on harmonic generation. The amplitudes of the second and third harmonics have been calculated varying the amplitude at the source. They are shown in Fig. 4. The second harmonic fits $p_2 = 0.0094p_0^2 + 0.042p_0 - 0.077$ at L/2 and the third harmonic fits $p_3 = 5.8 \times 10^{-6}p_0^4 - 0.00017p_0^3 + 0.0033p_0^2 - 0.014p_0 + 0.0082$ at 2L/3, where amplitudes are expressed in kPa.

3.1.1.4. Influence of bubble density on harmonic generation. A change of bubble density in the liquid modifies the acoustic characteristics of the medium [6]. For $N_g = 2 \times 10^{11}$ m^{-3}, corresponding to the volumetric void fraction $V_{vf} = 0.0076\%$, the sound speed is $c_f = 1002.2$ m/s and the attenuation coefficient is $\alpha = 6.01$ m^{-1}. For $N_g = 3 \times 10^9$ m^{-3}, corresponding to $V_{vf} = 0.00011\%$, $c_f = 1496.8$ m/s and $\alpha = 0.13$ m^{-1}. Namely, small changes in the volumetric void fraction produce important changes on the acoustic properties of the medium, such as the compressibility and nonlinearity, and modifications occurs in the generation of harmonics. Fig. 5 shows the amplitude of the second and third harmonics as a function of bubble density for the source amplitude $p_0 = 25$ kPa. They fit the following polynomials at L/2 and 2L/3, respectively, where harmonic amplitudes are expressed in Pa and N_g in mm^{-3}, $p_2 = -3.46 \times 10^{-10}N_g^6 - 2.57 \times 10^{-7}N_g^5 + 7.025 \times 10^{-5}N_g^4 - 0.0082N_g^3 + 0.31N_g^2 + 10.8N_g + 5979.2$ and $p_3 = -5.96 \times 10^{-10}N_g^6 + 4.44 \times 10^{-7}N_g^5 - 0.00012N_g^4 + 0.016N_g^3 - 0.92N_g^2 + 30.26N_g - 75.83$.

3.1.2. Other resonator lengths

We consider different cavity lengths, $L = n\lambda/4$, with $n = 1, 2, 3, 4$, $\lambda = c_f/f$ is the wavelength at frequency f in the bubbly liquid. For each resonator length 64, 128, 192, and 256 control volumes are used, respectively.

The generation of the second harmonic is studied in the four resonators. The objective of this study is to know the optimum resonator length that makes it possible to obtain the highest second-harmonic amplitude. Fig. 6 displays the fundamental and second-harmonic amplitude distributions for $p_0 = 1$ kPa. Lengths defined by odd multiples of $\lambda/4$ imply maximum amplitudes of 12.4 Pa (Fig. 6(a)) and 7.6 Pa (Fig. 6(b)), i.e., 1.24% and 0.76% of the source amplitude. When resonator lengths of even multiples of $\lambda/4$ are employed, maximum amplitudes of 1.794 kPa (Fig. 6(c)) and 1.849 kPa (Fig. 6(d)) are found, i.e., 179.4% and 184.9% of the source amplitude. With the use of lengths of odd multiples of $\lambda/4$, since Eq. (4) is assumed, the source acts as an anti-node that imposes the maximum pressure value reached in the resonator. However, by using even multiples of $\lambda/4$ to define the cavity length, Eq. (4) implies that the source point behaves like a node that does not set the maximum pressure value the wave can reach in the resonator. Therefore, resonators of even multiple of $\lambda/4$ are much more adequate to obtain large harmonic amplitude.

3.2. Two frequency experiment

The density $N_g = 5 \times 10^{11}$ m^{-3} of air bubbles of radius $R_{0g} = 2.5 \times 10^{-6}$ m is considered in the water. The time-dependent source function is defined here by $s(t) = p_0 \sin(\omega_1 t) + p_0 \sin(\omega_2 t)$ in Eq. (5), in which p_0 is the amplitude, f_1 and f_2 are the primary frequencies chosen to generate the difference frequency $f_d = f_2 - f_1$, $\omega_1 = 2\pi f_1$, and $\omega_2 = 2\pi f_2$. We set $f_d = 200$ kHz and $T_t = 400T_d$, where $T_d = 1/f_d$ is the acoustic period at f_d. $f_1 = 700$ kHz and $f_2 = 900$ kHz, except in Section 3.2.3.

The results obtained in Section 3.1.2 suggest the use of a resonant cavity of length $L = \lambda_d$ to enhance the difference-frequency

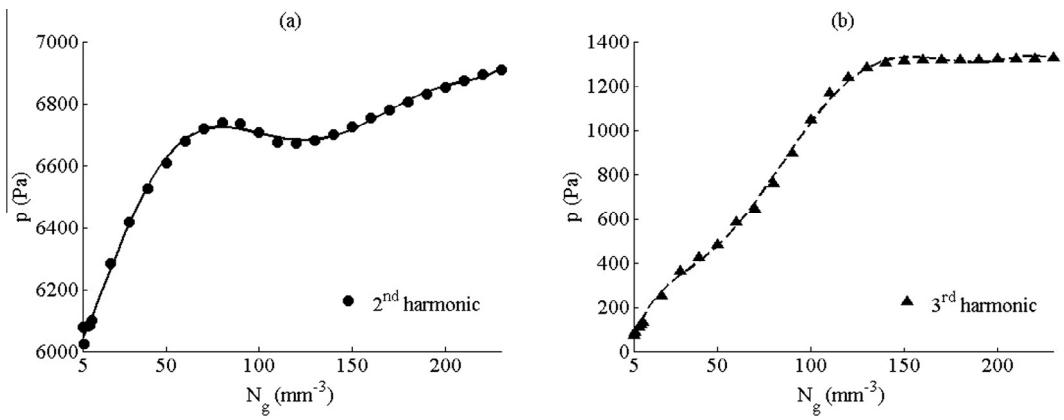

Fig. 5. (a) Second (at L/2) and (b) third (at 2L/3) harmonic amplitudes vs. bubble density. $R_{0g} = 4.5 \times 10^{-6}$ m, f = 200 kHz, $L = \lambda/4$, $p_0 = 25$ kPa.

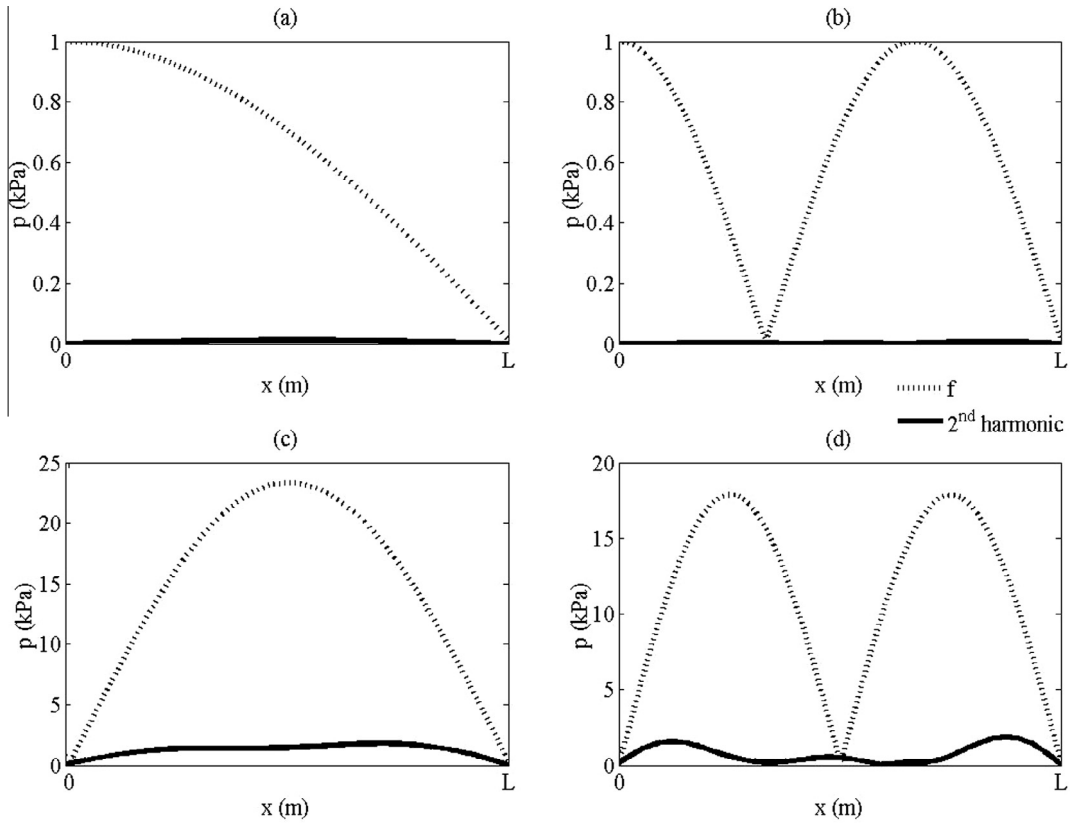

Fig. 6. Distribution of harmonics for different resonator lengths. $R_{0g} = 4.5 \times 10^{-6}$ m, $N_g = 2 \times 10^{11}$ m^{-3}, f = 200 kHz, $L = n\lambda/4$ (n = 1, 2, 3, 4), $p_0 = 1$ kPa. Top diagrams (odd numbers): (a) n = 1, (b) n = 3. Bottom diagrams (even numbers): (c) n = 2, (d) n = 4.

amplitude, where $\lambda_d = c_d/f_d$ is the wavelength and $c_d = 1223$ m/s is the sound speed in the bubbly liquid at f_d [16].

In this section the discretization is defined by $\tau = 3.125 \times 10^{-8}$ s and $h = 4.777 \times 10^{-5}$ m to ensure the convergence of the numerical solution, i.e., 160 points per period and 128 control volumes are employed.

3.2.1. Generation of difference frequency

Fig. 7 represents the frequency decomposition in the entire resonator for $p_0 = 14$ kPa obtained after applying a Fast Fourier Transform. The maximum amplitude p_d of the generated difference frequency f_d is 15.73 kPa obtained at 3L/4. It corresponds to 110% of the source amplitude. The sum frequency $f_s = f_1 + f_2$ reaches its maximum amplitude of 4.63 kPa at 0.001 m, corresponding to 33% of the source amplitude. These differences are due to the dispersive character of attenuation that affects the difference and the sum frequencies differently, $\alpha = 2.83$ m^{-1} at f_d and $\alpha = 3162.9$ m^{-1} at f_s. The source frequencies are also affected by attenuation in different ways, $\alpha = 58.71$ m^{-1} at f_1 and $\alpha = 157.67$ m^{-1} at f_2. It can also be seen that the f_2 component loses much more energy than the f_1 component in the cavity when the f_d component is created. In addition to attenuation considerations given above, this result suggests that during the nonlinear mixing process most of the energy gained by f_d comes from f_2.

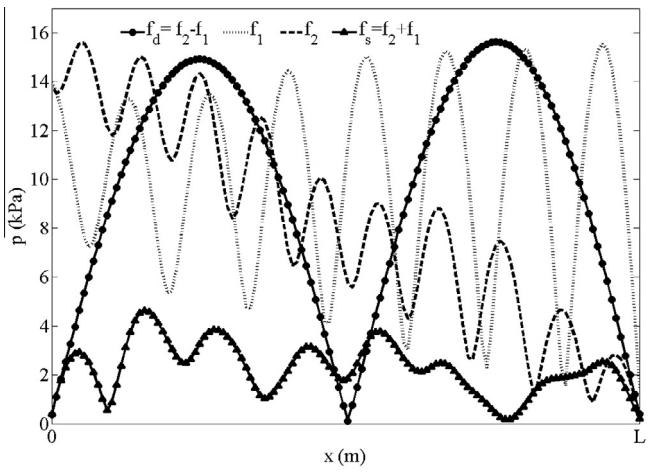

Fig. 7. Distribution of frequency components. $R_{0g} = 2.5 \times 10^{-6}$ m, $N_g = 5 \times 10^{11}$ m^{-3}, $f_1 = 700$ kHz, $f_2 = 900$ kHz, $L = \lambda_d$, $p_0 = 14$ kPa.

3.2.2. Influence of source amplitude on difference frequency amplitude

The maximum amplitude p_d of the difference frequency obtained in the cavity at 3L/4 is studied as a function of the source amplitude p_0. The result is represented in Fig. 8. It fits the following polynomial, in which p_d and p_0 are expressed in kPa, $p_d = 0.0017p_0^4 - 0.0549p_0^3 + 0.5042p_0^2 + 37.53p_0 - 0.0590$. Two different phases are observed: when p_0 rises from 0 to 7 kPa p_d grows rapidly; when p_0 is raised from 7 kPa p_d grows slower and slower and seems to reach a saturation behavior.

3.2.3. Influence of source frequency values on difference frequency amplitude

This section studies the influence of the localization of the primary frequencies on the maximum amplitude p_d values of the difference frequency. The source amplitude is set at $p_0 = 8$ kPa. Fig. 9 shows p_d at 3L/4 as a function of the half-sum of the source frequencies, $(f_1 + f_2)/2$. For frequencies below the peak of

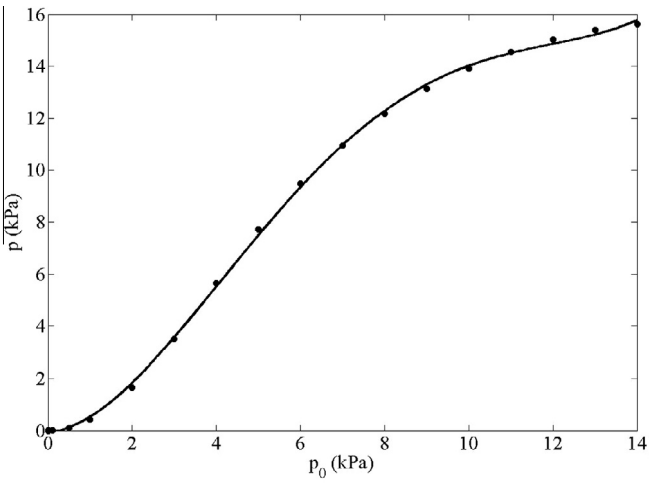

Fig. 8. Difference frequency amplitude at 3L/4 vs. source amplitude. $R_{0g} = 2.5 \times 10^{-6}$ m, $N_g = 5 \times 10^{11}$ m^{-3}, $f_1 = 700$ kHz, $f_2 = 900$ kHz, $L = \lambda_d$.

attenuation, i.e., between 0.5 and 1 MHz (Fig. 9(a)), the response of the system is high and we obtain a good efficiency in the difference-frequency generation because the attenuation affecting the wave is small (Fig. 10(b)) and the compressibility of the bubbly liquid is high (Fig. 10(c)). The highest amplitude is obtained for $f_1 = 0.7$ MHz and $f_2 = 0.9$ MHz: $p_d = 12.350$ kPa, which means a value equal to 154% of the source amplitude. For frequencies above the peak of attenuation, i.e., over 1.4 MHz (Fig. 9(b)), the response of the system is lower and we obtain a smaller efficiency of the generation process because the compressibility is small (Fig. 10(c)). The smallest response is $p_d = 997$ Pa, 12% of the source amplitude, corresponding to $f_1 = 1.4$ MHz and $f_2 = 1.6$ MHz. This value matches the frequency range for which the compressibility of the medium is minimum (Fig. 10(c)). Note that for source frequencies around the bubble resonance, $f_r = 1.347$ MHz, the compressibility is very high and no data have been obtained with the model.

Our new numerical model allows us to increase the source amplitude to higher values than other models found in the literature, in particular in relation to the finite-difference based model in Ref. [27], which is useful to observe nonlinear phenomena. Furthermore, comparing to the finite-difference techniques, the expansion to problems with higher space dimensions and involving other kinds of boundary conditions is made easier by the use of the finite-volume method, which is helpful to perform more complex developments and studies in the future. These benefits are possible because the method integrates the differential equations after dividing the whole domain in control volumes and imposes the continuity of variables between adjacent control volumes by interpolation.

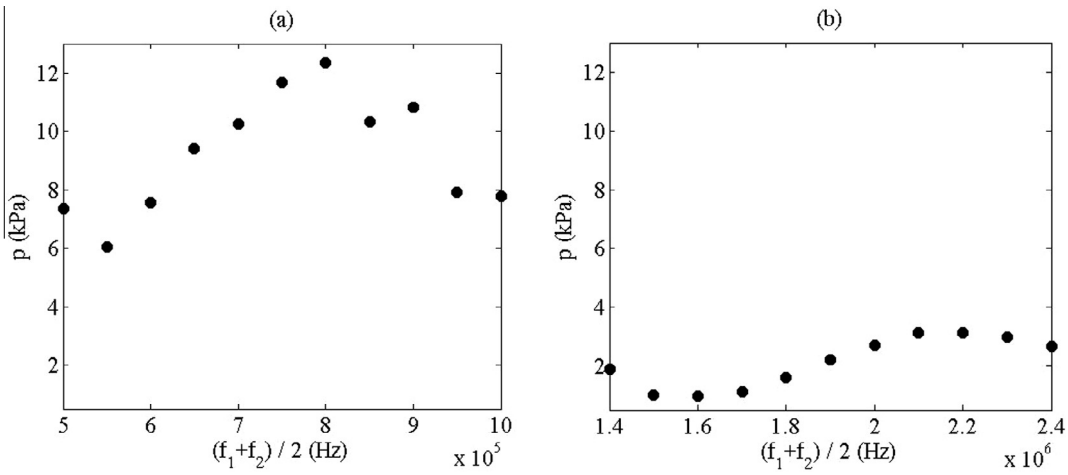

Fig. 9. Difference frequency amplitude at 3L/4 vs. localization of the primary frequencies $((f_1 + f_2)/2)$. (a) $((f_1 + f_2)/2) < f_r$, (b) $f_r < ((f_1 + f_2)/2)$. $R_{0g} = 2.5 \times 10^{-6}$ m, $N_g = 5 \times 10^{11}$ m^{-3}, $L = \lambda_d$, $p_0 = 8$ kPa.

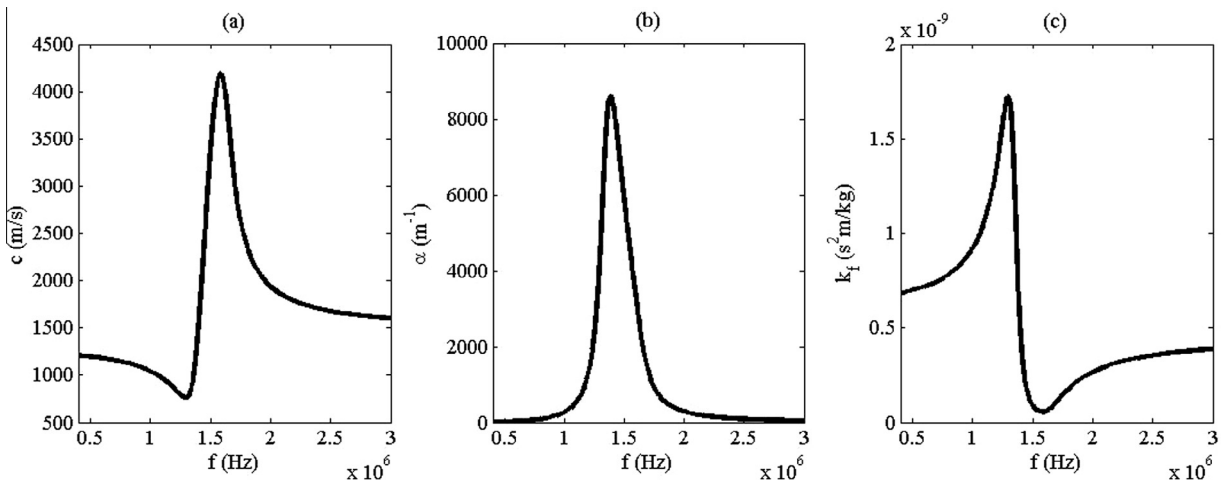

Fig. 10. Dispersion curves of sound speed (a), attenuation coefficient (b), and compressibility (c). $R_{0g} = 2.5 \times 10^{-6}$ m, $N_g = 5 \times 10^{11}$ m^{-3}.

It is worth noting that the difference-frequency amplitude obtained in this paper is much higher than the ones found in other studies of this phenomenon in bubbly liquids [30–33].

4. Conclusions

The numerical model developed here, based on a combination of the finite-volume and the finite-difference methods, allows us to study nonlinear ultrasonic standing waves in bubbly liquids. A differential system that models the interaction of acoustic pressure and bubble oscillations in a resonator has been solved. The numerical experiments shown here consider different amplitudes, frequencies, void fractions (bubble density or size), and resonator lengths. Nonlinearity, dispersion, and attenuation due to the bubbles have been observed. We have studied the generation of new frequencies in the resonator as a result of the nonlinear mixing of two primary ultrasonic signals. The behavior of the difference-frequency amplitude has been analyzed as a function of several parameters. The results obtained here suggest the use of primary frequencies located below the bubble resonance in a resonator whose length is set at one wavelength of the difference frequency in the bubbly medium to improve the frequency mixing response of the system. This study could be useful for some applications.

Acknowledgements

This work is supported by the Ministry of Economy and Competitiveness of Spain [DPI2012-34613, BES-2013-064399].

Christian Vanhille expresses his gratitude to Dr. Cleofé Campos-Pozuelo.

References

[1] J.A. Gallego-Juárez, K.F. Graff (Eds.), Power ultrasonics: applications of high-intensity ultrasound, Woodhead Publishing Series in Electronic and Optical Materials, vol. 66, Elsevier, Amsterdam, 2015.
[2] F. Chemat, Z. Huma, M. Kamran Khan, Applications of ultrasound in food technology: processing, preservation and extraction, Ultrason. Sonochem. 18 (2011) 813–835.
[3] O. Al-Bataineh, J. Jenne, P. Huber, Clinical and future applications of high intensity focused ultrasound in cancer, Cancer Treat. Rev. 38 (2012) 346–353.
[4] E. Riera-Franco de Sarabia, J.A. Gallego-Juárez, G. Rodríguez-Corral, L. Elvira-Segura, I. González-Gómez, Application of high-power ultrasound to enhance fluid/solid particle separation processes, Ultrasonics 38 (2000) 642–646.
[5] T.J. Mason, J.P. Lorimer, Applied Sonochemistry: The Uses of Power Ultrasound in Chemistry and Processing, Wiley-VCH, Weinheim, 2002.
[6] F. Grieser, P.K. Choi, N. Enomoto, H. Harada, K. Okitsu, K. Yasui (Eds.), Sonochemistry and the Acoustic Bubble, Elsevier, Amsterdam, 2015.
[7] K. Naugolnykh, L. Ostrovsky, Nonlinear Wave Processes in Acoustics, Cambridge University Press, New York, 1998.
[8] P.J. Westervelt, Parametric acoustic array, J. Acoust. Soc. Am. 35 (1963) 535–537.
[9] J.L.S. Bellin, R.T. Beyer, Experimental investigation of an end-fire array, J. Acoust. Soc. Am. 34 (1962) 1051–1054.
[10] T.S. Desser, R.B. Jeffrey, Tissue harmonic imaging techniques: physical principles and clinical applications, Semin. Ultrasound CT MR 22 (2001) 1–10.
[11] V.L. Newhouse, P.M. Shankar, Bubble size measurement using the nonlinear mixing of two frequencies, J. Acoust. Soc. Am. 75 (1984) 1473–1477.
[12] J.C. Buckey, D.A. Knaus, D.L. Alvarenga, M.A. Kenton, P.J. Magari, Dual-frequency ultrasound for detecting and sizing bubbles, Acta Astronaut. 56 (2005) 1041–1047.
[13] M. Cavaro, C. Payan, J. Moysan, Microbubble cloud characterization by nonlinear frequency mixing, J. Acoust. Soc. Am. 129 (2011) 179–183.
[14] D.N. Sinha, C. Pantea, Broadband unidirectional ultrasound propagation using sonic crystal and nonlinear medium, Emerg. Mater. Res. 2 (2013) 117–126.
[15] F.R. Young, Cavitation, McGraw-Hill, London, 1989.
[16] M.F. Hamilton, D.T. Blackstock, Nonlinear Acoustics, Academic Press, San Diego, 1998.
[17] I. Tudela, V. Sáez, M.D. Esclapez, M.I. Diez-Garcia, P. Bonete, J. González-García, Simulation of the spatial distribution of the acoustic pressure in sonochemical reactors with numerical methods: a review, Ultrason. Sonochem. 21 (2014) 909–919.
[18] V. Sáez, J. Frías-Ferrer, J. Iniesta, J. Gonzalez-García, A. Aldaz, E. Riera, Characterization of a 20 kHz sonoreactor: part I: analysis of mechanical effects by classical and numerical methods, Ultrason. Sonochem. 12 (2005) 59–65.
[19] J. Klíma, J. Frias-Ferrer, J. González-García, J. Ludvík, V. Sáez, J. Iniesta, Optimisation of 20 kHz sonoreactor geometry on the basis of numerical simulation of local ultrasonic intensity and qualitative comparison with experimental results, Ultrason. Sonochem. 14 (2007) 19–28.
[20] V.S. Sutkar, P.R. Gogate, L. Csoka, Theoretical prediction of cavitational activity distribution in sonochemical reactors, Chem. Eng. J. 158 (2010) 290–295.
[21] K.W. Commander, A. Prosperetti, Linear pressure waves in bubbly liquids: comparison between theory and experiments, J. Acoust. Soc. Am. 85 (1989) 732–746.
[22] R.E. Caflisch, M.J. Miksis, G.C. Papanicolau, L. Ting, Effective equations for wave propagation in bubbly liquids, J. Fluid Mech. 153 (1985) 259–273.
[23] S. Dähnke, K.M. Swamy, F.J. Keil, Modeling of three-dimensional pressure fields in sonochemical reactors with an inhomogeneous density distribution of cavitation bubbles. Comparison of theoretical and experimental results, Ultrason. Sonochem. 6 (1999) 31–41.
[24] S. Dähnke, K.M. Swamy, F.J. Keil, A comparative study on the modelling of sound pressure field distributions in a sonoreactor with experimental investigation, Ultrason. Sonochem. 6 (1999) 221–226.
[25] S. Nomura, M. Nakagawa, Analysis of an ultrasonic field attenuated by oscillating cavitation bubbles, Acoust. Sci. Tech. 22 (2001) 283–291.
[26] K. Yasui, T. Kozuka, T. Tuziuti, A. Towata, Y. Iida, J. King, P. Macey, FEM calculation of an acoustic field in a sonochemical reactor, Ultrason. Sonochem. 14 (2007) 605–614.
[27] C. Vanhille, C. Campos-Pozuelo, Numerical simulation of nonlinear ultrasonic standing waves in bubbly liquids, Int. J. Nonlinear Sci. Numer. Simul. 10 (2009) 751–757.
[28] C. Vanhille, C. Campos-Pozuelo, Nonlinear ultrasonic standing waves: two-dimensional simulations in bubbly liquids, Ultrason. Sonochem. 18 (2011) 679–982.
[29] C. Vanhille, C. Campos-Pozuelo, Numerical simulations of three-dimensional nonlinear acoustic waves in bubbly liquids, Ultrason. Sonochem. 20 (2013) 963–969.
[30] E.A. Zabolotskaya, S.I. Soluyan, Emission of harmonic and combination-frequency waves by air bubbles, Sov. Phys. Acoust. 18 (1973) 396–398.
[31] Y.A. Kobelev, A.M. Sutin, Difference-frequency sound generation in a liquid containing bubbles of differents sizes, Sov. Phys. Acoust. 26 (1980) 485–847.
[32] O.A. Druzhinin, L.A. Ostrovsky, A. Prosperetti, Low-frequency acoustic wave generation in a resonant bubble layer, J. Acoust. Soc. Am. 100 (1996) 3570–3580.
[33] C. Vanhille, C. Campos-Pozuelo, D.N. Sinha, Nonlinear frequency mixing in a resonant cavity: numerical simulations in a bubbly liquid, Ultrasonics 54 (2014) 2051–2054.
[34] H.K. Versteeg, W. Malalasekera, An Introduction to Computational Fluid Dynamics: The Finite Volume Method, Longman Scientific & Technical, Harlow, 1995.
[35] C. Vanhille, A. Lavie, C. Campos-Pozuelo, Modélisation numérique en mécanique: introduction et mise en pratique, Hermes Science Publications, Lavoisier, Paris, 2007.
[36] G.D. Smith, Numerical Solution of Partial Differential Equations, Finite Difference Methods, third ed., Clarendon, Oxford, 1985.
[37] M.T. Tejedor Sastre, C. Vanhille, Un modelo numérico para el análisis no lineal de ondas ultrasónicas estacionarias en líquidos con burbujas, 45°Congreso Español de Acústica, 8°Congreso Ibérico de Acústica y Simposio Europeo sobre Ciudades Inteligentes y Acústica Ambiental, Murcia 29–31 (2014) 1414–1419.

Capítulo 3

Modelos numéricos para el estudio de la mezcla no lineal de frecuencias en cavidades resonantes bi y tridimensionales llenas de un líquido con burbujas

Este capítulo se estudia el comportamiento de ondas ultrasónicas estacionarias en líquidos con burbujas en geometrías bidimensionales y tridimensionales que permitan el acercamiento a la realidad del problema físico que nos concierne en esta tesis. Este comportamiento se describe a partir de modelos matemáticos formados por la ecuación de ondas y una ecuación de Rayleigh-Plesset que relacionan la presión acústica con las vibraciones de las burbujas en dos y tres dimensiones respectivamente. Para ello se desarrollan modelos numéricos capaces de simular este comportamiento. Los modelos están basados en el método de los volúmenes finitos en las dimensiones espaciales y de las diferencias finitas en el dominio temporal.

Los experimentos numéricos se realizan para modos complejos en muchas cavidades diferentes considerando diferentes tipos de condiciones de contorno y aprovechando el carácter dispersivo del líquido con burbujas para que coincida con las resonancias

específicas de las cavidades. Los resultados permiten estudiar la generación de armónicos (con fuentes de una frecuencia) y la frecuencia diferencia (con fuentes de dos frecuencias) con distintos tipos de condiciones de contorno. Los modelos desarrollados muestran una enorme flexibilidad a la hora de simular cualquier tipo de geometría.

Se incluye la publicación en revista científica (Factor de impacto JCR-ISI: 6,012) cuya referencia es:

M.T. Tejedor Sastre, C. Vanhille, Numerical models for the study of the nonlinear frequency mixing in two an three-dimensional resonant cavities filled with a bubbly liquid, Ultrason. Sonochem. 39 (2017) 597-610.

Ultrasonics Sonochemistry

Jones, Jennifer (ELS-OXF)<J.Jones@elsevier.com>

vie 13/07/2018 10:54

Para:Christian Vanhille . <christian.vanhille@urjc.es>;

ELSEVIER

Dear Dr Christian Vanhille
We hereby grant María Teresa Tejedor Sastre permission to reproduce the material detailed below at no charge in her thesis, in print and on OpenDOAR and subject to the following conditions:

1. If any part of the material to be used (for example, figures) has appeared in our publication with credit or acknowledgement to another source, permission must also be sought from that source. If such permission is not obtained then that material may not be included in your publication/copies.

2. Suitable acknowledgment to the source must be made, either as a footnote or in a reference list at the end of your publication, as follows:

   "This article was published in Publication title, Vol number, Author(s), Title of article, Page Nos, Copyright Elsevier (or appropriate Society name) (Year)."

3. Her thesis may be submitted to her institution in either print or electronic form.

4. Reproduction of this material is confined to the purpose for which permission is hereby given.

5. This permission is granted for non-exclusive world **English** rights only. For other languages please reapply separately for each one required. Permission excludes use in an electronic form other than as specified above. Should she have a specific electronic project in mind please reapply for permission.

6. Should her thesis be published commercially, please reapply for permission.

Yours sincerely

Jennifer Jones
Permissions Specialist

Elsevier Limited, a company registered in England and Wales with company number 1982084, whose registered office is The Boulevard, Langford Lane, Kidlington, Oxford, OX5 1GB, United Kingdom.

03 Jul 2018 4:09pm

Question	Answer
Title	Dr.

Question	Answer
First name	Christian
Last name	Vanhille
Institute/company	Universidad Rey Juan Carlos
Address	Tulipán, s/n
Post/Zip Code	28933
City	Móstoles
State/Territory	Madrid
Country	Spain
Telephone	+34 916647482
Email	christian.vanhille@urjc.es
Please select the type of publication	Journal
Journal - Title	Ultrasonics Sonochemistry
Journal - ISSN	1350-4177
Journal - Volume	39
Journal - Issue	1
Journal - Year	2017
Journal - Pages from	597
Journal - Pages to	610
Journal - Author	María Teresa Tejedor Sastre, Christian Vanhille
Journal - Article Title	Numerical models for the study of the nonlinear frequency mixing in two and three-dimensional resonant cavities filled with a bubbly liquid
I would like to use (please select one of the following options)	Full article/chapter
If using figures/tables or illustrations please specify the quantity	
If using excerpts please provide a total word count	
Are you the author of the Elsevier material?	Yes
If not, is the Elsevier author involved with your project?	Yes
If yes, please provide details of how the Elsevier author is involved	
In what format will you use the material?	Print and Electronic
Will you be translating the material?	No
If yes, please specify the languages	
Information about your proposed use	Reuse in a thesis/dissertation
Proposed use text	Posting in a repository.
AdditionalComments/Information	I would need this permission as soon as possible since the dissertation of María Teresa Tejedor Sastre must be submitted next week (I am the doctoral thesis director). Thank you.

Ultrasonics - Sonochemistry 39 (2017) 597–610

Contents lists available at ScienceDirect

Ultrasonics - Sonochemistry

journal homepage: www.elsevier.com/locate/ultson

Numerical models for the study of the nonlinear frequency mixing in two and three-dimensional resonant cavities filled with a bubbly liquid

María Teresa Tejedor Sastre, Christian Vanhille*

Universidad Rey Juan Carlos, Tulipán, s/n. 28933 Móstoles, Madrid, Spain

ARTICLE INFO

Keywords:
Ultrasound
Nonlinear acoustics
Bubbly liquids
Multi-dimensional numerical simulations
Frequency mixing
Complex modes

ABSTRACT

The objective of this work is to develop versatile numerical models to study the nonlinear distortion of ultrasounds and the generation of low-ultrasonic frequency signals by nonlinear frequency mixing in two and three-dimensional resonators filled with bubbly liquids. The interaction of the acoustic field and the bubble vibrations is modeled through a coupled differential system formed by the multi-dimensional wave equation and a Rayleigh-Plesset equation. The numerical models we develop are based on multi-dimensional finite-volume techniques and a time discretization carried out by finite differences. Numerical experiments are performed for complex modes in many different cavities considering different kinds of boundary conditions and taking advantage of the dispersive character of the bubbly fluid to match specific resonances of the cavities. Results show the distribution of fundamental and harmonics for single frequency excitation and difference-frequency component for two-frequency excitation that are promoted by the strong nonlinearity of the bubbly medium. The numerous simulations analyzed suggest that the new numerical models developed and proposed in this paper are useful to understand the behavior of ultrasounds in bubbly liquids for sonochemical processes and applications of nonlinear frequency mixing.

1. Introduction

The nonlinear propagation of power ultrasound in homogeneous and multiphasic media, fluids and solids, has been the topic of many works in the last decades [1,2]. The nonlinear effects on the acoustic field are visible through the harmonic distortion that can lead to the formation of shock waves, the generation of sub and super-harmonics, and the mixing of all these components [3,4]. These nonlinear features induce phenomenon useable in many different applications [2]. Bubbly liquids are biphasic media that have a very high nonlinear acoustic parameter [3–5]. A small amount of gas bubbles in a homogeneous liquid modifies its compressibility and makes this parameter be several orders of magnitude higher [3–6]. These media are thus very interesting in several applications for which bubbles are required or cavitation is present [7,8]. Other physical properties of the liquid are changed by adding bubbles [3–5]. Besides compressibility, sound speed and attenuation acquire a dispersive character that depends on the bubble resonance. Bubbly liquids have been the subject of many theoretical and applied researches in recent years [3,9,10]. Several studies have been carried out in this framework to characterize the acoustic field in sonoreactors [11], by taking into account different aspects such as the geometry [12], attenuation [13–15], inhomogeneous distribution of bubbles [16], wall vibrations [17], nonlinearity [18–20].

The formation of the sum and difference-frequency signals by nonlinear mixing of two primary waves was described in [21,22]. Applications of this phenomenon are based on the high directivity and low attenuation of the difference frequency component, in underwater communication or nondestructive testing [23–25]. Frequency mixing can be used to detect and characterize bubbles [26–28] in disciplines as diverse as the safety in aerospace or nuclear industry.

Several experimental works and theoretical studies in one-dimensional space have been carried out to analyze the harmonic generation and frequency mixing in bubbly liquids. Zabolotskaya and Soluyan [29] analyze theoretically the emission of harmonics and combination of frequencies. Kovelev and Sutin [30] study theoretically and experimentally the difference-frequency sound generation in a liquid containing bubbles of different sizes. Druzhinin et al. [31] explore the low-frequency generation through a resonant bubble layer analytically and numerically. Ma et al. [32] examine theoretically and experimentally the difference-frequency generation from microbubbles. Vanhille et al. [18,33,34] analyze numerically the harmonic generation and difference frequency in several configurations. Some multidimensional studies exist in the literature about harmonic distortion [19,20] and frequency mixing [35]. It must be noted that, unlike what is performed

* Corresponding author.
E-mail address: christian.vanhille@urjc.es (C. Vanhille).

http://dx.doi.org/10.1016/j.ultsonch.2017.05.009
Received 27 February 2017; Received in revised form 28 April 2017; Accepted 5 May 2017
Available online 13 May 2017
1350-4177/

here, this latest does not consider resonant cavities.

Obtaining experimental data from the propagation of ultrasound in a liquid with a stable population of gas bubbles is not straightforward. On the other hand, a lack of versatile multidimensional numerical models for the study of nonlinear ultrasound in bubbly liquids exists in the literature. This deficiency limits the possibility to progress in the understanding of both the nonlinear distortion and the frequency mixing in realistic configurations. Moreover, as Tudela et al. point out [36], the design of more efficient sonoreactors requires more accurate models able to simulate different realistic multidimensional acoustic modes. It is thus necessary to develop new models able to go forward in this direction.

In this paper we present new versatile multidimensional tools able to simulate the nonlinear effects (harmonic generation, frequency mixing) that take place in cavities filled with bubbly liquids in different configurations. We develop several numerical models, based on the finite-difference method [37,38] in time domain and on the finite-volume method [38,39] in space dimensions, to solve the differential system formed by the wave equation and a Rayleigh-Plesset equation. These equations model the nonlinear coupling between the acoustic field and the bubble vibrations. The main reason to use the finite-volume method is the possibility to increase the number of dimension easily and the straightforward implementation of boundary conditions. This advantage is due to the integration of the differential system after dividing the entire space domain in small control volumes and imposing the continuity of variables between adjacent control volumes by interpolation.

The objective of this work is to study the harmonic and the difference frequency generation in different multidimensional configurations. In Section 2.1 we present the physical problem treated here. In Section 2.2 we describe the mathematical problem for three geometries with different boundary conditions both in two (Section 2.2.1) and three (Section 2.2.2) dimensions. Section 2.3 presents the discretized equations corresponding to each mathematical problem and geometry. In Section 3 we present the results obtain from multiple simulations of complex modes in all the cases developed in Section 2. Our models are suitable to observe the nonlinear distortion of ultrasounds and the generation of the difference frequency produced by nonlinear frequency mixing. Both could be useful in sonochemistry and in applications of the difference-frequency component.

2. Material and methods

2.1. Physical problem

We consider a mixture of water and air bubbles in different kinds of resonant cavities. We suppose spherical bubbles that are evenly distributed in the liquid. For a given mixture, these bubbles are of the same size. The system is excited by a continuous pressure source at one or two frequencies. We study the nonlinear mutual interaction between the pressure field and the bubble vibrations for different geometries and assuming several types of initial and boundary conditions (Dirichlet and Neumann). This problem is set out in two and three-dimensional configurations, and modeled through the corresponding differential systems in Sections 2.2.1 and 2.2.2, respectively.

It must be noted that the model developed here considers the nonlinear interaction of ultrasound and bubble vibrations by assuming one bubble size in each experiment, and neglects the Bjerknes forces of the acoustic field on bubbles.

2.2. Mathematical problem

2.2.1. Two-dimensional resonant cavity

We consider a cavity of dimensions $L_2(y)-L_1(y)$ in the x-direction and L_y in the y-direction, where (x,y) are the two-dimensional coordinates. The interaction between the acoustic pressure p(x,y,t) and the volume variation of the bubbles $v(x,y,t) = V(x,y,t)-v_{0g}$, where $v_{0g} = 4\pi R_{0g}^3/3$ is the initial volume of the bubbles, R_{0g} is their initial radius, and t is the time coordinate, is described by the following differential system [3–5]:

$$\frac{\partial^2 p}{\partial x^2} + \frac{\partial^2 p}{\partial y^2} - \frac{1}{c_{0l}^2}\frac{\partial^2 p}{\partial t^2} = -\rho_{0l} N_g \frac{\partial^2 v}{\partial t^2},$$
$$L_1(y) < x < L_2(y),\ 0 < y < L_y,\ 0 < t < T_t, \tag{1}$$

$$\frac{\partial^2 v}{\partial t^2} + \delta\omega_{0g}\frac{\partial v}{\partial t} + \omega_{0g}^2 v + \eta p = a v^2 + b\left(2v\frac{\partial^2 v}{\partial t^2} + \left(\frac{\partial v}{\partial t}\right)^2\right),$$
$$L_1(y) \leqslant x \leqslant L_2(y),\quad 0 \leqslant y \leqslant L_y,\quad 0 < t < T_t. \tag{2}$$

Eq. (1) is the wave equation, where c_{0l} and ρ_{0l} are the sound speed and the density at the equilibrium state of the liquid. N_g is the density of bubbles. Eq. (2) is a Rayleigh-Plesset equation, where $\delta = 4\nu_l/(\omega_{0g}R_{0g}^2)$ is the viscous damping coefficient of the bubbly fluid, in which ν_l is the cinematic viscosity of the liquid, $\omega_{0g} = \sqrt{3\gamma_g p_{0g}/\rho_{0l}R_{0g}^2}$ is the resonance frequency of the bubbles, for which γ_g is the specific heats ratio of the gas, $p_{0g} = \rho_{0g}c_{0g}^2/\gamma_g$ is its atmospheric pressure, ρ_{0g} and c_{0g} are the density and sound speed at the equilibrium state in the gas. The parameters $\eta = 4\pi R_{0g}/\rho_{0l}$, $a = (\gamma_g + 1)\omega_{0g}^2/(2v_{0g})$, and $b = 1/(6v_{0g})$ are constants. The experiment is performed until time T_t is reached.

We suppose that the bubbles are at rest in the unperturbed liquid when the experiment starts:

$$p(x,y,0) = 0,\quad v(x,y,0) = 0,\quad \frac{\partial p}{\partial t}(x,y,0) = 0,\quad \frac{\partial v}{\partial t}(x,y,0) = 0,$$
$$L_1(y) \leqslant x \leqslant L_2(y),\quad 0 \leqslant y \leqslant L_y. \tag{3}$$

2.2.1.1. Rectangular cavity. We consider that $L_1(y) = 0$ and $L_2(y) = L_x$ is a constant (Fig. 1a and b). The pressure source s(t) is placed at y= 0:

$$p(x,0,t) = s(t),\quad 0 < x < L_x,\quad 0 \leqslant t \leqslant T_t. \tag{4}$$

2.2.1.1.1. Rectangular cavity with free walls. We impose a free-wall condition at the other boundaries of the cavity:

$$p(0,y,t) = p(x,L_y,t,) = p(L_x,y,t) = 0,\quad 0 \leqslant x \leqslant L_x,\quad 0 < y \leqslant L_y,\quad 0 \leqslant t \leqslant T_t. \tag{5}$$

2.2.1.1.2. Rectangular cavity with rigid walls. We impose a free-wall condition at $y = L_y$ and a rigid-wall condition at x= 0 and $x = L_x$:

$$p(x,L_y,t) = 0,\quad 0 \leqslant x \leqslant L_x,\quad 0 \leqslant t \leqslant T_t, \tag{6}$$

$$\frac{\partial p}{\partial x}(0,y,t) = \frac{\partial p}{\partial x}(L_x,y,t) = 0,\quad 0 < y \leqslant L_y,\quad 0 \leqslant t \leqslant T_t. \tag{7}$$

2.2.1.2. Trapezoidal cavity with free walls. We consider that $L_1(y) = yL_x/4L_y$ and $L_2(y) = L_x - yL_x/4L_y$ (Fig. 1c). The pressure source s(t) is placed at $y = L_y$ and we impose a free-wall condition at the other boundaries of the cavity:

$$p(x,L_y,t) = s(t),\quad L_x/4 < x < 3L_x/4,\quad 0 \leqslant t \leqslant T_t, \tag{8}$$

$$p(yL_x/4L_y,y,t) = p(x,0,t) = p(L_x - yL_x/4L_y,y,t) = 0,$$
$$0 \leqslant x \leqslant L_x,\quad 0 \leqslant y < L_y,\quad 0 \leqslant t \leqslant T_t. \tag{9}$$

2.2.1.3. Horn cavity with rigid walls. We consider that $L_1(y) = L_x/4\sqrt{y/L_y}$ and $L_2(y) = L_x - L_x/4\sqrt{y/L_y}$ (Fig. 1d). The pressure source s(t) is placed at $y = L_y$. We impose a free-wall condition at y= 0 and a rigid-wall condition at the other boundaries of the cavity:

$$p(x,L_y,t) = s(t),\quad L_x/4 < x < 3L_x/4,\quad 0 \leqslant t \leqslant T_t, \tag{10}$$

$$p(x,0,t) = 0,\quad 0 \leqslant x \leqslant L_x,\quad 0 \leqslant t \leqslant T_t, \tag{11}$$

$$\frac{\partial p}{\partial x}\left(L_x/4\sqrt{y/L_y},y,t\right) = \frac{\partial p}{\partial x}\left(L_x - L_x/4\sqrt{y/L_y},y,t\right) = 0,\quad 0 \leqslant y < L_y,\quad 0 \leqslant t \leqslant T_t. \tag{12}$$

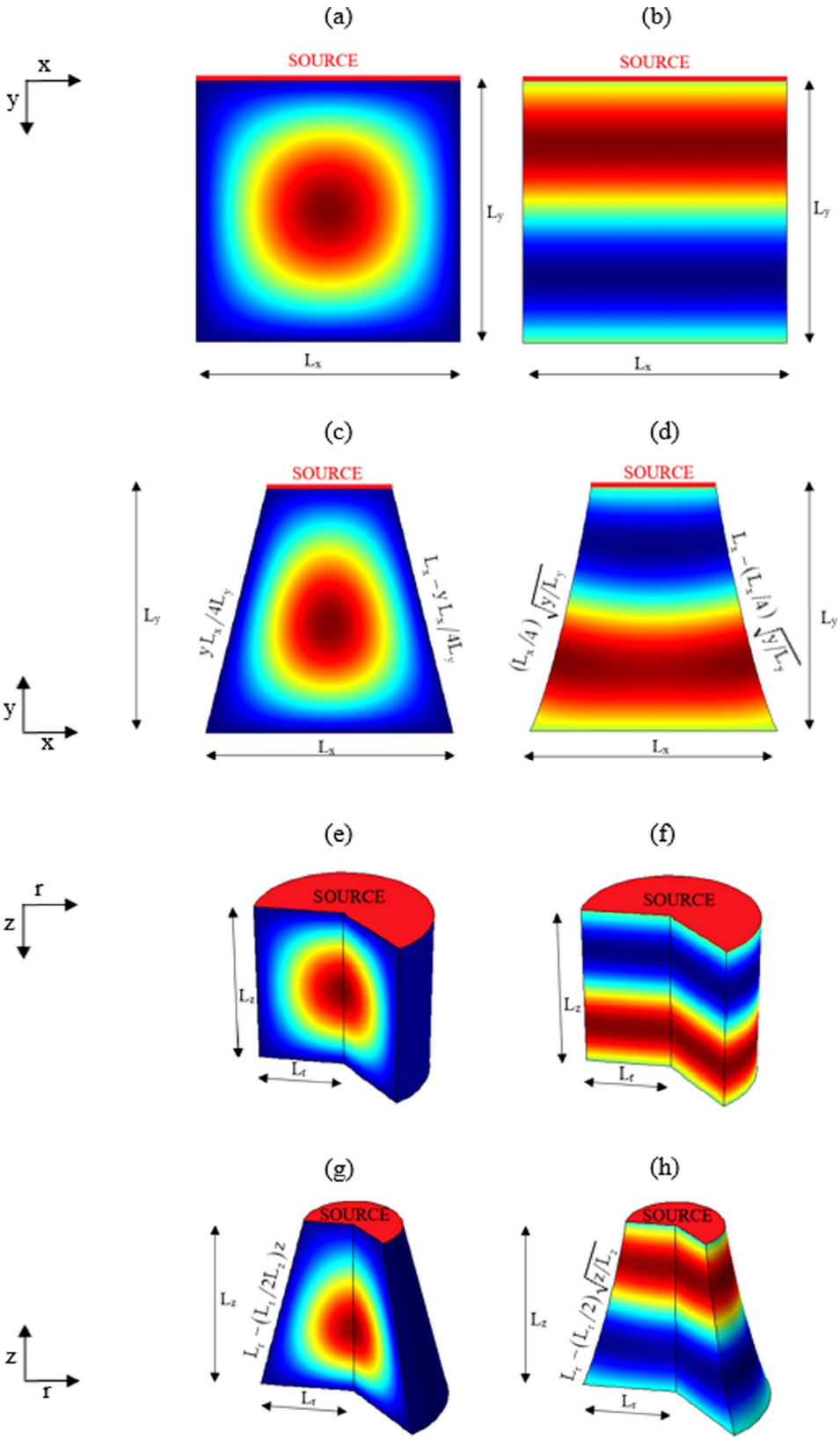

Fig. 1. Schematic representation of the cavities and mode shapes. Two-dimensional resonators: (a) Rectangular cavity with free walls and mode (1, 1); (b) Rectangular cavity with rigid walls and mode (0, 2); (c) Trapezoidal cavity with free walls and mode (1, 1); (d) Horn cavity with rigid walls and mode (0, 2). Three-dimensional resonators: (e) Cylindrical cavity with free walls and mode (1, 1); (f) Cylindrical cavity with rigid walls and mode (0, 2); (g) Truncated cone cavity with free walls and mode (1, 1); (h) Horn cavity with rigid walls and mode (0, 2).

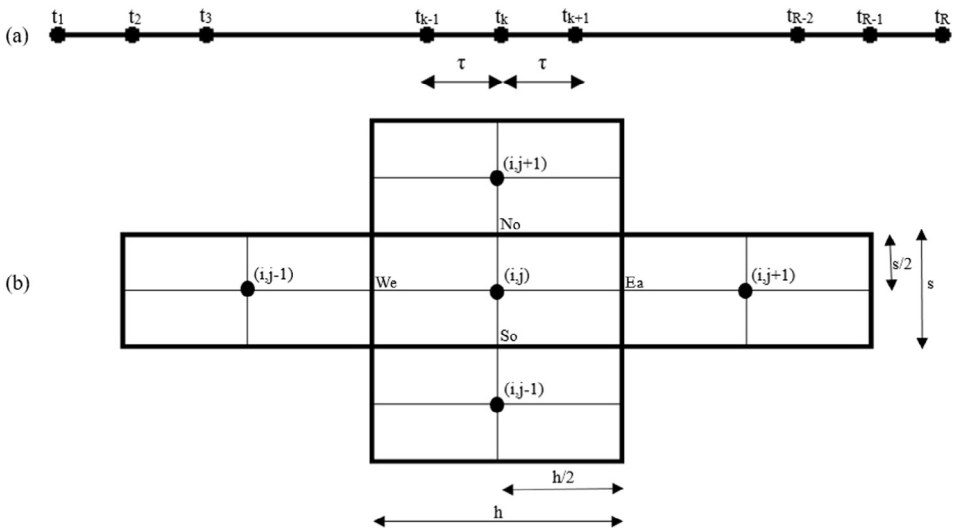

Fig. 2. (a) Finite-difference discretization of the time domain (subscript k). (b) Finite volume discretization of the space domain. Subscript i is valid for the x dimension in Section 2.3.2.1 and for the r dimension in Section 2.3.2.2. Subscript j is valid for the y dimension in Section 2.3.2.1 and for the z dimension in Section 2.3.2.2.

2.2.2. Three-dimensional resonant cavity

We assume a symmetry of the problem around the z-axis in the three-dimensional space (x,y,z) that allows us to reduce the problem and use the cylindrical coordinates (r,z). We consider a cavity of length $L_2(z)$ in the r-direction and L_z in the z-direction. The interaction between the acoustic pressure p(r,z,t) and the volume variation of the bubbles $v(r,z,t) = V(r,z,t) - v_{0g}$ is modeled by the wave equation, Eq. (13), and the Rayleigh-Plesset equation, Eq. (14), written in cylindrical coordinates [3–5]:

$$\frac{\partial^2 p}{\partial r^2} + \frac{1}{r}\frac{\partial p}{\partial r} + \frac{\partial^2 p}{\partial z^2} - \frac{1}{c_{0l}^2}\frac{\partial^2 p}{\partial t^2} = -\rho_{0l} N_g \frac{\partial^2 v}{\partial t^2}, \quad 0 < r < L_2(z), \quad 0 < z < L_z, \quad 0 < t < T_t, \tag{13}$$

$$\frac{\partial^2 v}{\partial t^2} + \delta\omega_{0g}\frac{\partial v}{\partial t} + \omega_{0g}^2 v + \eta\, p = a v^2 + b\left(2v\frac{\partial^2 v}{\partial t^2} + \left(\frac{\partial v}{\partial t}\right)^2\right), \quad 0 \leqslant r \leqslant L_2(z), \quad 0 \leqslant z \leqslant L_z, \quad 0 < t < T_t. \tag{14}$$

The symbols used in this system are identical to the ones used in Eqs. (1) and (2). We also suppose that at the onset of the experiment no wave affects the fluid and the bubbles are at rest:

$$p(r,z,0) = 0, \quad v(r,z,0) = 0, \quad \frac{\partial p}{\partial t}(r,z,0) = 0, \quad \frac{\partial v}{\partial t}(r,z,0) = 0, \quad 0 \leqslant r \leqslant L_2(z), \quad 0 \leqslant z \leqslant L_z. \tag{15}$$

2.2.2.1. Cylindrical cavity. We consider that $L_2(z) = L_r$ is constant (Fig. 1e and f). The pressure source s(t) is placed at z= 0. We use the axial symmetry condition to obtain the three-dimensional solution of the problem:

$$p(r,0,t) = s(t), \quad 0 < r < L_r, \quad 0 \leqslant t \leqslant T_t, \tag{16}$$

$$\frac{\partial p}{\partial r}(0,z,t) = 0, \quad 0 \leqslant z \leqslant L_z, \quad 0 < t \leqslant T_t. \tag{17}$$

2.2.2.1.1. Cylindrical cavity with free walls. We consider a free-wall condition at the other boundaries of the cavity:

$$p(r,L_z,t) = p(L_r,z,t) = 0, \quad 0 \leqslant r \leqslant L_r, \quad 0 < z \leqslant L_z, \quad 0 \leqslant t \leqslant T_t. \tag{18}$$

2.2.2.1.2. Cylindrical cavity with rigid walls. We impose a free-wall condition at $z = L_z$ and a rigid-wall condition at $r = L_r$:

$$p(r,L_z,t) = 0, \quad 0 \leqslant r \leqslant L_r, \quad 0 \leqslant t \leqslant T_t, \tag{19}$$

$$\frac{\partial p(L_r,z,t)}{\partial r} = 0, \quad 0 < z \leqslant L_z, \quad 0 \leqslant t \leqslant T_t. \tag{20}$$

2.2.2.2. Truncated cone with free walls. We consider that $L_2(z) = L_r - zL_r/2L_z$ (Fig. 1g). The pressure source s(t) is placed at $z = L_z$. We impose a free-wall condition at the other boundaries of the cavity:

$$p(r,L_z,t) = s(t), \quad 0 < r < L_r/2, \quad 0 \leqslant t \leqslant T_t, \tag{21}$$

$$p(L_r - zL_r/2L_z,z,t) = p(r,0,t) = 0, \quad 0 \leqslant r \leqslant L_r, \quad 0 < z \leqslant L_z, \quad 0 \leqslant t \leqslant T_t. \tag{22}$$

2.2.2.3. Horn cavity with rigid walls. We consider that $L_2(z) = L_r - L_r/2\sqrt{z/L_z}$ (Fig. 1h). The pressure source s(t) is placed at $z = L_z$ We impose a free-wall condition at z= 0 and a rigid-wall condition at $r = L_r - L_r/2\sqrt{z/L_z}$:

$$p(r,L_z,t) = s(t), \quad 0 < r < L_r/2, \quad 0 \leqslant t \leqslant T_t, \tag{23}$$

$$p(r,0,t) = 0, \quad 0 \leqslant r \leqslant L_r, \quad 0 \leqslant t \leqslant T_t, \tag{24}$$

$$\frac{\partial p(L_r - L_r/2\sqrt{z/L_z},z,t)}{\partial r} = 0, \quad 0 < z \leqslant L_z, \quad 0 \leqslant t \leqslant T_t. \tag{25}$$

2.3. Numerical model

To solve the mathematical problems exposed in Section 2.2, we develop several numerical models that are inspired by the one-dimensional method developed in [34]. The increase of the space dimensions (two and three) and the consideration of new initial and boundary conditions (Dirichlet and Neumann) require specific developments.

2.3.1. Time approximations

A finite-difference technique is developed in the time domain. The total time T_t is divided into R−1 intervals of duration τ. Each time point is denoted by t_k (k= 2,…,R−1) (Fig. 2a). The following equations are used to approximate the time derivatives that appear in Eqs. (1), (2), (13), and (14).

$$\frac{\partial^2 p_k}{\partial t^2} \approx \frac{p_{k+1} - 2p_k + p_{k-1}}{\tau^2}, \quad \frac{\partial^2 v_k}{\partial t^2} \approx \frac{v_{k+1} - 2v_k + v_{k-1}}{\tau^2}, \quad \frac{\partial v_k}{\partial t} \approx \frac{v_k - v_{k-1}}{\tau}, \quad \frac{\partial p_k}{\partial t} \approx \frac{p_k - p_{k-1}}{\tau}. \tag{26}$$

We use these approximations in all the models described in Sections 2.2.1 and 2.2.2. The error is $O(\tau^2)$ for the second-order derivatives and $O(\tau)$ for the first-order derivatives.

2.3.2. Space approximations

We develop a finite-volume model to approximate the space dimensions.

2.3.2.1. Two-dimensional resonant cavity. We divide the cavity in N× M control volumes V_C of dimensions h in the x-direction and s in the y-direction. We denote the central point of each V_C by x_i (i= 1,…,N) and y_j (j= 1,…,M). The differential equations are integrated over each V_C. The following equations approximate the integrals that come from Eqs. (1) and (2), where Ea, We, No, and So indicate the East, West, North and South sides of V_C, respectively, and K is a generic constant (Fig. 2b):

$$\int_{V_C}\frac{\partial^2 p_i}{\partial x^2}dv=\int_{So}^{No}\int_{We}^{Ea}\frac{\partial^2 p_i}{\partial x^2}dxdy=s\left(\frac{\partial p}{\partial x}\bigg|_{Ea}-\frac{\partial p}{\partial x}\bigg|_{We}\right)\approx s\left(\frac{p_{i+1}-p_i}{h}-\frac{p_i-p_{i-1}}{h}\right)=s\left(\frac{p_{i+1}-2p_i+p_{i-1}}{h}\right),\tag{27}$$

$$\int_{V_C}\frac{\partial^2 p_i}{\partial y^2}dv=\int_{We}^{Ea}\int_{So}^{No}\frac{\partial^2 p_i}{\partial y^2}dxdy=h\left(\frac{\partial p}{\partial y}\bigg|_{No}-\frac{\partial p}{\partial y}\bigg|_{So}\right)\approx h\left(\frac{p_{j+1}-p_j}{s}-\frac{p_j-p_{j-1}}{s}\right)=h\left(\frac{p_{j+1}-2p_j+p_{j-1}}{s}\right),\tag{28}$$

$$\int_{V_C}K\,dv=\int_{We}^{Ea}\int_{So}^{No}K\,dxdy\approx Khs.\tag{29}$$

The error in theses equations is O(h,s) .

2.3.2.2. Three-dimensional resonant cavity. We divide the cavity in N× M control volumes V_C of dimensions h in the r-direction and s in the z-direction. We denote the central point of each control volume by r_i (i= 1,…,N) and by z_j (j= 1,…,M). The differential equations are integrated over each V_C. The following equations are used to approximate the integrals that come from Eqs. (13) and (14), where Ea, We, No, and So indicate the East, West, North, and South sides of V_C, respectively, and K is a generic constant (Fig. 2b):

$$\begin{aligned}\int_{V_C}r\frac{\partial^2 p_i}{\partial r^2}dv+\int_{V_C}r\frac{1}{r}\frac{\partial p_i}{\partial r}dv&=\int_{So}^{No}\int_{We}^{Ea}r\frac{\partial^2 p_i}{\partial r^2}dzdr+\int_{So}^{No}\int_{We}^{Ea}\frac{\partial p_i}{\partial r}dzdr\\&=s\left(r\frac{\partial p}{\partial r}\bigg|_{We}^{Ea}-\int_{We}^{Ea}\frac{\partial p}{\partial r}dr+\int_{We}^{Ea}\frac{\partial p}{\partial r}dr\right)\\&=sr\frac{\partial p}{\partial r}\bigg|_{We}^{Ea}=shi\left(\frac{p_{i+1}-p_i}{h}\right)-sh(i-1)\left(\frac{p_i-p_{i-1}}{h}\right)\\&=isp_{i+1}+(1-2i)sp_i+(i-1)sp_{i-1},\end{aligned}\tag{30}$$

$$\int_{V_C}\frac{\partial^2 p_j}{\partial z^2}dv=\int_{We}^{Ea}\int_{So}^{No}\frac{\partial^2 p_j}{\partial z^2}rdzdr=\left(\frac{\partial p}{\partial z}\bigg|_{No}-\frac{\partial p}{\partial z}\bigg|_{So}\right)\int_{We}^{Ea}rdr\approx\frac{h^2}{2}(2i-1)\left(\frac{p_{j+1}-p_j}{s}-\frac{p_j-p_{j-1}}{s}\right)=\frac{h^2}{2}(2i-1)\left(\frac{p_{j+1}-2p_j+p_{j-1}}{s}\right),\tag{31}$$

$$\int_{V_C}K\,dv=\int_{We}^{Ea}\int_{So}^{No}K\,rdzdr=\frac{h^2}{2}(2i-1)(Kz|_{So}^{No})=\frac{Ksh^2}{2}(2i-1).\tag{32}$$

The error in theses equations is O(h,s) .

2.3.3. Discretized equations

The space and time approximations given in Sections 2.3.1 and 2.3.2 are applied to the differential equations of Section 2.2, leading to an explicit numerical scheme in both the two and the three-dimensional configurations.

2.3.3.1. Two-dimensional case. Applying the approximations given above, Eqs. (26)–(29), to Eqs. (1) and (2) we obtain the following equations for any control volume (i,j) and any t_k (k= 2,…,R−1):

$$\begin{aligned}\frac{h^2s^2}{c_{0l}^2}p_{i,j,k+1}-\rho_{0l}N_gh^2s^2v_{i,j,k+1}&=\tau^2s^2(Ap_{i+1,j,k}+Bp_{i-1,j,k})\\&+\tau^2h^2(Cp_{i,j+1,k}+Dp_{i,j-1,k})\\&+(-E\tau^2s^2-F\tau^2h^2+\frac{2h^2s^2}{c_{0l}^2})p_{i,j,k}-\frac{h^2s^2}{c_{0l}^2}p_{i,j,k-1}\\&+\rho_{0l}N_gh^2s^2(-2v_{i,j,k}+v_{i,j,k-1}),\end{aligned}\tag{33}$$

$$\begin{aligned}(2bv_{i,j,k}-1)v_{i,j,k+1}&=(-2+\delta\tau\omega_{0g}+\tau^2\omega_{0g}^2-\tau^2av_{i,j,k}+3bv_{i,j,k})v_{i,j,k}\\&+(1-\delta\tau\omega_{0g}-bv_{i,j,k-1})v_{i,j,k-1}+\eta\tau^2p_{i,j,k},\end{aligned}\tag{34}$$

where A, B, C, D, E, F in Eq. (33) take different values that depends on the geometry of the cavity and whether V_C is on the boundary of the cavity or not. Equation (34) is common to all geometries and V_C.

2.3.3.2. Three-dimensional case. Applying the approximations given above, Eqs. (26), (30–32), to Eqs. (13) and (14) we obtain the following equation for any control volume (i,j) and any t_k (k= 2,…,R−1):

$$\begin{aligned}\frac{h^2s^2(2i-1)}{2c_{0l}^2}p_{i,j,k+1}-\frac{\rho_{0l}N_gh^2s^2(2i-1)}{2}v_{i,j,k+1}&=\tau^2s^2(Ap_{i+1,j,k}+Bp_{i-1,j,k})\\&+\frac{\tau^2h^2}{2}(Cp_{i,j+1,k}+Dp_{i,j-1,k})\\&+\left(-E\tau^2s^2-\frac{F\tau^2h^2}{2}+\frac{h^2s^2(2i-1)}{c_{0l}^2}\right)p_{i,j,k}\\&-\frac{h^2s^2(2i-1)}{2c_{0l}^2}p_{i,j,k-1}+\frac{\rho_{0l}N_gh^2s^2(2i-1)}{2}\\&(-2v_{i,j,k}+v_{i,j,k-1}),\end{aligned}\tag{35}$$

where A, B, C, D, E, F in Eq. (35) take different values that depends on the geometry of the cavity and whether V_C is on the boundary of the cavity or not. Eq. (34) remains unchanged.

2.3.4. Specific cavities

All the resonant cavities used in Section 3 require a specific numerical development.

2.3.4.1. Two-dimensional cavities

2.3.4.1.1. Rectangular cavity. The equations of Table 1 and Eq. (34) allows us to solve the acoustic pressure and volume variation in the whole rectangular cavity in each time step. The valid values for the rectangular cavity are the parameters of Table 1. Note that the values appearing in bold font in column E are only valid with free walls (Section 2.2.1.1.1), whereas italic font is used with rigid walls (Section 2.2.1.1.2).

2.3.4.1.2. Trapezoidal cavity with free walls. The system formed by the equations of Table 2 and Eq. (34) allows us to solve the total pressure and volume variation in the whole cavity in each time step.

2.3.4.1.3. Horn cavity with rigid walls. The system formed by the equations of Table 3 and Eq. (34) allows us to solve the total pressure

Table 1
Parameters for the rectangular cavity in Eq. (33).

	A	B	C	D	E		F
i= 1 ,j= 1	1	0	1	$2s(t)/p_{i,j-1,k}$	**3**	*1*	3
i= 1 ,j= M	1	0	0	1	**3**	*1*	3
i= 1 ,j= (2,…,M−1)	1	0	1	1	**3**	*1*	2
i= N, j= 1	0	1	1	$2s(t)/p_{i,j-1,k}$	**3**	*1*	3
i= N, j= M	0	1	0	1	**3**	*1*	3
i= N,j = (2,...,M−1)	0	1	1	1	**3**	*1*	2
i= (2,...,N−1),j = 1	1	1	1	$2s(t)/p_{i,j-1,k}$	2		3
i= (2,...,N−1),j = M	1	1	0	1	2		3
i= (2,...,N−1),j = (2,...,M−1)	1	1	1	1	2		2

Table 2
Parameters for the trapezoidal cavity in Eq. (33).

	A	B	C	D	E	F
i= 1 , j= 1	1	0	1	0	3	3
i<N/4 , j= 4iM/N	1	0	0	1	3	3
i= 1, 1 < j< 4iM/N i⩽ N/4, 4(i−1)M/ N< j< 4iM/N	1	0	1	1	3	2
1 < i< N−1 , j= 1	1	1	1	0	2	3
i= N/4 , j= M	1	0	$2s(t)/p_{i,j-1,k}$	1	3	3
i= 3N/4 + 1 , j= M	0	1	$2s(t)/p_{i,j-1,k}$	1	3	3
N/4 < i< 3N/4 + 1 , j= M	1	1	$2s(t)/p_{i,j-1,k}$	1	2	3
i⩽ N/4,j < 4(N−i)M/Ni⩾ 3N/4 + 1,j < 4(N−i)M/N N/4 < i< 3N/4 + 1, (j= 2,…,M−1)	1	1	1	1	2	2
i⩾ 3N/4 + 1, 4(N−i)M/ N< j< 4(N+ 1−i)M/N i= N, 1 < j< 4(N+ 1−i)M/N	0	1	1	1	3	2
i>3N/4 + 1 , j= 4(N+ 1−i)M/N	0	1	0	1	3	3
i= N, j= 1	0	1	1	0	3	3

and volume variation in the whole cavity in each time step.

2.3.4.2. Three-dimensional resonant cavity

2.3.4.2.1. Cylindrical cavity. The system formed by the equations of Table 4 and Eq. (34) allows us to solve the total pressure and volume variation in the whole cylindrical cavity in each time step. The valid values for the cylindrical cavity are the parameters of Table 4. Note that the values appearing in bold font in column E are only valid with free walls (Section 2.2.2.1.1), whereas italic font is used with rigid walls (Section 2.2.2.1.2).

2.3.4.2.2. Truncated cone with free walls. The system formed by the equations of Table 5 and Eq. (34) allows us to solve the total pressure and volume variation in the whole cavity in each time step.

2.3.4.2.3. Horn cavity with rigid walls. The system formed by the equations of Table 6 and Eq. (34) allows us to solve the total pressure and volume variation in the whole cavity in each time step.

3. Results

We show here the results obtained from the application of the models proposed in Section 2. We consider the following data for the liquid (water), $c_{0l} = 1500$ m/s, $\rho_{0l} = 1000$ kg/m^3, $\nu_l = 1.43 \times 10^{-6}$ m^2/s, and for the gas (air), $c_{0g} = 340$ m/s, $\rho_{0g} = 1.29$ kg/m^3, $\gamma_g = 1.4$.

Section 3.1 presents the results obtained with three models applied to two-dimensional resonant cavities: rectangular (Section 3.1.1), trapezoidal (Section 3.1.2), and horn (Section 3.1.3) cavities. Section 3.2 provides the results obtained with three models applied to three-dimensional resonant cavities: cylindrical (Section 3.2.1), truncated cone (Section 3.2.2), and horn (Section 3.2.3) cavities.

Two different kinds of source are used: one-frequency excitation (Sections 3.1.1.1.1,3.1.1.2.1,3.1.2.1,3.1.3.1,3.2.1.1.1,3.2.1.2.1,3.2.2.1, and 3.2.3.1) and two-frequency excitation (Sections 3.1.1.1.2,3.1.1.2.2,3.1.2.2,3.1.3.2,3.2.1.1.2,3.2.1.2.2,3.2.2.2, and 3.2.3.2). In the first case we use bubbles of radius $R_{0g} = 4.5 \times 10^{-6}$ m at the density $N_g = 2 \times 10^{11}$ m^{-3}, whereas in the second case we use bubbles of radius $R_{0g} = 2.5 \times 10^{-6}$ m at the density $N_g = 5 \times 10^{11}$ m^{-3}. All the experiments last the required time to ensure that the steady state is reached.

3.1. Two-dimensional resonant cavity

The dimensions of the two-dimensional cavities are $L_x = 0.0035$ m and $L_y = 0.0035$ m. We use N× M= 100 × 100 V_C.

3.1.1. Rectangular cavity

The source s(t) is situated at the central area of the wall and expands over 10% of this dimension (Fig. 3a). On the remaining 90% of the wall the source grows as $s(t)\left(\frac{\alpha+i}{GN+1}\right)^6$ for i⩽ GN and $s(t)\left(\frac{\beta-i}{GN+1}\right)^6$ for i>(G+ 0.1)N, where α = 0, β = N+ 1, and G= 0.45.

3.1.1.1. Rectangular cavity with free walls

3.1.1.1.1. One-frequency experiment. We consider a continuous pressure source $s(t) = p_0 \sin(\omega t)$ of amplitude $p_0 = 7$ kPa and frequency f, where ω = 2πf. The total time of the experiment is $T_t = 400$ T, where the period is T= 1/f. We choose the frequency that matches the mode (1,1) of the cavity (Fig. 1a). We use the method given in Ref. [4] to obtain the sound speed of the bubbly medium. We use a finite-element based commercial software [40] to calculate a first approximation of the resonance frequency. This first frequency is not the real resonance neither the one corresponding to our model since both geometrical approximations are different. We calculate a second resonance frequency with our model doing a frequency sweep close to the first approximation. We do this in linear regime with a source amplitude of $p_0 = 1$ Pa. We take the frequency with higher maximum pressure, f= 2.0247 × 10^5 Hz. We carry out this process in all the cases presented in this paper.

The sound speed for this medium and this frequency is c= 1001.7 m/s. We use 400 temporal steps per period. Fig. 4a, b, c show the amplitude of the first three harmonics obtained after applying a Fast Fourier Transform (FFT) in the whole resonator. We obtain the maximum pressure amplitude for the fundamental, the second, and the third harmonics: $p_f = 22.495$ kPa (321.4% of p_0), $p_{2f} = 11.002$ kPa (157.2% of p_0), $p_{3f} = 6.579$ kPa (94.0% of p_0), respectively.

3.1.1.1.2. Two-frequency experiment. We use a continuous pressure

Table 3
Parameters for the horn cavity in Eq. (33).

	A	B	C	D	E	F
i= 1 , j= 1	1	0	0	0	1	2
i= 2 , j= 1	1	1	0	0	2	2
(i= 3,…,N−2),j = 1	1	1	1	0	2	3
i⩽ N/4, j < 4^2(i−1)^{2}M/N^{2}i⩾ 3N/4,j < 4^2(N−i)^{2}M/N^{2}N/4 < i< 3N/4 + 1 , j= 2,….,M−1	1	1	1	1	2	2
i⩽ N/4, 4^2(i−1)^{2}M/N^2 < j< 4^2i^2M/N^2	1	0	1	1	1	2
i⩽ N/4 , j= 4^2i^2M/N^2	1	0	0	1	1	1
i= N/4 , j= M	1	0	$2s(t)/p_{i,j+1,k}$	1	1	3
i⩾ 3N/4 + 1, 4^2(N−i)^{2}M/N^2 < j< 4^2(N+ 1−i)^{2}M/N^2	0	1	1	1	1	2
i= 3N/4 + 1 , j= M	0	1	$2s(t)/p_{i,j+1,k}$	1	1	3
i>3N/4 + 1 , j= 4^2i^2M/N^2	0	1	0	1	1	1
N/4 < i< 3N/4 + 1 , j= M	1	1	$2s(t)/p_{i,j+1,k}$	1	2	3
i= N−1 , j= 1	1	1	0	0	2	2
i= N, j= 1	0	1	0	0	1	2

Table 4
Parameters for the cylindrical cavity in Eq. (35).

	A	B	C	D	E		F
i= 1 ,j= 1	i	0	2i−1	$2(2i-1)s(t)/p_{i,j-1,k}$	i		3(2i−1)
i= 1 ,j= M	i	0	0	2i−1	i		3(2i−1)
i= 1 ,j= (2,…,M−1)	i	0	2i−1	2i−1	i		2(2i−1)
i= N, j= 1	0	i−1	2i−1	$2(2i-1)s(t)/p_{i,j-1,k}$	**3i−1**	*i−1*	3(2i−1)
i= N, j= M	0	i−1	0	2i−1	**3i−1**	*i−1*	3(2i−1)
i= N,j = (2,...,M−1)	0	i−1	2i−1	2i−1	**3i−1**	*i−1*	2(2i−1)
i= (2,…,N−1),j = 1	i	i−1	2i−1	$2(2i-1)s(t)/p_{i,j-1,k}$	2i−1		3(2i−1)
i= (2,…,N−1),j = M	i	i−1	0	2i−1	2i−1		3(2i−1)
i= (2,…,N−1),j = (2,…,M−1)	i	i−1	2i−1	2i−1	2i−1		2(2i−1)

source $s(t) = p_0\sin(\omega_1 t) + p_0\sin(\omega_2 t)$ of amplitude $p_0 = 12$ kPa and frequencies f_1 and f_2, where $\omega_1 = 2\pi f_1$ and $\omega_2 = 2\pi f_2$. The total time is $T_t = 400T_d$, where $T_d = 1/f_d$ is the period at the difference frequency $f_d = f_2 - f_1$. We take $f_1 = 6 \times 10^5$ Hz and $f_2 = 8.4666 \times 10^5$ Hz so that $f_d = 2.4666 \times 10^5$ Hz and we consider the mode (1,1). The sound speed for this medium and this frequency is $c_d = 1220.4$ m/s. We consider 400 temporal intervals per period. Fig. 4d shows the amplitude of the difference frequency in the whole resonator obtained by FFT. The maximum amplitude at f_d is $p_d = 3.032$ kPa (25.3% of p_0).

It must be noted that, since the bubbly liquid is dispersive, the primary frequencies f_1 and f_2 are chosen so that both of them are not very close to the bubble resonance, $f_{0g} = 1.347$ MHz, i) to avoid the peak of attenuation at frequencies close to the bubble resonance, ii) to work in a frequency range that allows the nonlinearity of the medium to be high enough to obtain the desired nonlinear effects. Assuming this commitment between nonlinearity and attenuation, we set the frequencies such that the difference frequency component is resonant in the cavity. This procedure is followed for all the two-frequency experiments presented in this paper.

3.1.1.2. Rectangular cavity with rigid walls

3.1.1.2.1. One-frequency experiment. We consider a continuous pressure source $s(t) = p_0\sin(\omega t)$ of amplitude $p_0 = 18$ kPa and frequency f, where $\omega = 2\pi f$. The total time of the experiment is $T_t = 400$ T, where the period is T= 1/f. We choose the frequency f= 2.7992×10^5 Hz that matches the mode (0,2) of this cavity (Fig. 1b). The sound speed for this medium and this frequency is c= 980.9 m/s. We use 400 temporal steps per period. Fig. 5a, b, c show the amplitude of the first three harmonics obtained after applying a FFT in the whole resonator. We obtain the maximum pressure amplitude for the fundamental, the second, and the third harmonics: $p_f = 31.678$ kPa (176.0% of p_0), $p_{2f} = 9.741$ kPa (54.1% of p_0), $p_{3f} = 2.988$ kPa (16.6% of p_0), respectively.

3.1.1.2.2. Two-frequency experiment. We use a continuous pressure source $s(t) = p_0\sin(\omega_1 t) + p_0\sin(\omega_2 t)$ of amplitude $p_0 = 9$ kPa and frequencies f_1 and f_2, where $\omega_1 = 2\pi f_1$ and $\omega_2 = 2\pi f_2$. The total time is $T_t = 400T_d$ where $T_d = 1/f_d$ is the period at the difference frequency $f_d = f_2 - f_1$. We take $f_1 = 6 \times 10^5$ Hz and $f_2 = 9.4646 \times 10^5$ Hz so that $f_d = 3.4646 \times 10^5$ Hz and we consider the mode (0,2). The sound speed for this medium and this frequency is $c_d = 1213.3$ m/s. We take 400 temporal intervals per period. Fig. 5d shows the amplitude of the difference frequency in the whole resonator obtained by FFT. The maximum amplitude at f_d is $p_d = 1.464$ kPa (16.3% of p_0).

3.1.2. Trapezoidal cavity with free walls

The source s(t) is situated at the central area of the wall and expands over 20% of this dimension (Fig. 3a). On the remaining 80% of the wall the source grows as $s(t)\left(\frac{\alpha+i}{GN+1}\right)^6$ for N/4 < i⩽ N/4 + GN and $s(t)\left(\frac{\beta-i}{GN+1}\right)^6$ for N/4 + (G+ 0.1) N< i⩽ 3N/4, where $\alpha = -N/4$, $\beta = 3N/4 + 1$, and G= 0.2 .

3.1.2.1. One-frequency experiment. We consider a continuous pressure source $s(t) = p_0\sin(\omega t)$ of amplitude $p_0 = 16$ kPa and frequency f, where $\omega = 2\pi f$. The total time of the experiment is $T_t = 400T$, where the period is T= 1/f. We choose the frequency f= 2.3726×10^5 Hz that matches the mode (1,1) of this cavity (Fig. 1c). The sound speed for this medium and this frequency is c= 993.74 m/s. We use 400 temporal steps per period. Fig. 6a, b, c show the amplitude of the first three harmonics obtained after applying a FFT in the whole resonator. We obtain the maximum pressure amplitude for the fundamental, the second, and the third harmonics: $p_f = 30.612$ kPa (191.3% of p_0), $p_{2f} = 11.301$ kPa (70.6% of p_0), $p_{3f} = 4.306$ kPa (26.9% of p_0), respectively.

3.1.2.2. Two-frequency experiment. We use a continue pressure source $s(t) = p_0\sin(\omega_1 t) + p_0\sin(\omega_2 t)$ of amplitude $p_0 = 12$ kPa and frequencies f_1

Table 5
Parameters for the truncated cone cavity with free walls in Eq. (35).

	A	B	C	D	E	F
i= 1 ,j= 1	i	0	2i−1	0	i	3(2i−1)
i= 1 ,j= M	i	0	$2(2i-1)s(t)/p_{i,j+1,k}$	2i−1	i	3(2i−1)
i= 1 ,j= (2,…,M−1)	i	0	2i−1	2i−1	i	2(2i−1)
1 < i< N−1 ,j= 1	i	i−1	2i−1	0	2i−1	3(2i−1)
1 < i< N/2 ,j= M	i	i−1	$2(2i-1)s(t)/p_{i,j+1,k}$	2i−1	2i−1	3(2i−1)
i= N/2 ,j= M	0	i−1	$2(2i-1)s(t)/p_{i,j+1,k}$	2i−1	3i−1	3(2i−1)
i>N/2,j = 2(N+ 1−i)M/N	0	i−1	0	2i−1	3i−1	3(2i−1)
i>N/2,2(N−i)M/ N< j< 2(N+ 1−i)M/Ni = N,1 < j = 4M/N	0	i−1	2i−1	2i−1	3i−1	2(2i−1)
i= N,j = 1	0	i−1	0	2i−1	3i−1	3(2i−1)
i<N/2, j = (2,…,M−1) i ⩾ N/2,j < 2(N−i)M/N	i	i−1	2i−1	2i−1	2i−1	2(2i−1)

Table 6
Parameters for the horn cavity with free walls in Eq. (35).

	A	B	C	D	E	F
i= 1 ,j= 1	i	0	2i−1	0	i	3(2i−1)
i= 1 ,j= M	i	0	$2(2i-1)s(t)/p_{i,j+1,k}$	2i−1	i	3(2i−1)
i= 1 ,j= (2,…,M−1)	i	0	2i−1	2i−1	i	2(2i−1)
1 < i< N−2 ,j= 1	i	i−1	2i−1	0	2i−1	3(2i−1)
1 < i< N/2 ,j= M	i	i−1	$2(2i-1)s(t)/p_{i,j+1,k}$	2i−1	2i−1	3(2i−1)
i= N/2 ,j= M	0	i−1	$2(2i-1)s(t)/p_{i,j+1,k}$	2i−1	i−1	3(2i−1)
$i>N/2, j = 4(N+1-i)^2M/N^2$	0	i−1	0	2i−1	i−1	2i−1
$i>N/2,\ 4(N-i)^2M/N^2 < j< 4(N+1-i)^2M/N^2$	0	i−1	2i−1	2i−1	i−1	2(2i−1)
i= N,j = 1	0	i−1	0	2i−1	i−1	2(2i−1)
$i<N/2, j = (2,\ldots,M-1)\quad i\geqslant N/2, j < 4(N-i)^2M/N^2$	i	i−1	2i−1	2i−1	2i−1	2(2i−1)

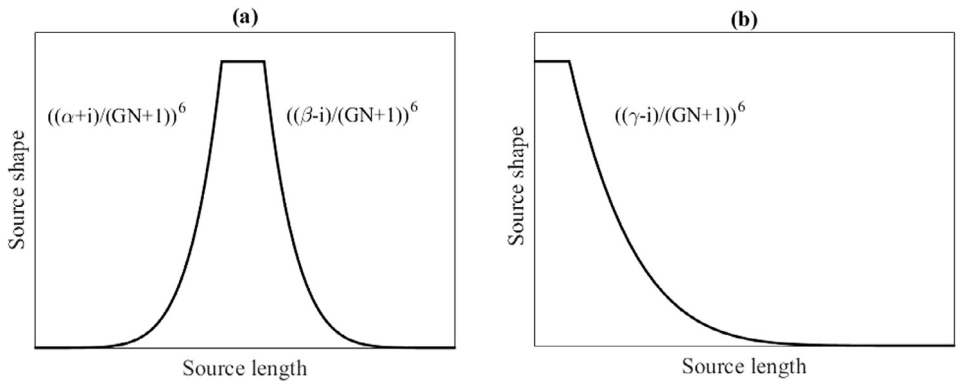

Fig. 3. Source shape. (a) Two-dimensional source. (b) Three-dimensional source with axial symmetry.

and f_2, where $\omega_1 = 2\pi f_1$ and $\omega_2 = 2\pi f_2$. The total time is $T_t = 400T_d$ where $T_d = 1/f_d$ is the period at the difference frequency $f_d = f_2 - f_1$. We take $f_1 = 5 \times 10^5$ Hz and $f_2 = 7.9082 \times 10^5$ Hz so that $f_d = 2.90820 \times 10^5$ Hz and we consider the mode (1,1). The sound speed for this medium and this frequency is $c_d = 1217.6$ m/s. We take 400 temporal intervals per period. Fig. 6d shows the amplitude of the difference frequency in the whole resonator obtained by FFT. The maximum amplitude at f_d is $p_d = 2.507$ kPa (20.9% of p_0).

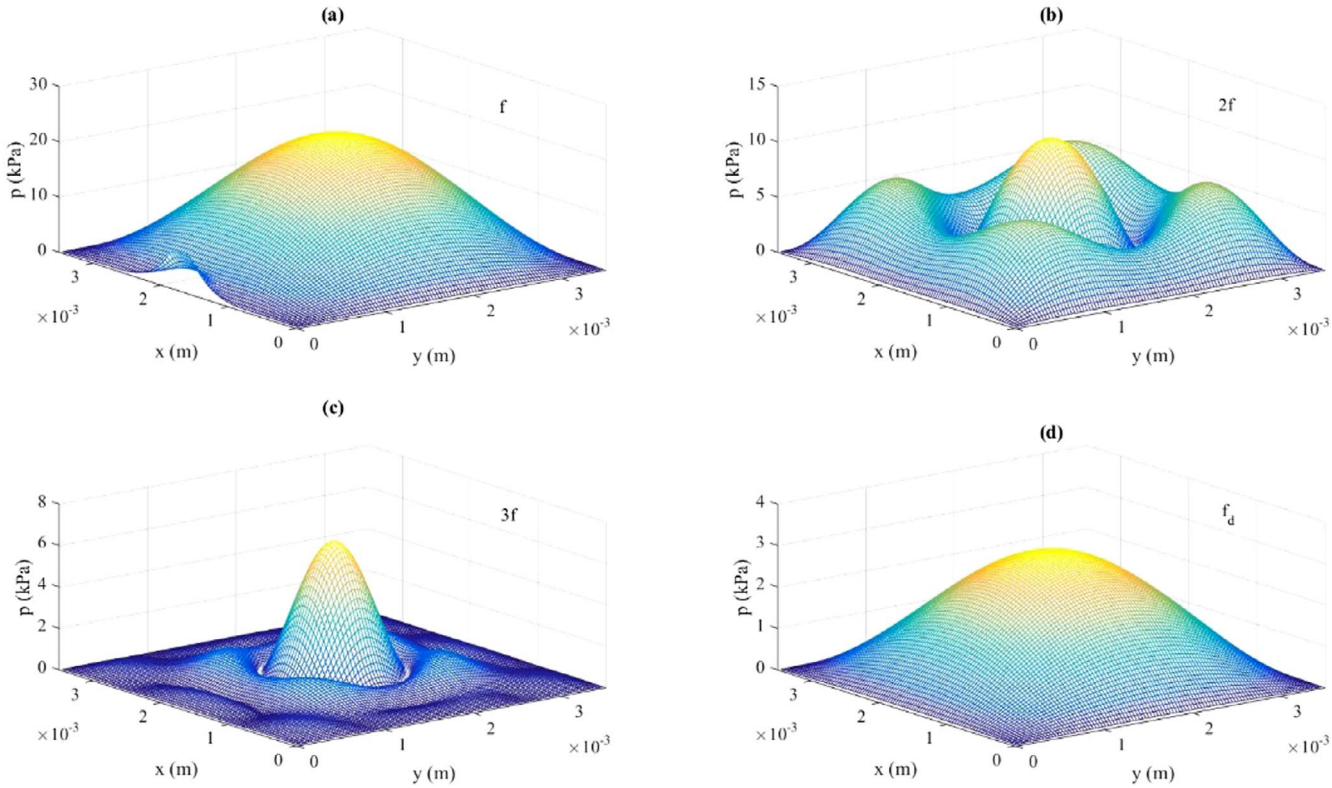

Fig. 4. Distribution of frequencies. Two-dimensional rectangular cavity with free walls. (a) Fundamental frequency. (b) 2nd harmonic. (c) 3rd harmonic. (d) Difference frequency.

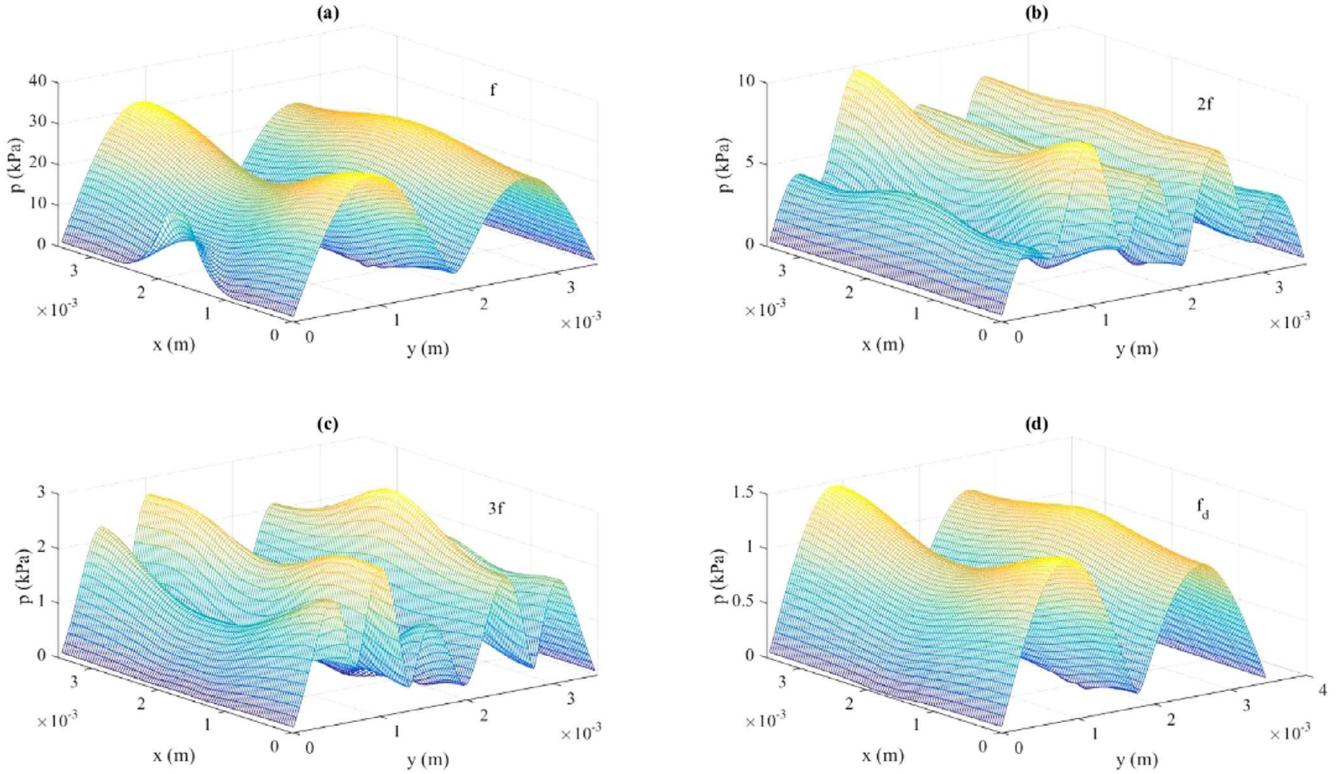

Fig. 5. Distribution of frequencies. Two-dimensional rectangular cavity with rigid walls. (a) Fundamental frequency. (b) 2nd harmonic. (c) 3rd harmonic. (d) Difference frequency.

3.1.3. Horn cavity with rigid walls

The source is situated like in Section 3.1.2.

3.1.3.1. One-frequency experiment. We consider a continuous pressure source $s(t) = p_0 \sin(\omega t)$ of amplitude $p_0 = 19$ kPa and frequency f, where $\omega = 2\pi f$. The total time of the experiment is $T_t = 400\,T$, where the period is $T = 1/f$. We choose the frequency $f = 2.7927 \times 10^5$ Hz that matches the mode (0,2) of this cavity (Fig. 1d). The sound speed for this medium and this frequency is c= 981.1 m/s. We use 400 temporal steps per period. Fig. 7a, b, c show the amplitude of the first three harmonics

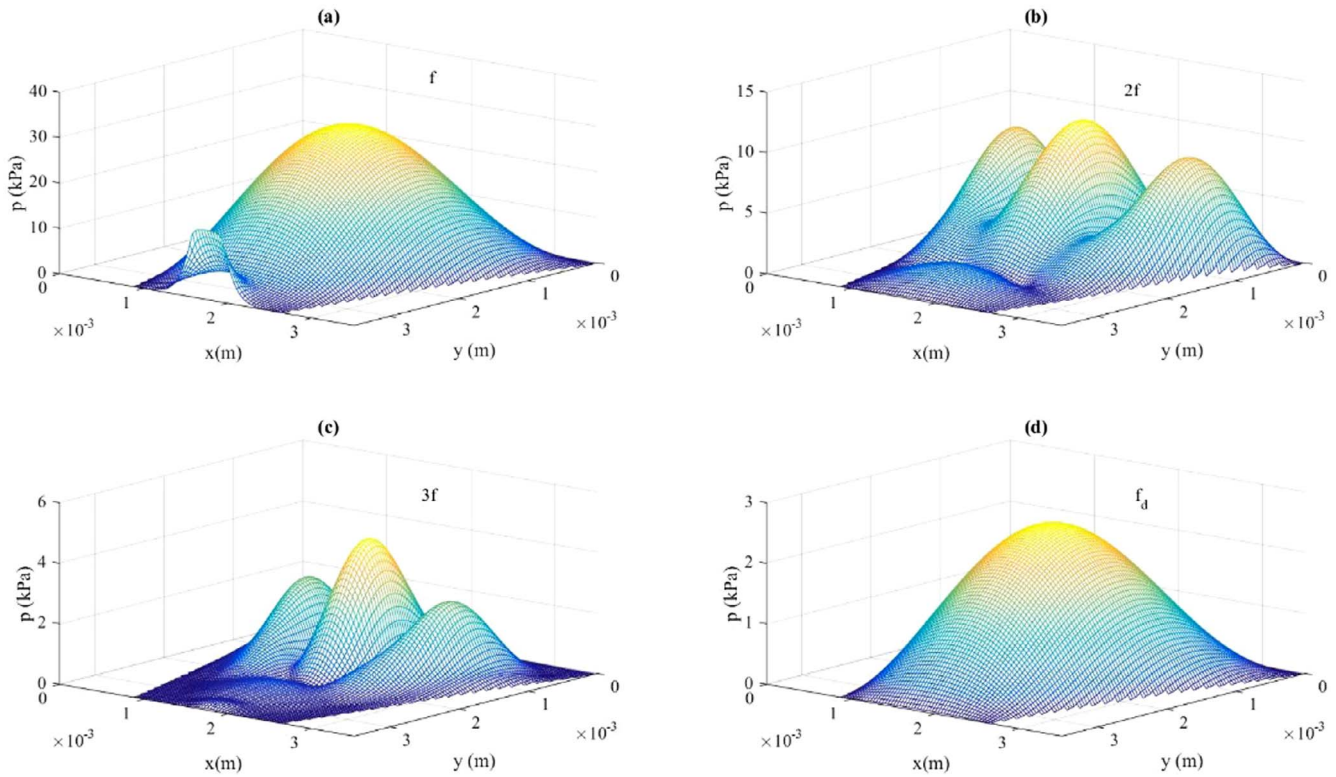

Fig. 6. Distribution of frequencies. Two-dimensional trapezoidal cavity with free walls. (a) Fundamental frequency. (b) 2nd harmonic. (c) 3rd harmonic. (d) Difference frequency.

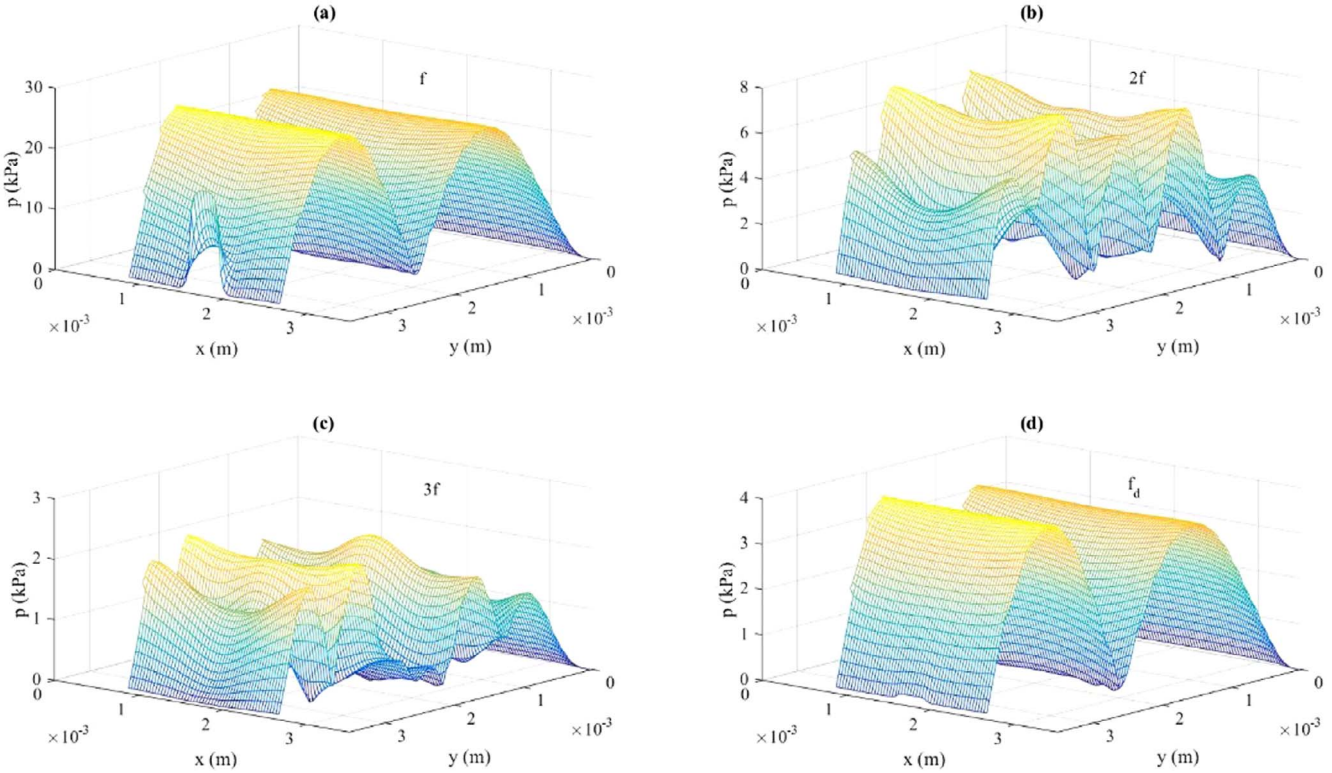

Fig. 7. Distribution of frequencies. Two-dimensional horn cavity with rigid walls. (a) Fundamental frequency. (b) 2nd harmonic. (c) 3rd harmonic. (d) Difference frequency.

obtained after applying a FFT in the whole resonator. We obtain the maximum pressure amplitude for the fundamental, the second, and the third harmonics: $p_f = 26.539$ kPa (139.7% of p_0), $p_{2f} = 7.820$ kPa (41.2% of p_0), $p_{3f} = 2.279$ kPa (12.0% of p_0), respectively.

3.1.3.2. Two-frequency experiment. We use a continuous pressure source $s(t) = p_0\sin(\omega_1 t) + p_0\sin(\omega_2 t)$ of amplitude $p_0 = 12$ kPa and frequencies f_1 and f_2, where $\omega_1 = 2\pi f_1$ and $\omega_2 = 2\pi f_2$. The total time is $T_t = 400T_d$ where $T_d = 1/f_d$ is the period at the difference frequency $f_d = f_2 - f_1$. We take $f_1 = 5 \times 10^5$ Hz and $f_2 = 8.4543 \times 10^5$ Hz so that $f_d = 3.4543 \times 10^5$ Hz and we consider the mode (0,2). The sound speed for this medium and this frequency is $c_d = 1213.4$ m/s. We take 400 temporal intervals per period. Fig. 7d shows the amplitude of the difference frequency in the whole resonator obtained by FFT. The maximum amplitude at f_d is $p_d = 3.936$ kPa (32.8% of p_0).

3.2. Three-dimensional resonant cavity

The dimensions of the three-dimensional cavities are $L_r = 0.00175$ m and $L_z = 0.0035$ m. We use N× M= 50 × 100 V_C.

3.2.1. Cylindrical cavity

The source s(t) takes 10% of the wall (Fig. 3b). On the remaining 90% of the wall the source grows as $s(t)\left(\frac{\gamma - i}{GN + 1}\right)^6$ for i>N−GN, where γ = N+ 1 and G= 0.9 .

3.2.1.1. Cylindrical cavity with free walls

3.2.1.1.1. One-frequency experiment. We consider a continuous pressure source $s(t) = p_0\sin(\omega t)$ of amplitude $p_0 = 20$ kPa and frequency f, where $\omega = 2\pi f$. The total time of the experiment is $T_t = 400$ T where the period is T= 1/f. We choose the frequency f= 2.58×10^5 Hz that matches the mode (1,1) of this cavity (Fig. 1e). The sound speed for this medium and this frequency is c= 987.63 m/s .We take 400 temporal steps per period. Fig. 8a, b, c show the amplitude of the first three harmonics obtained after applying a FFT in the plane that defines the axisymmetric. We obtain the maximum pressure amplitude for the fundamental, the second, and the third harmonics: $p_f = 29.310$ kPa (146.6% of p_0), $p_{2f} = 5.7054$ kPa (28.6% of p_0), $p_{3f} = 0.857$ kPa (4.3% of p_0), respectively.

3.2.1.1.2. Two-frequency experiment. We use a continuous pressure source $s(t) = p_0\sin(\omega_1 t) + p_0\sin(\omega_2 t)$ of amplitude $p_0 = 12$ kPa and frequencies f_1 and f_2, where $\omega_1 = 2\pi f_1$ and $\omega_2 = 2\pi f_2$. The total time is $T_t = 400T_d$ where $T_d = 1/f_d$ is the period at the difference frequency $f_d = f_2 - f_1$. We take $f_1 = 6 \times 10^5$ Hz and $f_2 = 9.1758 \times 10^5$ Hz so that $f_d = 3.1758 \times 10^5$ Hz and we consider the mode (1,1). The sound speed for this medium and this frequency is $c_d = 1215.7$ m/s. We take 400 temporal intervals per period. Fig. 8d shows the amplitude of the difference frequency in the plane that defines the axisymmetric obtained by FFT. The maximum amplitude at f_d is $p_d = 0.643$ kPa (5.4% of p_0).

3.2.1.2. Cylindrical cavity with rigid walls

3.2.1.2.1. One-frequency experiment. We consider a continuous pressure source $s(t) = p_0\sin(\omega t)$ of amplitude $p_0 = 20$ kPa and frequency f, where $\omega = 2\pi f$. The total time of the experiment is $T_t = 400T$ where the period is T= 1/f. We choose the frequency f= 2.7992×10^5 Hz that matches the mode (0,2) of this cavity (Fig. 1f). The sound speed for this medium and this frequency is c= 980.88 m/s. We take 400 temporal steps per period. Fig. 9a, b, c show the amplitude of the first three harmonics obtained after applying a FFT in the plane that defines the axisymmetric. We obtain the maximum pressure amplitude for the fundamental, the second, and the third harmonics: $p_f = 18.911$ kPa (94.6% of p_0), $p_{2f} = 3.249$ kPa (16.2% of p_0), $p_{3f} = 0.678$ kPa (3.4% of p_0), respectively.

3.2.1.2.2. Two-frequency experiment. We use a continuous pressure source $s(t) = p_0\sin(\omega_1 t) + p_0\sin(\omega_2 t)$ of amplitude $p_0 = 12$ kPa and frequencies f_1 and f_2, where $\omega_1 = 2\pi f_1$ and $\omega_2 = 2\pi f_2$. The total time is $T_t = 400T_d$ where $T_d = 1/f_d$ is the period at the difference frequency $f_d = f_2 - f_1$. We take $f_1 = 5 \times 10^5$ Hz and $f_2 = 8.4636 \times 10^5$ Hz so that $f_d = 3.4636 \times 10^5$ Hz and we consider the mode (0,2). The sound speed

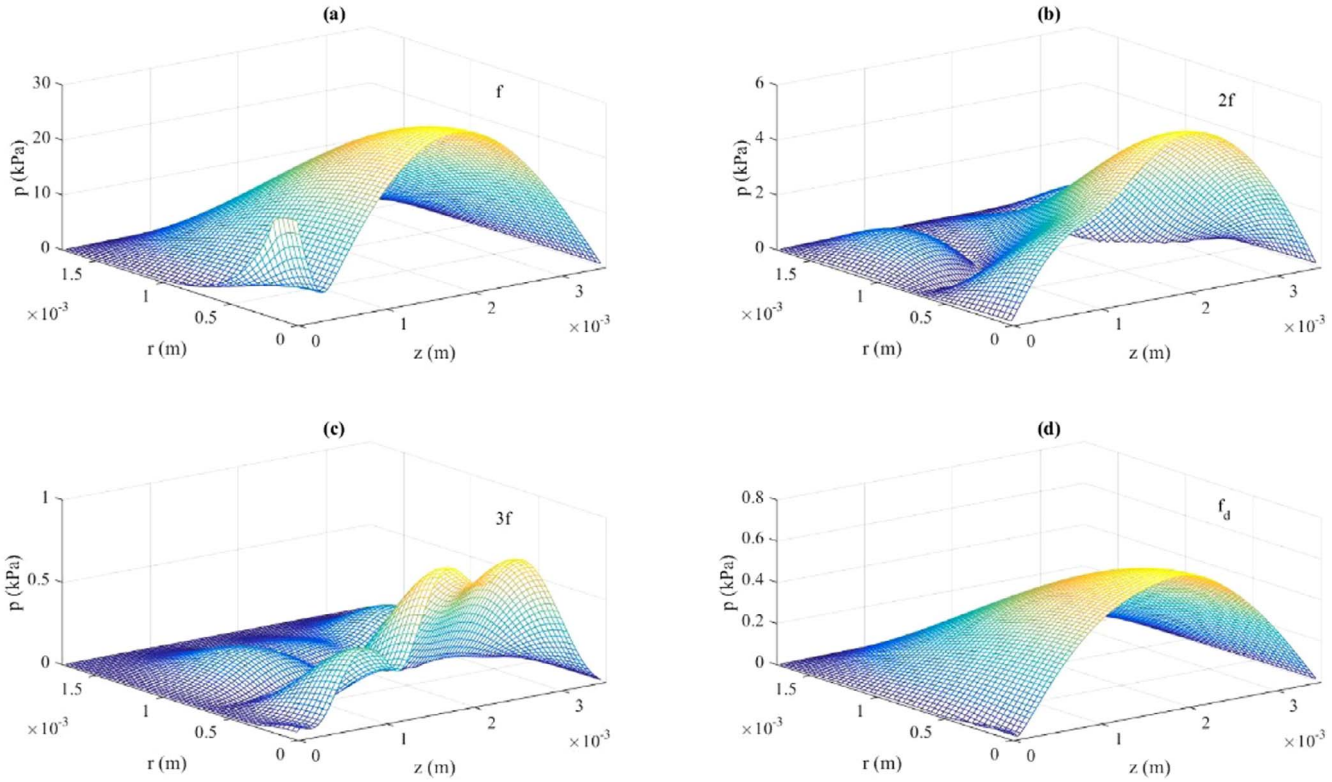

Fig. 8. Distribution of frequencies. Three-dimensional cylindrical cavity with free walls. (a) Fundamental frequency. (b) 2nd harmonic. (c) 3rd harmonic. (d) Difference frequency.

for this medium and this frequency is c_d = 1213.3 m/s. We take 400 temporal intervals per period. Fig. 9d shows the amplitude of the difference frequency in the plane that defines the axisymmetric obtained by FFT. The maximum amplitude at f_d is p_d = 0.596 kPa (5% of p_0).

3.2.2. Truncated cone cavity with free walls

The source s(t) takes 20% of the wall (Fig. 3b). On the remaining 80% the source grows as $s(t)\left(\frac{\gamma - i}{GN+1}\right)^6$ for N/2−NG < i⩽ N/2, where γ = N/2 + 1 and G= 0.4.

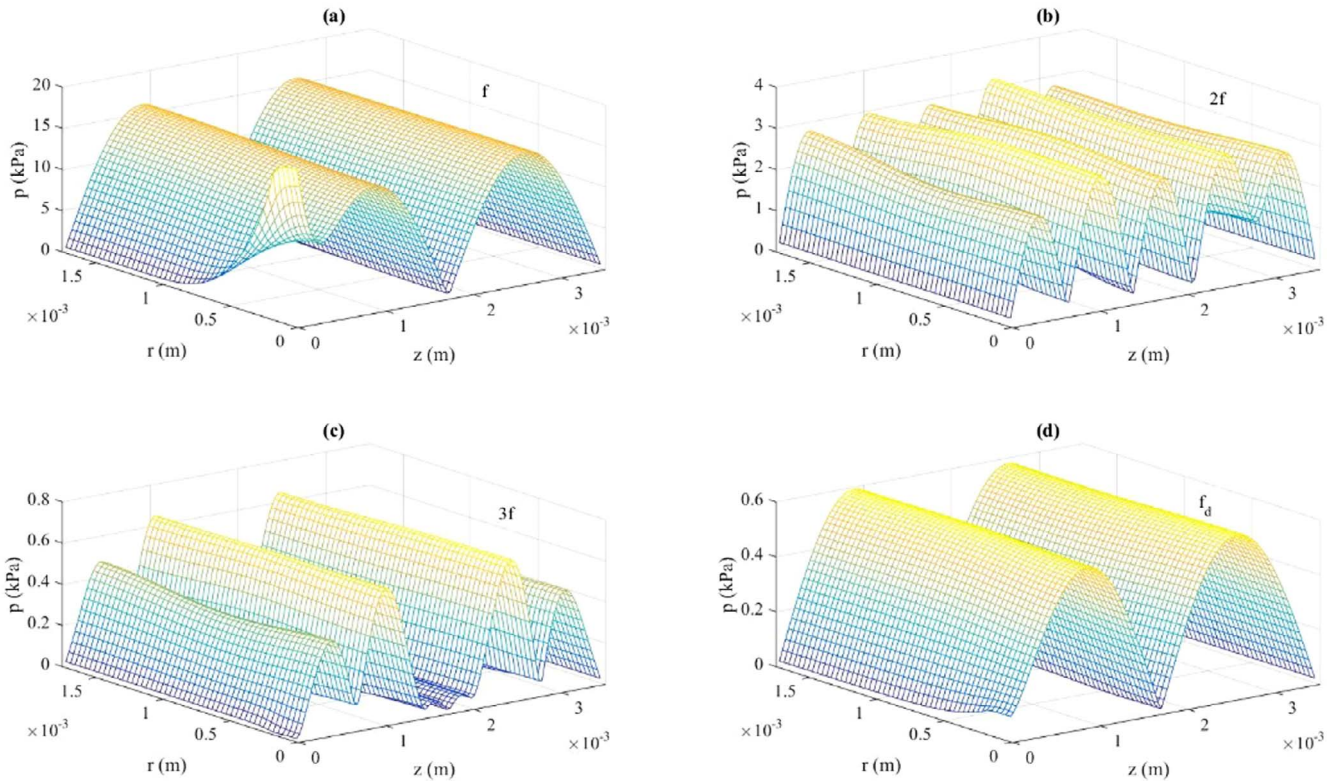

Fig. 9. Distribution of frequencies. Three-dimensional cylindrical cavity with rigid walls. (a) Fundamental frequency. (b) 2nd harmonic. (c) 3rd harmonic. (d) Difference frequency.

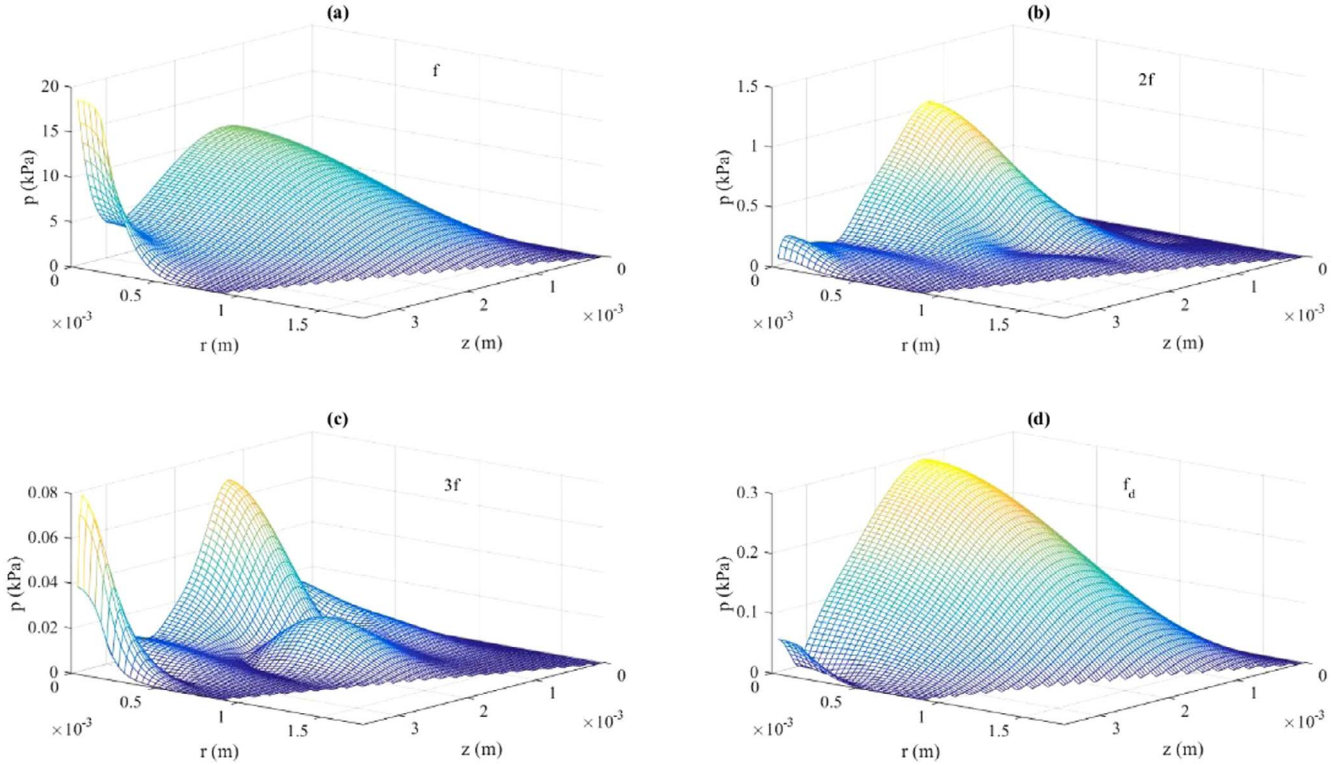

Fig. 10. Distribution of frequencies. Three-dimensional truncated cone cavity with free walls. (a) Fundamental frequency. (b) 2nd harmonic. (c) 3rd harmonic. (d) Difference frequency.

3.2.2.1. One-frequency experiment. We consider a continuous pressure source $s(t) = p_0\sin(\omega t)$ of amplitude $p_0 = 20$ kPa and frequency f, where $\omega = 2\pi f$. The total time is $T_t = 400\,T$ where the period is $T = 1/f$. We choose the frequency $f = 3.109 \times 10^5$ Hz that matches the mode (1,1) of this cavity (Fig. 1g). The sound speed for this medium and this frequency is c= 970.02 m/s. We take 400 temporal steps per period. Fig. 10a, b, c show the amplitude of the first three harmonics obtained after applying a FFT in the plane that defines the axisymmetric. We obtain the maximum pressure amplitude for the fundamental, the second, and the third harmonics: $p_f = 18.696$ kPa (93.5% of p_0), $p_{2f} = 1.065$ kPa (5.3% of p_0), $p_{3f} = 0.079$ kPa (0.4% of p_0), respectively

3.2.2.2. Two-frequency experiment. We use a continuous pressure source $s(t) = p_0\sin(\omega_1 t) + p_0\sin(\omega_2 t)$ of amplitude $p_0 = 12$ kPa and frequencies f_1 and f_2, where $\omega_1 = 2\pi f_1$ and $\omega_2 = 2\pi f_2$. The total time is $T_t = 400T_d$ where $T_d = 1/f_d$ is the period at the difference frequency $f_d = f_2 - f_1$. We take $f_1 = 6 \times 10^5$ Hz and $f_2 = 9.8756 \times 10^5$ Hz so that $f_d = 3.8756 \times 10^5$ Hz and we consider the mode (1,1). The sound speed for this medium and this frequency is $c_d = 1209.6$ m/s. We take 400 temporal intervals per period. Fig. 10d shows the amplitude of the difference frequency in the plane that defines the axisymmetric obtained by FFT. The maximum amplitude at f_d is $p_d = 0.285$ kPa (2.4% of p_0).

3.2.3. Horn cavity with rigid walls

The source is situated like in Section 3.2.2.

3.2.3.1. One-frequency experiment. We consider a continuous pressure source $s(t) = p_0\sin(\omega t)$ of amplitude $p_0 = 20$ kPa and frequency f, where $\omega = 2\pi f$. The total time is $T_t = 400\,T$ where the period $T = 1/f$. We choose the frequency $f = 2.7951 \times 10^5$ Hz that matches the mode (0,2) of this cavity (Fig. 1h). The sound speed for this medium and this frequency is c= 981 m/s. We take 400 temporal steps per period. Fig. 11a, b, c show the amplitude of the first three harmonics obtained after applying a FFT in the plane that defines the axisymmetric. We obtain the maximum pressure amplitude for the fundamental, the second, and the third harmonics: $p_f = 19.955$ kPa (100.0% of p_0), $p_{2f} = 4.511$ kPa (22.6% of p_0), $p_{3f} = 1.261$ kPa (6.3% of p_0), respectively.

3.2.3.2. Two-frequency experiment. We use a continuous pressure source $s(t) = p_0\sin(\omega_1 t) + p_0\sin(\omega_2 t)$ of amplitude $p_0 = 12$ kPa and frequencies f_1 and f_2, where $\omega_1 = 2\pi f_1$ and $\omega_2 = 2\pi f_2$. The total time is $T_t = 400T_d$ where $T_d = 1/f_d$ is the period at the difference frequency $f_d = f_2 - f_1$. We take $f_1 = 5 \times 10^5$ Hz and $f_2 = 8.4571 \times 10^5$ Hz so that $f_d = 3.4571 \times 10^5$ Hz and we consider the mode (0,2). The sound speed for this medium and this frequency is $c_d = 1213.4$ m/s. We take 400 temporal intervals per period. Fig. 11d shows the amplitude of the difference frequency in the plane that defines the axisymmetric after obtained by FFT. The maximum amplitude at f_d is $p_d = 0.812$ kPa (6.8% of p_0).

The results shown in this paper are highly dependent on the choice of the geometry, the kind of boundary conditions, and the size of the source. The results obtained in a specific configuration cannot be compared quantitatively to the data produced by simulations in other cases.

This paper proves that the versatility of the numerical models allows us to choose and design the geometries that potentiate the effects of nonlinear distortion or nonlinear frequency mixing. This can be very useful for the design of efficient sonochemical reactors. Moreover, when free boundaries are assumed, this design could have a prime importance in applications when the propagation of the difference-frequency component in open-field media is useful.

4. Conclusions

The new numerical models proposed in this paper (based on the finite-volume and finite-difference methods) allow us to increase the knowledge on the interaction of oscillating bubbles and ultrasound in different multi-dimensional resonant cavities filled with bubbly fluids. We analyze the harmonic and difference-frequency generation, consequence of the strong nonlinearity of bubbly liquids. The versatility of

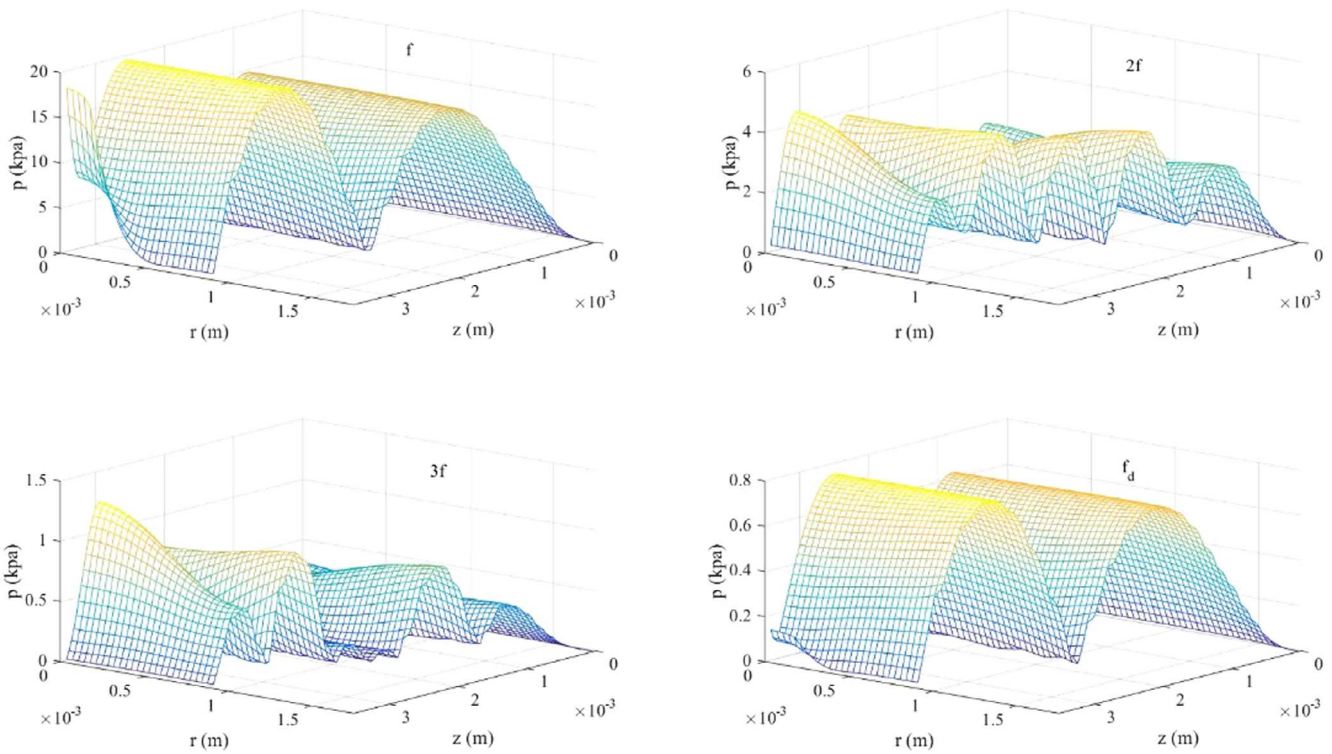

Fig. 11. Distribution of frequencies. Three-dimensional horn cavity with rigid walls. (a) Fundamental frequency. (b) 2nd harmonic. (c) 3rd harmonic. (d) Difference frequency.

the models developed here makes it possible to study many different geometries and boundary conditions. The analysis of the simulations suggests that these tools could be helpful to understand the behavior of ultrasounds in bubbly liquids in different application frameworks, to design more efficient resonators in sonochemical processes and to enhance the generation of low ultrasonic signals obtained indirectly by frequency mixing for parametric arrays. Moreover, this study allows us to observe which geometries are the most adequate to enhance the amplitude of the difference-frequency component. This result is even more important with free-wall boundary conditions for applications of parametric arrays that require open-field propagation beyond the edges of the resonator.

ACKNOWLEDGEMENTS

This work is supported by the Ministry of Economy and Competitiveness of Spain [DPI2012-34613, BES-2013-064399].

Christian Vanhille dedicates this work to Dr. Cleofé Campos-Pozuelo.

References

[1] L. Bjorno, Forty years of nonlinear ultrasound, Ultrasonics 40 (2002) 11–17.
[2] J.A. Gallego-Juárez, K.F. Graff (Eds.), Power ultrasonics: applications of high-intensity ultrasound, Woodhead Publishing Series in Electronic and Optical Materials, vol. 66, Elsevier, Amsterdam, 2015.
[3] K. Naugolnykh, L. Ostrovsky, Nonlinear Wave Processes in Acoustics, Cambridge University Press, New York, 1998.
[4] M.F. Hamilton, D.T. Blackstock (Eds.), Nonlinear Acoustics, Academic Press, San Diego, 1998.
[5] F. Grieser, P.K. Choi, N. Enomoto, H. Harada, K. Okitsu, K. Yasui (Eds.), Sonochemistry and the Acoustic Bubble, Elsevier, Amsterdam, 2015.
[6] C. Vanhille, C. Pantea, D.N. Sinha, Acoustic characterization of Fluorinert FC-43 liquid with helium gas bubbles: numerical experiments, Shock Vib. 2017 (2017) 2518168.
[7] Y. Matsumoto, J.S. Allen, S. Yoshizawa, T. Ikeda, Y. Kaneko, Medical ultrasound with microbubbles, Exp. Therm. Fluid Sci. 29 (2005) 255–265.
[8] T.J. Mason, J.P. Lorimer, Applied Sonochemistry: The Uses of Power Ultrasound in Chemistry and Processing, Wiley-VCH, Weinheim, 2002.
[9] N.A. Fernandez, L. Rodriguez-Freire, M. Keswani, R. Sierra-Alvarez, Effect of chemical structure on the sonochemical degradation of prefluoroalkyl and polyfluoroalkyl substances (PFASs), Environ. Sci.: Water Res. Technol. 2 (2016) 975–983.
[10] H. Koruk, A. El Ghamrawy, A.N. Pouliopoulos, J.J. Choi, Acoustic particle palpation for measuring tissue elasticity, Appl. Phys. Lett. 107 (2015) 223701.
[11] V. Sáez, J. Frías-Ferrer, J. Iniesta, J. González-García, A. Aldaz, E. Riera, Characterization of a 20 kHz sonoreactor: part I: analysis of mechanical effects by classical and numerical methods, Ultrason. Sonochem. 12 (2005) 59–65.
[12] J. Klíma, J. Frías-Ferrer, J. González-García, J. Ludvík, V. Sáez, J. Iniesta, Optimisation of 20 kHz sonoreactor geometry on the basis of numerical simulation of local ultrasonic intensity and qualitative comparison with experimental results, Ultrason. Sonochem. 14 (2007) 19–28.
[13] V.S. Sutkar, P.R. Gogate, L. Csoka, Theoretical prediction of cavitational activity distribution in sonochemical reactors, Chem. Eng. J. 158 (2010) 290–295.
[14] K.W. Commander, A. Prosperetti, Linear pressure waves in bubbly liquids: comparison between theory and experiments, J. Acoust. Soc. Am. 85 (1989) 732–746.
[15] S. Nomura, M. Nakagawa, Analysis of an ultrasonic field attenuated by oscillating cavitation bubbles, Acoust. Sci. Tech. 22 (2001) 283–291.
[16] S. Dähnke, K.M. Swamy, F.J. Keil, A comparative study on the modelling of sound pressure field distributions in a sonoreactor with experimental investigation, Ultrason. Sonochem. 6 (1999) 221–226.
[17] K. Yasui, T. Kozuka, T. Tuziuti, A. Towata, Y. Iida, J. King, P. Macey, FEM calculation of an acoustic field in a sonochemical reactor, Ultrason. Sonochem. 14 (2007) 605–614.
[18] C. Vanhille, C. Campos-Pozuelo, Numerical simulation of nonlinear ultrasonic standing waves in bubbly liquids, Int. J. Nonlinear Sci. Numer. Simul. 10 (2009) 751–757.
[19] C. Vanhille, C. Campos-Pozuelo, Nonlinear ultrasonic standing waves: two-dimensional simulations in bubbly liquids, Ultrason. Sonochem. 18 (2011) 679–982.
[20] C. Vanhille, C. Campos-Pozuelo, Numerical simulations of three-dimensional nonlinear acoustic waves in bubbly liquids, Ultrason. Sonochem. 20 (2013) 963–969.
[21] P.J. Westervelt, Parametric acoustic array, J. Acoust. Soc. Am. 35 (1963) 535–537.
[22] J.L.S. Bellin, R.T. Beyer, Experimental investigation of an end-fire array, J. Acoust. Soc. Am. 34 (1962) 1051–1054.
[23] B.N. Kim, S.W. Yoon, Nonlinear parameter estimation in water-satured sandy sediment with difference frequency acoustic wave, Ultrasonics 49 (2009) 438–445.
[24] D.N. Sinha, C. Pantea, Broadband unidirectional ultrasound propagation using sonic crystal and nonlinear medium, Emerg. Mater. Res. 2 (2013) 117–126.
[25] H.O. Berktay, Possible exploitation of non-linear acoustics in underwater transmitting applications, J. Sound Vib. 2 (1965) 435–461.
[26] J.C. Buckey, D.A. Knaus, D.L. Alvarenga, M.A. Kenton, P.J. Magari, Dual-frequency ultrasound for detecting and sizing bubbles, Acta Astronaut. 56 (2005) 1041–1047.
[27] M. Cavaro, C. Payan, J. Moysan, F. Baqué, Microbubble cloud characterization by nonlinear frequency mixing, J. Acoust. Soc. Am. 129 (2011) 179–183.
[28] V.L. Newhouse, P.M. Shankar, Bubble size measurement using the nonlinear mixing of two frequencies, J. Acoust. Soc. Am. 75 (1984) 1473–1477.
[29] E.A. Zabolotskaya, S.I. Soluyan, Emission of harmonic and combination-frequency waves by air bubbles, Sov. Phys. Acoust. 18 (1973) 396–398.

[30] Y.A. Kobelev, A.M. Sutin, Difference-frequency sound generation in a liquid containing bubbles of differents sizes, Sov. Phys.-Acoust. 26 (1980) 485–847.
[31] O.A. Druzhinin, L.A. Ostrovsky, A. Prosperetti, Low-frequency acoustic wave generation in a resonant bubble layer, J. Acoust. Soc. Am. 100 (1996) 3570–3580.
[32] Q.Y. Ma, Y.Y. Qiu, B. Huang, D. Zhang, X.F. Gong, Difference-frequency ultrasound generation from microbubbles under dual-frequency excitation, Chin. Phys. B. 19 (2010) 094302.
[33] C. Vanhille, C. Campos-Pozuelo, D.N. Sinha, Nonlinear frequency mixing in a resonant cavity: numerical simulations in a bubbly liquid, Ultrasonics 54 (2014) 2051–2054.
[34] M.T. Tejedor Sastre, C. Vanhille, A numerical model for the study of the difference frequency generated from nonlinear mixing of standing ultrasonic waves in bubbly liquids, Ultrason. Sonochem. 34 (2017) 881–888.
[35] C. Vanhille, Two-dimensional numerical simulations of ultrasound in liquids with gas bubble agglomerates: Examples of bubbly-liquid-type acoustic metamaterials (BLAMMs), Sensors 17 (2017) 173.
[36] I. Tudela, V. Sáez, M.D. Esclapez, M.I. Díez-García, P. Bonete, J. González-García, Simulation of the spatial distribution of the acoustic pressure in sonochemical reactors with numerical methods: a review, Ultrason. Sonochem. 21 (2014) 909–919.
[37] G.D. Smith, Numerical Solution of Partial Differential Equations, Finite Difference Methods, third ed., Clarendon, Oxford, 1985.
[38] C. Vanhille, A. Lavie, C. Campos-Pozuelo, Modélisation Numérique En Mécanique: Introduction Et Mise En Pratique, Hermes Science Publications, Lavoisier, Paris, 2007.
[39] H.K. Versteeg, W. Malalasekera, An Introduction to Computational Fluid Dynamics: The Finite Volume Method, Longman Scientific & Technical, Harlow, 1995.
[40] Comsol Multiphysics™.

Capítulo 4

Resonancia no lineal de cavidades llenas de líquidos con burbujas: Un estudio numérico

Este capítulo surge a partir de las observaciones hechas en el Capítulo 3. En la búsqueda de la frecuencia de resonancia de las cavidades multidimensionales llenas de un líquido con burbujas del Capítulo 3 se observó un aumento en la respuesta (trabajando en régimen no lineal) si se trabajaba con frecuencias un poco inferiores a la frecuencia de resonancia obtenida para el régimen lineal.

En este capítulo se hace un estudio del cambio que tiene lugar en la frecuencia de resonancia de una cavidad llena de líquido con burbujas, es decir, en la velocidad de propagación de la onda, en resonadores unidimensionales cuando se trabaja en régimen no lineal. Las simulaciones permiten proponer leyes de la variación en la frecuencia de resonancia de la cavidad y por tanto en la velocidad de propagación como función de la amplitud de presión. Los resultados indican un ablandamiento del medio (disminución en la velocidad de propagación). Además se da una aplicación en la generación de la frecuencia diferencia ya que se consigue aumentar en gran medida su generación al tener en cuenta este fenómeno.

Se incluye el manuscrito enviado a una revista científica (Factor de impacto JCR-ISI: 1,320):

M.T. Tejedor Sastre, C. Vanhille, Nonlinear resonance of cavities filled with bubbly liquids: A numerical study, Shock Vib. (2018) Enviado.

Nonlinear resonance of cavities filled with bubbly liquids: A numerical study

This paper studies the resonance of a system composed by a nonlinear biphasic medium made of a liquid and gas bubbles in a cavity. The analysis is performed through numerical simulations at different pressure amplitudes. The finite-volume and finite-difference based model developed in the time domain simulates the nonlinear interaction of ultrasound and bubble dynamics via the resolution of a differential system formed by the wave and a Rayleigh-Plesset equations. The results reveal the existence of a nonlinear resonance of the system, which is observed by a frequency shift of the resonance of the cavity that rises with pressure amplitude. This effect evidences the fact that under finite amplitudes the bubbly medium undergoes global changes, i.e., the sound speed decreases and the softening of the medium is produced as acoustic pressure amplitude grows. Numerical experiments show that this effect is more pronounced when the bubble density in the liquid is raised. Moreover, this nonlinear resonance effect is used to enhance the generation of the frequency-difference signal by nonlinear frequency mixing in the medium by maximizing its amplitude.

4.1. Introduction

Adding bubbles to a liquid modifies its acoustic properties [1-4]. The nonlinear parameter increases several orders of magnitude. The sound speed, attenuation coefficient, compressibility, and nonlinear parameter acquire dispersive dependence on bubble resonance. The nonlinear interaction of ultrasound and bubble oscillations must be understood to take advantage of these properties in different applied frameworks such as sonochemistry [5], medicine [6], and others [7,8].

The nonlinearity of the medium is responsible of the generation of harmonics from the fundamental frequency and generates combinations of frequencies by nonlinear frequency mixing (sum frequency and difference frequency) when several ultrasonic signals travel through the medium [9]. These effects have multiple applications. Med-

ical imaging can be generated from higher harmonic components [10]. Underwater exploration or transmission and nondestructive testing are fields where the difference frequency signal has a huge interest because of its low attenuation, good directivity, and high penetration [11,12]. Characterization and detection of bubbles are also attractive applications of the frequency mixing phenomenon [13-16].

Several studies based on linear models have been performed to understand the behavior of ultrasonics waves in bubbly liquids inside a cavity [17-19]. Other works that analyze the behavior of standing ultrasonics waves are based on nonlinear models [20,21]. In those papers both the sound speed and the resonance frequencies are calculated without taking into account the amplitude of the waves [2,3]. In this paper we aim at showing that the pressure amplitude of the signal changes the resonance frequency of the cavity (and the sound speed).

The dependence of the resonance frequency on drive amplitude has been observed in solids, for which the nonlinear features of ultrasound are used in areas as damage diagnostics in materials [22], granular media and dynamic earthquake triggering [23] and fluids in closed tubes of variable cross-section [24].This effect has also been studied in bubbly liquids for a resonance frequency associated to the multiple scattering of bubbles that changes as a function of the amplitude of an incident Gaussian pulse [25].

The objective of this work is to study the variation with pressure amplitude of the resonance of a one-dimensional resonator filled with a fluid made of a liquid and gas bubbles when working at nonlinear regime with finite-amplitude signals. A continuous excitation at a frequency well below the bubble resonance is used to take advantage of the nonlinearity with a relative low attenuation.

In Section 4.2 we present the physical problem and the corresponding mathematical model used in this work. Some numerical results obtained in a specific case by varying the amplitude at the source are shown in Section 4.3. They allows us to observe the nonlinear resonance phenomenon of the cavity. This variation of resonance frequency is then analyzed when the bubble density in the liquid is changed. Finally, we apply this phenomenon to maximize the difference frequency component generated by nonlinear frequency mixing. Section 4.4 gives the discussion of this work.

4.2. Materials and methods

We consider a one-dimensional cavity of length L filled with a mixture of water and air bubbles. Under the Rayleigh-Plesset approximation, we suppose that, among others, the bubbles are spherical and have the same size. We also assume that they are evenly distributed in the liquid. The model assumes that bubbles are the only source of attenuation, dispersion and nonlinearity. The buoyancy, Bjerknes and viscous drag forces are not considered in this work. The interaction between the acoustic pressure $p(x,t)$, and the volume variation of the bubbles $v(x,t) = V(x,t) - v_{0g}$ is modeled by the wave equation, Eq. (4.1), and a Rayleigh-Plesset equation, Eq. (4.2) [26,3], where x is the one-dimensional space coordinate, t is the time, V is the current volume of the bubble, and $v_{0g} = 4/3\pi R_{0g}^3$ is the initial bubble volume, with R_{0g} the initial radius.

$$\frac{\partial^2 p}{\partial x^2} - \frac{1}{c_{0l}^2}\frac{\partial^2 p}{\partial t^2} = -\rho_{0l} N_g \frac{\partial^2 v}{\partial t^2},\ 0 < x < L,\ 0 < t < T_t \tag{4.1}$$

$$\frac{\partial^2 v}{\partial t^2} + \delta\omega_{0g}\frac{\partial v}{\partial t} + \omega_{0g}^2 v + \eta p = av^2 + b\left(2v\frac{\partial^2 v}{\partial t^2} + \left(\frac{\partial v}{\partial t}\right)^2\right),\ 0 \le x \le L,\ 0 < t < T_t \tag{4.2}$$

In Eq. (4.1) c_{0l} and ρ_{0l} are the sound speed and the density at the equilibrium state of the liquid. N_g is the density of bubbles, i.e., the bubble number per m^3. In Eq. (4.2) $\delta = 4\nu_l/\omega_{0g}R_{0g}^2$ is the viscous damping coefficient of the bubbly fluid, in which ν_l is the cinematic viscosity of the liquid, $\omega_{0g} = \sqrt{3\gamma_g p_{0g}/\rho_{0l}R_{0g}^2}$ is the resonance frequency of the bubbles, in which γ_g is the specific heats ratio of the gas, $p_{0g} = \rho_{0g}c_{0g}^2/\gamma_g$ is its atmospheric pressure, ρ_{0g} and c_{0g} are the density and sound speed at the equilibrium state of the gas. The parameter $\eta = 4\pi R_{0g}/\rho_{0l}$, and the nonlinear coefficients $a = (\gamma_g + 1)\omega_{0g}^2/2v_{0g}$ and $b = 1/6v_{0g}$, are constant. The numerical experiments last a total time T_t. In the following studies, Section 4.3, the value of this parameter T_t is high enough to ensure that the steady state of the waves is reached. The system is closed by supposing that the liquid and the bubbles are unperturbed at the onset of the studies:

$$p(x \neq 0, 0) = 0, v(x,0) = 0,\ \frac{\partial p}{\partial t}(x \neq 0, 0) = 0,\ \frac{\partial v}{\partial t}(x,0) = 0,\ 0 \le x \le L, \tag{4.3}$$

that the resonator is excited by a time-dependent pressure source $s(t)$ placed at $x = 0$:

$$p(x = 0, t) = s(t),\ 0 \leq t \leq T_t, \tag{4.4}$$

and that a free-wall condition is imposed at the reflector:

$$p(L, t) = 0,\ 0 \leq t \leq T_t. \tag{4.5}$$

To solve this differential system we use a numerical model developed in [21] based on a finite-volume method in the space dimension and a finite-difference method in the time domain.

4.3. Results

We show the results obtained by setting the following data into the model: $c_{0l} = 1500\, m/s$, $\rho_{0l} = 1000\, kg/m^3$, $\nu_l = 1.43 \times 10^{-6}\, m^2/s$ for the liquid (water) and $c_{0g} = 340\, m/s$, $\rho_{0g} = 1.29\, kg/m^3$, $\gamma_g = 1.4$ for the gas (air). We use bubbles of radius $R_{0g} = 2.5\, \mu m$.

4.3.1. Single bubble density

The pressure source used is $s(t) = p_0 sin(\omega_f t)$ where p_0 is the amplitude, $\omega_f = 2\pi f$ and f is the frequency. The length of the cavity is set at $L = \lambda/2$ to reach a resonant mode, where $\lambda = c_f/f$ is the wavelength and c_f is the sound speed in this biphasic medium at this frequency [3]. The bubble density used here is $N_g = N_{g2} = 5 \times 10^{11} m^{-3}$. For this medium and $f = 200\, kHz$ the sound speed is $c_f = 1222.8\, m/s$. Therefore, we set the cavity length at $L = c_f/2f = 0.0031\, m$. We apply a frequency sweep to the source of amplitude $p_0 = 1\, Pa$ with an interval $\Delta f = 10\, Hz$ around f to check that the frequency able to achieve the better response matches our considered frequency f, and thus ensure that we work at the resonance frequency for this amplitude (linear resonance of the cavity). The maximum pressure is found in the cavity by applying a Fast Fourier Transform for the signal obtained at each frequency. We now perform the same procedure for higher amplitude values at the source, up to $p_0 = 250\, Pa$. Figure

4.1 shows the maximum pressure reached in the resonator for each source amplitude over the studied frequency range. The maximum pressure value in the linear case, $p_0 = 1\ Pa$, is $p_{max} = 113\ Pa$, corresponding to $f = 200\ kHz$, as expected. For the lowest amplitudes (linear case) the curve is perfectly symmetrical. However, we observe that by increasing the source amplitude the resonance frequency, i.e., the frequency that allows the higher response of the system, decreases, and that the nonlinear attenuation implies a decrease of the maximum pressure reached in relation to the source amplitude and a loss of symmetry around the nonlinear resonance. The resonance of the cavity is thus a function of the pressure amplitude. This means that by changing the amplitude a frequency shift from the linear resonance f is observed. For the source amplitude $p_0 = 250\,Pa$ the frequency that permits the best response is $f_{250} = 198.74\,kHz$, and the frequency shift is therefore $\Delta f_{250} = f - f_{250} = 1.26\,kHz$. Since the length of the cavity remains the same for all the amplitudes, the sound speed in the medium changes with amplitudes. For $p_0 = 250Pa$ the sound speed is modified to $c_{250} = 2Lf_{250} = 1215.1m/s$. Thus, the medium undergoes a modification of its acoustic properties, not only on a local basis (velocity of particles) when nonlinear distortion occurs (e.g., as for a shock wave), but on a global basis. The medium is modified when amplitudes change. Specifically, it suffers a softening process when pressure amplitudes are raised. This effect is due to the increase of the effective bubble volume. At nonlinear regime the positive volume variations prevail over the negative values. This makes the oscillations of the bubble produced around a volume bigger than the initial one, $v_{0g}^{+} > v_{0g}$, and thus, the sound speed in the effective medium is lower [3], i.e., it undergoes a softening process. Section 4.3.2 gives more details about this effect.

4.3.2. Several bubble densities

We now study this nonlinear resonance shift for three different bubble densities by keeping the same amplitude sweeping range as in Section 4.3.1, N_{g2}, $N_{g1} = 3\times10^{11}m^{-3}$, and $N_{g3} = 7 \times 10^{11}\ m^{-3}$. For N_{g2} the sound speed and resonator length remain the same as in Section 4.3.1. For $N_{g1} = 3 \times 10^{11}\ m^{-3}$ we use $c_f = 1314.1\ m/s$ and $L = c_f/2f = 0.0033\ m$. For $N_{g3} = 7 \times 10^{11}\ m^{-3}$ we use $c_f = 1148.2\ m/s$ and $L =$

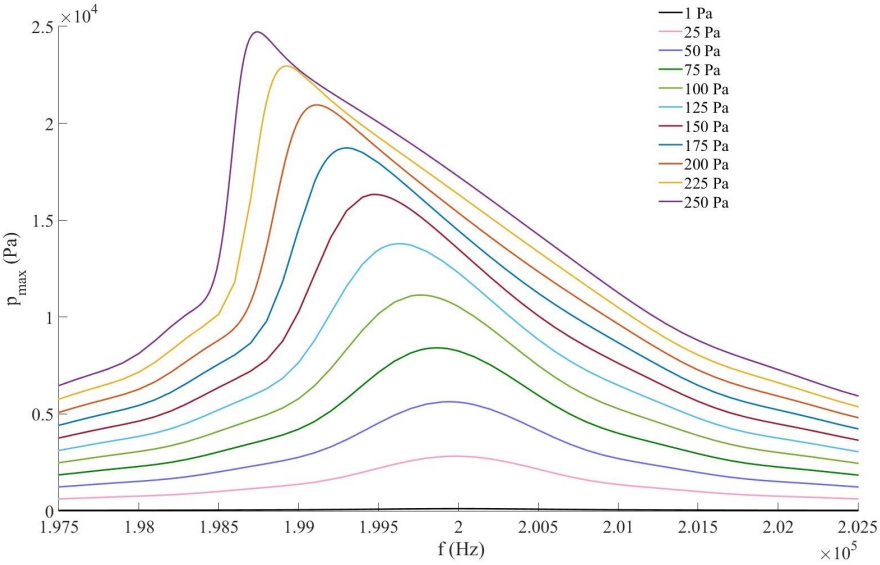

Figure 4.1: Maximum pressure in the cavity vs. source frequency for different source amplitudes.

$c_f/2f = 0.0029\,m$. Figure 4.2 represents the resonance frequency variation from the linear resonance at $f = 200\,kHz$ as a function of the maximum pressure achieved in the cavity for each bubble density, including the third degree polynomial fitting of the resonance frequency variation: $\Delta f = 8.4\times10^{-12}p_{max}^3+2.3\times10^{-6}p_{max}^2+0.00018p_{max}+2.5$ for N_{g3} , $\Delta f = 1.2\times10^{-11}p_{max}^3 + 1.8\times10^{-6}p_{max}^2 - 1.4\times10^{-5}p_{max} + 1.9$ for N_{g2}, and $\Delta f = 3.5\times10^{-11}p_{max}^3 + 3\times10^{-7}p_{max}^2 + 0.0062p_{max} - 5.2$ for N_{g1}, where Δf is expressed in Hz and p_{max} in Pa. We observe that for the same maximum pressure the frequency shift is higher in the media with higher bubble density, since their nonlinear acoustic parameter is higher, i.e., as the bubble density rises the frequency shift is more pronounced. Nevertheless, for the same source amplitude the maximum pressure reached is higher when the bubble density is lower, since there is less attenuation in the medium. Figure 4.3 shows the frequency shift (the resonance frequency variation from the linear resonance of the cavity) as a function of the average volume increase Δv for the three bubble densities. We observe that the frequency shift increases (higher maximum pressure, Fig. 4.2) with Δv , i.e., when the effective bubble volume is higher, following a linear fit: $\Delta f = 1.3986\times10^{21}\Delta v - 19.83$ for N_{g1} , $\Delta f = 2.0129\times10^{21}\Delta v +$

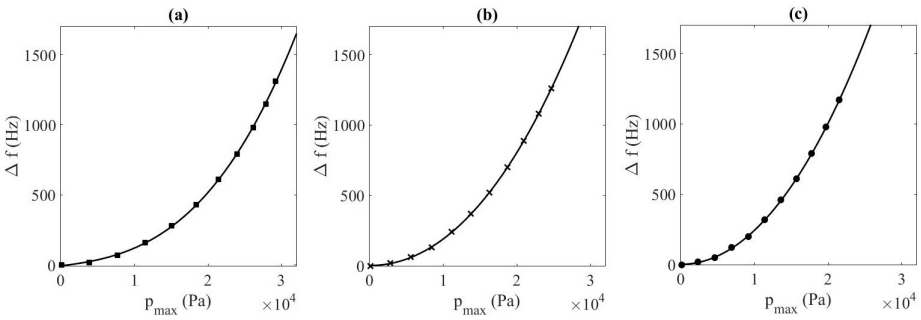

Figure 4.2: Fitting curves of the resonance frequency shift vs. maximum pressure in the cavity for different bubbly densities. (a) $N_{g1} = 3\times10^{11} m^{-3}$, (b) $N_{g2} = 5\times10^{11} m^{-3}$, (c) $N_{g3} = 7 \times 10^{11}\ m^{-3}$.

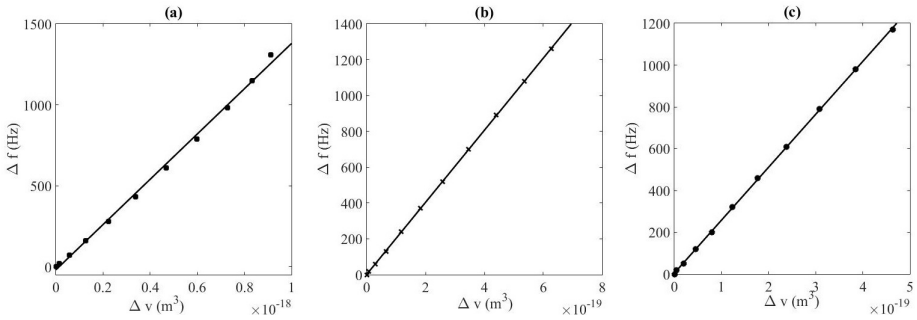

Figure 4.3: Fitting curves of the resonance frequency shift vs. average volume increase Δv for different bubbly densities (a) $N_{g1} = 3 \times 10^{11}\ m^{-3}$, (b) $N_{g2} = 5 \times 10^{11}\ m^{-3}$, (c) $N_{g3} = 7 \times 10^{11}\ m^{-3}$.

1.2361 for N_{g2} , and $\Delta f = 2.5326 \times 10^{21}\Delta v + 4.6884$ for N_{g3} , where Δf is expressed in Hz and Δv in m^3 .

4.3.3. Application to frequency mixing and difference-frequency generation

The nonlinear frequency shift effect observed in the previous sections is now used to maximize the amplitude of the difference-frequency component generated in the context of the nonlinear frequency mixing [1, 27]. The pressure source used is $s(t) = p_0 sin(\omega_1 t) + p_0 sin(\omega_2 t)$, where f_1 and f_2 are the primary source frequencies chosen to generate the difference frequency $f_d = f_2 - f_1$, $\omega_1 = 2\pi f_1$ and $\omega_2 = 2\pi f_2$. Like in Section 4.3.1 the bubble density is $N_g = N_{g2} = 5 \times 10^{11}\ m^{-3}$ and the length of the cavity is

$L = 0.0031$. This length is chosen to fit the linear resonance at the difference frequency 200 kHz, thus $L = \lambda_{dL}/2$, $f_{dL} = 200\,kHz$, where $\lambda_{dL} = c_{dL}/f_{dL}$ is the wavelength and $c_{dL} = 1222.8\,m/s$ is the sound speed for this frequency in this medium. The source amplitude for this study is $p_0 = 10\,kPa$, and we analyze the difference frequency generation for two difference frequencies, $f_{dL} = 200\,kHz$ and $f_{dNL} = 198.41\,kHz$ to compare the results when we take into account the resonance frequency shift, which is the frequency that produces the highest response by parametric emission in this case. The primary frequencies at the source are respectively $f_{1L} = 700\,kHz$ and $f_{2L} = f_{1L} + f_{dL} = 900 kHz$, and $f_{1NL} = 700 kHz$ and $f_{2NL} = f_{1NL} + f_{dNL} = 898.41 kHz$. These frequencies are chosen close to half the resonance frequency of the bubbles since the nonlinearity is high at this frequency in the dispersive medium [3]. Figure 4.4 shows the amplitude distribution along the cavity of the primary frequencies f_{1L}, f_{2L}, the difference frequency f_{dL} (continuous lines), the primary frequencies f_{1NL}, f_{2NL}, and the difference frequency f_{dNL} (dashed lines) obtained after applying a Fast Fourier Transform. Different amplitudes are observed for f_{dL} and f_{dNL}. Whereas the maximum pressure for f_{dL} is $p_{dL} = 12.092\,kPa$ (121% of p_0), the corresponding value for f_{dNL} is $p_{dNL} = 17.376\,kPa$ (174% respect to p_0, which is a very high value for parametric emission). The benefit drawn in terms of difference-frequency amplitude is 53%. It is also interesting to note that the energy of the primary frequencies is distributed differently by changing one of them, $f_{1L} = f_{1NL}$, $f_{2L} \neq f_{2NL}$. By taking into account the shift of the resonance frequency both primary frequencies undergo a strong loss of intensity whereas the difference frequency is much stronger.

4.4. Discussion

This work shows the existence of a nonlinear resonance effect of a system composed by a nonlinear biphasic medium made of a liquid and gas bubbles in a cavity, i.e., the observation of a frequency shift of its resonance that grows with pressure amplitudes. The numerical results at different pressure amplitudes and for several bubble densities reveal that the bubbly medium undergoes global modifications dependent on pressure amplitudes. The decrease of the sound speed as acoustic pressure amplitude

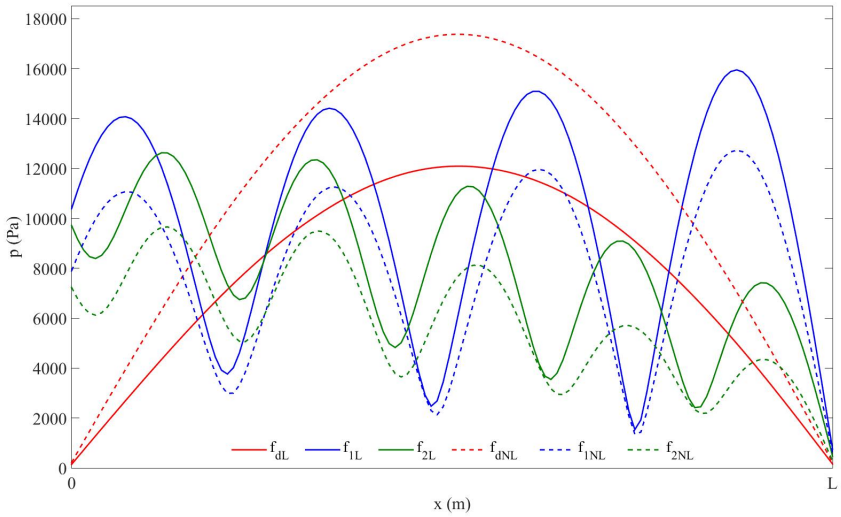

Figure 4.4: Amplitude distribution of frequency components along the resonator. $f_{1L} = 700\,kHz$, $f_{2L} = 900\,kHz$, $f_{dL} = 200\,kHz$ (continuous lines), $f_{1NL} = 700\,kHz$, $f_{2NL} = 898.41\,kHz$ and $f_{dNL} = 198.41\,kHz$ (dashed lines).

grows suggests a softening of the medium. This effect is due to the increase of the effective bubble volume with acoustic pressure amplitude. This nonlinear resonance effect of the cavity is then used to maximize the frequency-difference amplitude generated by nonlinear frequency mixing in the bubbly medium.

Acknowledgements

This work is supported by the National Agency for Research (Agencia Estatal de Investigación, AEI), Ministry of Economy, Industry, and Competitiveness of Spain (Ministerio de Economía, Industria y Competitividad), Ministry of Science, Innovation, and Universities of Spain (Ministerio de Ciencia, Innovación y Universidades), and the European Regional Development Fund (FEDER) [grant numbers DPI2012-34613, BES-2013-064399, and DPI2017-84758].

Christian Vanhille dedicates this work to Dr. Cleofé Campos-Pozuelo.

References

[1] K. Naugolnykh, L. Ostrovsky, Nonlinear Wave Processes in Acoustics, Cambridge University Press, New York, 1998.

[2] F. Grieser, P.K. Choi, N. Enomoto, H. Harada, K. Okitsu, K. Yasui (Eds.), Sonochemistry and the Acoustic Bubble, Elsevier, Amsterdam, 2015.

[3] M.F. Hamilton, D.T. Blackstock (Eds.), Nonlinear Acoustics, Academic Press, San Diego, 1998.

[4] O.V. Rudenko, S.I. Soluian, Theoretical foundations of nonlinear acoustics, Consultants Bureau, New York, 1977.

[5] T.J. Mason, J.P. Lorimer, Applied sonochemistry: the uses of power ultrasound in chemistry and processing, Wiley-VCH, 2002.

[6] Y. Matsumoto, J.S. Allen, S. Yoshizawa, T. Ikeda, Y. Kaneko, Medical ultrasound with microbubbles, Exp. Therm. Fluid Sci. 29 (2005) 255-265.

[7] O.V. Abramov, Ultrasound in Liquid and Solid Metals, CRC Press, Boca Ratón, 1994.

[8] J.A. Gallego-Juárez, K.F.E. Graff, Power Ultrasonics: Applications of High-Intensity Ultrasound, Elsevier, Amsterdam, 2014.

[9] W. Lauterborn, Nonlinear Acoustics and Acoustic Chaos, Springer Berlin Heidelberg, Berlin, 2002.

[10] T.S. Desser, R.B. Jeffrey, Tissue harmonic imaging techniques: Physical principles and clinical applications, Semin. Ultrasound CT 22 (2001) 1-10.

[11] B.N. Kim, S.W. Yoon, Nonlinear parameter estimation in water-saturated sandy sediment with difference frequency acoustic wave, Ultrasonics 49 (2009) 438-445.

[12] D.N. Sinha, C. Pantea, Broadband unidirectional ultrasound propagation using sonic crystal and nonlinear medium, Emer. Mater. Res. 2 (2013) 117-126.

[13] V.L. Newhouse, P.M. Shankar, Bubble size measurements using the nonlinear mixing of two frequencies, J. Acoust. Soc. Am. 75 (1984) 1473-1477.

[14] J.C. Buckey, D.A. Knaus, D.L. Alvarenga, M.A. Kenton, P.J. Magari, Dual-frequency ultrasound for detecting and sizing bubbles, Acta Astronaut. 56 (2005) 1041-1047.

[15] M. Cavaro, C. Payan, J. Moysan, Microbubble cloud characterization by nonlinear frequency mixing, J. Acoust. Soc. Am. 129 (2011) 179-183.

[16] C. Vanhille, Two-dimensional numerical simulations of ultrasound in liquids with gas bubble agglomerates: Examples of bubbly-liquid-type acoustic metamaterials (BLAMMs), Sensors, 17 (2017) 173.

[17] G. Servant, J.P. Caltagirone, A. Gérard, J.L. Laborde, A. Hita, Numerical simulation of cavitation bubble dynamics induced by ultrasound waves in a high frequency reactor, Ultrason. Sonochem. 7 (2000) 217-227.

[18] S. Dähnke, F.J. Keil, Modeling of three-dimensional linear pressure fields in sonochemical reactors with homogeneous and inhomogeneous density distributions of cavitation bubbles, Ind. Eng. Chem. Res.37 (1998) 848-864.

[19] K.W. Commander, A. Prosperetti, Linear pressure waves in bubbly liquids:Comparison between theory and experiments, The J. Acoust. Soc. Am. 85 (1989) 732-746.

[20] C. Vanhille, C. Campos-Pozuelo, Numerical simulation of nonlinear ultrasonic standing waves in bubbly liquid, Int. J. Nonlinear Sci. Numer. Simul. 10 (2009) 751-757.

[21] M.T. Tejedor Sastre, C. Vanhille, A numerical model for the study of thedifference frequency generated from nonlinear mixing of standing ultrasonic waves in bubbly liquids, Ultrason. Sonochem. 34 (2017) 881-888.

[22] U. Polimeno, M. Meo, Detecting barely visible impact damage detection on aircraft composites structures, Compos, Struct. 91 (2009) 398-402.

[23] P.A. Johnson, X. Jia, Nonlinear dynamics, granular media and dynamic earthquake triggering, Nature, 437 (2005) 871-874.

[24] M.P. Mortel, B.R. Seymour, Nonlinear resonant oscillations in closed tubesof variable cross-section, J. Fluid Mech. 519 (2004) 183-199.

[25] J.-B. Doc, J.-M. Conoir, R. Marchiano, D. Fuster, Nonlinear acoustic propagation in bubbly liquids: Multiple scattering, softening and hardening phenomena, J. Acoust. Soc. Am. 139 (2016) 1703-1712.

[26] E.A. Zabolotskaya, S.I. Soluyan, Emission of harmonic and combination-frequency waves by air bubbles. Sov. Phys. Acoust. 18 (1973) 396-398.

[27] S. Karpov, A. Prosperetti, L. Ostrovsky, Nonlinear wave interactions in bubble layers, TJ. Acoust. Soc. Am. 113 (2003) 1304-1316.

Capítulo 5

Estudio numérico de la mezcla de frecuencias en un campo ultrasónico focalizado en líquidos con burbujas a partir de una fuente esférica de dos frecuencias

En este capítulo se pretende estudiar el comportamiento de campos ultrasónicos focalizados en líquidos con burbujas en campos abiertos generados mediante un transductor esférico. Este comportamiento se describe a partir del modelo matemático formado por la ecuación de ondas y una ecuación de Rayleigh-Plesset que describen el acoplamiento entre la presión acústica y las vibraciones de las burbujas. Para ello se desarrollan modelos numéricos basados en el método de los volúmenes finitos en las dimensiones espaciales y de las diferencias finitas en el dominio temporal.

Los resultados permiten analizar los armónicos (con fuentes de una frecuencia) y proponer leyes que rigen su comportamiento como función de la amplitud de la fuente. También se consigue estudiar las frecuencias suma y diferencia (con fuentes de dos frecuencias) y a proponer leyes físicas que describen su generación como función de la amplitud de la fuente. Además en este trabajo se incluye un estudio de la convergencia

y de la estabilidad del modelo desarrollado.

Se incluye el manuscrito enviado a una revista científica (Factor de impacto JCR-ISI: 2,147):

M.T. Tejedor Sastre, C. Vanhille, Numerical study of frequency mixing in a focused ultrasonic field in bubbly liquids from a dual-frequency spherical source, Results Phys. (2018) Enviado.

Numerical study of frequency mixing in a focused ultrasonic field in bubbly liquids from a dual-frequency spherical source

The aim of this work is to study the nonlinear frequency mixing that comes out in the focus region in a bubbly liquid when a spherical transducer emits a dual-frequency ultrasonic wave of finite amplitude in a three-dimensional open domain with axial symmetry. The nonlinear interaction between the acoustic field and the bubble vibrations is modeled through a coupled differential system formed by the wave equation and a Rayleigh-Plesset equation. Simulations are performed by means of an ad-hoc numerical model developed on the basis of multi-dimensional finite-volume and finite-difference techniques. Results show the nonlinear response of the system by showing the space distribution of the fundamental and harmonics for a single-frequency excitation (for which a convergence study is also carried out) and the space distribution of the difference and sum-frequency components for a two-frequency excitation. In the former case a law is proposed for the evolution of each one of the second and third harmonics vs. amplitude. In the latter configuration a law is proposed for the evolution of each one of the difference and sum frequencies vs. amplitude. This work suggests that the combination of two frequencies emitted from a spherical transducer can allow the enhancement of the generation of the difference and sum-frequencies in a restricted volume of the bubbly liquid. This could be used to control the amplitude and space extent of these frequency components by modifying the shape of the spherical transducer, the primary frequencies, and the pressure amplitude. Our results can be useful for industrial and medical processes based on nonlinear frequency mixing.

5.1. Introduction

Bubbly liquids are dispersive media that affect the propagation of an ultrasonic wave differently depending on the ratio of the driven frequency to the bubble resonance. These media can strongly attenuate and nonlinearly distort the wave. They are very

interesting media since at some frequency ranges this nonlinear distortion (harmonic generation) can become huge even at relatively small amplitudes and for small void fractions (low bubble density in the liquid) [1-3]. When a dual-frequency wave travels in a bubbly liquid, the nonlinearity of the medium produces the mixing of these frequency that generates new frequency components in the signal, in particular the difference and sum frequencies of the two primary ones. Harmonic generation from a single-frequency signal is used in medical imaging [4]. Nonlinear mixing from a dual-frequency signal is useful for applications such as bubble detection and characterization [5-7] and underwater communication [8,9], mainly because of the low attenuation and high directivity of the created difference frequency.

Theoretical, experimental, and applied studies about nonlinear frequency mixing exist in the literature [9-11]. In bubbly liquids, few works about nonlinear frequency mixing have been reported [12-19]. Zabolotskaya and Soluyan derived a differential model to analyze the combination of frequencies in a bubbly liquid [12]. The difference-frequency is analyzed theoretically and experimentally in a liquid containing bubbles of different sizes by Kobelev and Sutin in Ref. [13]. Druzhinin et al. explore analytically and numerically the low-frequency generation in a resonant bubble layer [14]. Ma et al. analyze the difference-frequency generation from microbubbles theoretically and experimentally [15]. Vanhille et al. study numerically the difference frequency in several configurations in one or more dimensions [16-19].

Although the effect of a dual-frequency HIFU field is studied experimentally in Ref. [20] to show the efficiency of the therapeutic effects due to the cavitation field obtained at the low difference frequency signal, the nonlinear frequency mixing produced in a focused ultrasonic field in a liquid containing bubbles evenly distributed has not been analyzed in the literature, even if its implication in some industrial and medical applications could be interesting because of the specific properties of the difference-frequency component [9-11,21]. In the present work, we draw our attention on this topic.

The aim of this work is the study of the difference and sum frequencies generated by a focused ultrasonic field created by a spherical transducer in a bubbly liquid in an axi-symmetric three-dimensional open domain. To this end, we chose to develop a

numerical model able to perform simulations at several pressure amplitude ranges. Section 5.2 presents the physical problem we consider and the differential equations used to perform its modeling. This section also describes the numerical model developed to solve the mathematical model. In Section 5.3 we present the results obtained from numerical simulations when the source is driven at one and two frequencies. Section 5.4 gives the discussion of this study. An appendix gives the results of the study of the convergence in the one-frequency source case.

5.2. Material and methods

5.2.1. Physical problem

We consider a mixture of water and air bubbles in a three-dimensional open domain, with variables (x, y, z), excited by a spherical transducer (Fig. 5.1), in which bubbles are evenly distributed in the liquid. We assume that all the bubbles are spherical, have the same size, and that bubbles are the only source of attenuation, nonlinearity, and dispersion in the medium. We also consider that bubbles are monodisperse and oscillate at their first radial mode, the surface tension is neglected, and the bubble collapse is not modeled. Buoyancy, Bjerknes and viscous drag forces are not considered in this work. The transducer excites the system with a continuous pressure source driven at one frequency, f, or at two frequencies, f_1 and f_2. We study the nonlinear mutual interaction between the pressure field and the bubble oscillations in the time, variable t, and space domains.

5.2.2. Mathematical model

We assume a symmetry of the problem around the z-axis in the three-dimensional space that reduces the problem to an axi-symmetric space domain and allows us to use cylindrical coordinates (r, z). The interaction between acoustic pressure $p(r, z, t)$ and bubble volume variation $v(r, z, t) = V(r, z, t) - v_{0g}$ is modeled by the coupling of the wave equation, Eq. (5.1), and the Rayleigh-Plesset equation, Eq. (5.2), [1-3],

$$\frac{\partial^2 p}{\partial r^2} + \frac{1}{r}\frac{\partial p}{\partial r} + \frac{\partial^2 p}{\partial z^2} - \frac{1}{c_{0l}^2}\frac{\partial^2 p}{\partial t^2} = -\rho_{0l} N_g \frac{\partial^2 v}{\partial t^2},$$
$$0 < r < R/2,\ R - \sqrt{R^2 - r^2} < z < L,\ 0 < t < T_t, \tag{5.1}$$

$$\frac{\partial^2 v}{\partial t^2} + \delta\omega_{0g}\frac{\partial v}{\partial t} + \omega_{0g}^2 v + \eta p = av^2 + b\left(2v\frac{\partial^2 v}{\partial t^2} + \left(\frac{\partial v}{\partial t}\right)^2\right),$$
$$0 \le r \le R/2,\ R - \sqrt{R^2 - r^2} \le z \le L,\ 0 < t < T_t, \tag{5.2}$$

in which c_{0l} and ρ_{0l} are the sound speed and the density at the equilibrium state of the liquid, N_g is the density of bubbles in the liquid, $\delta = 4\nu_l/\omega_{0g}R_{0g}^2$ is the viscous damping coefficient of the bubbly fluid, ν_l is the cinematic viscosity of the liquid, $\omega_{0g} = \sqrt{3\gamma_g p_{0g}/\rho_{0l}R_{0g}^2}$ is the resonance frequency of bubbles, γ_g is the specific heats ratio of the gas, $p_{0g} = \rho_{0g}c_{0g}^2/\gamma_g$ is the atmospheric pressure of the gas, ρ_{0g} and c_{0g} are the density and sound speed at the equilibrium state in the gas, R is the radius of curvature ($R/2$ is the opening radius) of the transducer, and L is the length of the space domain in the main axis direction. Parameters $\eta = 4\pi R_{0g}/\rho_{0l}$, $a = (\gamma_g + 1)\omega_{0g}^2/(2v_{0g})$, and $b = 1/(6v_{0g})$ are constants. Our simulations are performed from $t = 0$ up to time T_t is reached. We suppose that the bubbles are at rest in the unperturbed liquid when the experiment starts:

$$p(r,z,0) = 0,\ v(r,z,0) = 0,\ \frac{\partial p}{\partial t}(r,z,0) = 0,\ \frac{\partial v}{\partial t}(r,z,0) = 0,$$
$$0 \le r \le R/2,\ R - \sqrt{R^2 - r^2} \le z \le L(r). \tag{5.3}$$

The axi-symmetrical condition is also set:

$$\frac{\partial p}{\partial r}(0,z,t) = 0,\ R - \sqrt{R^2 - r^2} \le z \le L(r),\ 0 < t < T_t. \tag{5.4}$$

The source $s(t)$ is placed at the bottom part in Fig. 5.1. The other boundary conditions, including the open-domain condition, are

$$s(t) = p(r, z = R - \sqrt{R^2 - r^2}, t),\ 0 < r < R/2,\ 0 \le t \le T_t, \tag{5.5}$$

$$\frac{\partial p}{\partial r}(R/2,z,t) = -\frac{1}{c_{0l}^2}\frac{\partial p}{\partial t}(R/2,z,t),\ R(1 - \sqrt{3}/2) < z < L,\ 0 \le t \le T_t, \tag{5.6}$$

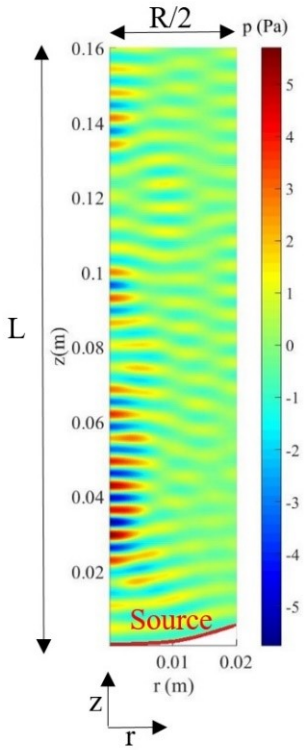

Figure 5.1: Schematic representation of the open space domain (linear regime) showing the axi-symmetric plan section, the spherical transducer, and the region of the focus.

$$\frac{\partial p}{\partial z}(r, L, t) = -\frac{1}{c_{0l}^2}\frac{\partial p}{\partial t}(r, L, t),\ 0 < r < R/2,\ 0 \leq t \leq T_t, \tag{5.7}$$

5.2.3. Numerical model

The numerical model developed is based on our previous works developed for resonators in one and several dimensions [17,18]. This new model solves the differential system formed by Eqs. (5.1-5.7). It is based on a combination of numerical techniques, the finite-volume method in the space dimensions and the finite-difference method in the time domain [22-24]. The space discretization is performed by dividing the domain $R/2 \times L$ in a number of $N \times M$ control volumes, each one of size $h \times h$. We define each control volume of the axi-symmetric plane (r, z) by its central point denoted by the subscripts (i, j). The differential equations are then integrated in each volume control

assuming a linear relation between adjacent control volumes. The truncation error of the space scheme is $O(h)$. The time discretization is carried out by dividing the total time T_t in Q_t intervals, each one of dimension τ. We denote each time point by the subscript k. We use central finite-difference formulas to approximate the second-order time derivatives and central backward finite-difference formulas to approximate the first-order time derivatives. The truncation error in these approximations is $O(\tau^2)$ and $O(\tau)$, respectively. These developments for Eqs. (5.2)(5.3) lead to the following discretized system, valid for any control volume (i, j) and any time point such that $k = 3, ..., Q_t + 1$,

$$\begin{aligned}\frac{h^2 B}{c_{0l}^2} p_{i,j,k+1} - \rho_{0l} N_g h^2 B v_{i,j,k+1} &= \tau^2 (A_1 p_{i+1,j,k} + A_2 p_{i-1,j,k}) \\ &+ \tau^2 B (A_3 p_{i,j+1,k} + A_4 p_{i,j-1,k}) + \left(-\frac{h^2 B}{c_{0l}^2} + A_5 \right) p_{i,j,k-1} \\ + \rho_{0l} N_g h^2 B (-2 v_{i,j,k} + v_{i,j,k-1}) &+ \left(A_6 \tau^2 + A_7 B \tau^2 + \frac{2Bh^2}{c_{0l}^2} + A_8 \right) p_{i,j,k},\end{aligned} \tag{5.8}$$

$$\begin{aligned}(2bv_{i,j,k} - 1) v_{i,j,k+1} &= (-2 + \delta\tau\omega_{0g} + \tau^2 \omega_{0g}^2 - \tau^2 a v_{i,j,k} + 3b v_{i,j,k}) v_{i,j,k} \\ &+ (1 - \delta\tau\omega_{0g} - b v_{i,j,k}) v_{i,j,k-1} + \eta \tau^2 p_{i,j,k}\end{aligned} \tag{5.9}$$

where $B = (1 - 2i)/2$ and A_c, with $c = (1, 2, 3, 4, 5, 6, 7, 8)$. A_c takes different values that depend on whether the control volume is in the interior of the space domain, at the boundary of the space domain, at the symmetry axis, or at the source. We have thus the following cases:

- in the former case, within the interior of the space domain, $A_1 = i$, $A_2 = i - 1$, $A_3 = 1$, $A_4 = 1$, $A_5 = 0$, $A_6 = 1 - 2i$, $A_7 = -2$, and $A_8 = 0$;

- if the volume is at the source, $A_1 = i$, $A_2 = i - 1$, $A_3 = 1$, $A_4 = 2s(t)/p_{i,j-1,k}$, $A_5 = 0$, $A_6 = 1 - 2i$, $A_7 = -3$, and $A_8 = 0$;

- if the volume is at the source and at the symmetry axis, $A_1 = i$, $A_2 = 0$, $A_3 = 1$, $A_4 = 2s(t)/p_{i,j-1,k}$, $A_5 = 0$, $A_6 = -i$, $A_7 = -3$, and $A_8 = 0$;

- if the volume is at the source and at the right boundary, $A_1 = 0$, $A_2 = i - 1$, $A_3 = 1$, $A_4 = 2s(t)/p_{i,j-1,k}$, $A_5 = \tau^2/c_{0l}^2$, $A_6 = 1 - i$, $A_7 = -3$, and $A_8 = -\tau^2/c_{0l}^2$;

- if the volume is at the right boundary, $A_1 = 0$, $A_2 = i - 1$, $A_3 = 1$, $A_4 = 1$, $A_5 = \tau^2/c_{0l}^2$, $A_6 = 1 - i$, $A_7 = -2$, and $A_8 = -\tau^2/c_{0l}^2$;

- if the volume is at the right boundary and at the top boundary, $A_1 = 0$, $A_2 = i - 1$, $A_3 = 0$, $A_4 = 1$, $A_5 = \tau^2(1 + B)/c_{0l}^2$, $A_6 = 1 - i$, $A_7 = -1$, and $A_8 = -\tau^2(1 + B)/c_{0l}^2$;

- if the volume is at the top boundary, $A_1 = i$, $A_2 = i - 1$, $A_3 = 0$, $A_4 = 1$, $A_5 = \tau^2 B/c_{0l}^2$, $A_6 = 1 - 2i$, $A_7 = -1$, and $A_8 = -\tau^2 B/c_{0l}^2$;

- if the volume is at the top boundary and at the symmetry axis, $A_1 = i$, $A_2 = 0$, $A_3 = 0$, $A_4 = 1$, $A_5 = \tau^2 B/c_{0l}^2$, $A_6 = -i$, $A_7 = -1$, and $A_8 = \tau^2 B/c_{0l}^2$;

- if the volume is at the symmetry axis, $A_1 = i$, $A_2 = 0$, $A_3 = 1$, $A_4 = 1$, $A_5 = 0$, $A_6 = -i$, $A_7 = -2$, and $A_8 = 0$.

Eq. (5.9) is valid for all control volumes. This set of discretized equations, considering the different values of A_c for each control volume, leads to the explicit scheme that allows us obtain the solution $(v_{i,j,k}, p_{i,j,k})$ in each space volume and at each time point.

5.3. Results

In this section we consider the following data for the liquid (water), $c_{0l} = 1500\ m/s$, $\rho_{0l} = 1000\ kg/m^3$, $\nu_l = 1.43 \times 10^{-6}\ m/s$, and for the gas (air), $c_{0g} = 340\ m/s$, $\rho_{0g} = 1.29\ kg/m^3$, $\gamma_g = 1.4$. We use bubbles of radius $R_{0g} = 2.5 \times 10^{-6}\ m$ at density $N_g = 5 \times 10^{11}\ m^{-3}$. The dimensions of the space domain simulated here is given by the opening radius of the spherical transducer $R/2 = 0.02\ m$, since its radius is set at $R = 0.04\ m$, and the length in the main axial direction $L = 0.16\ m$ (Fig. 5.1). For the numerical discretization we set $N = 100$ and thus use $N \times 8N = 80000$ control volumes of size $h^2 = 4 \times 10^{-8}\ m^2$. Two cases are considered. The first one assumes a one-frequency source (Section 5.3.1). The other one considers a two-frequency source (5.3.2). The frequency components shown in the following are obtained after applying a Fast Fourier Transform to the solution calculated in the time domain.

5.3.1. One-frequency experiment

We use the single-frequency continuous pressure source $s(t) = p_0 sin(\omega t)$ of amplitude $p_0 = 6\ kPa$ and frequency $f = 200\ kHz$. The sound speed in this medium at

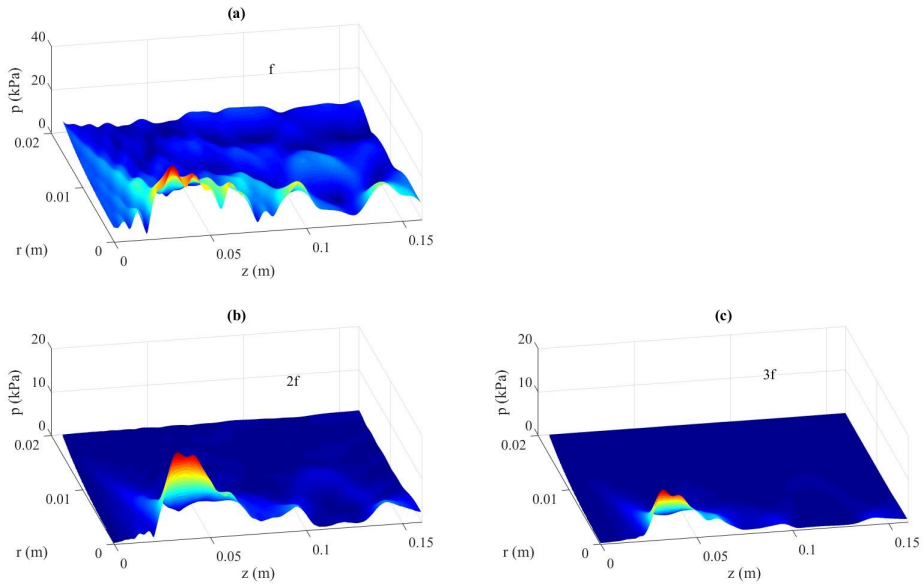

Figure 5.2: Space distribution of frequencies in the open domain: (a) fundamental frequency f; (b) 2nd harmonic $2f$; (c) 3rd harmonic $3f$. Single-frequency source case.

f, $2f$, and $3f$ is $c = 1222.8\ m/s$, $c = 1208.4\ m/s$, and $c = 1180.7\ m/s$, respectively [2]. The experiment lasts $T_t = 50T$, where $T = 1/f$ and we use $Q = 400$ time intervals of length $\tau = 1.25 \times 10^{-8}\ s$ per period.

Figure 5.2 displays the space distribution in the open domain of the fundamental frequency, (a) f, 2nd harmonic, (b) $2f$, and 3rd harmonic, (c) 3f. Figure 5.3 presents the distribution along the axis of symmetry of the open domain of the fundamental frequency f, 2nd harmonic $2f$, and 3rd harmonic $3f$. Figure 5.4 shows the fitting curves of maximum pressure obtained in the open domain as a function of the amplitude at the source, of the 2nd and 3rd harmonics, (a) $2f$ and (b) $3f$.

The maximum pressure amplitude of the fundamental frequency obtained in the space domain (Figs. 5.2 and 5.3), $p_{mf} = 32.391kPa$, which is 539.9% of p_0, indicates a high-pressure focus on the symmetry axis. The second and third harmonics also reach high values, respectively the maximum pressure amplitudes, $p_{m2f} = 19.910kPa$ (331.8% of p_0) and $p_{m3f} = 11.280kPa$ (188.0% of p_0). It can be seen in Fig. 5.3 that these maximum values, corresponding to the three frequency components, are obtained at the same position, i.e., the focus which is situated near the center of curvature of the

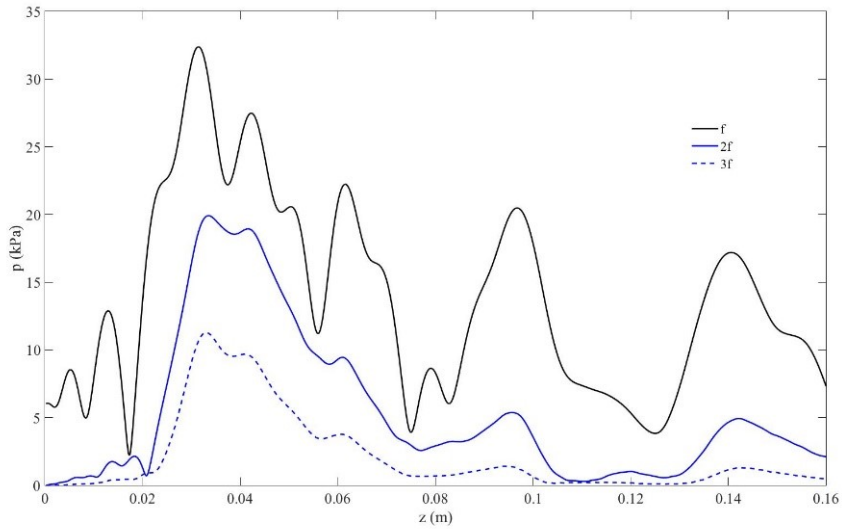

Figure 5.3: Distribution of fundamental frequency f, 2nd harmonic $2f$, and 3^r harmonic $3f$ along the symmetry axis of the open domain. Single-frequency source case.

spherical source. As expected, both harmonics increase only once the amplitude of the pressure wave is high enough, i.e., when the traveling wave approaches the theoretical focus region. Moreover, it is interesting to observe that the third harmonic allows us to clearly localize the place of the real focus on the symmetry axis in the bubbly liquid, in a much precise way than using the fundamental or the second harmonic. The fitting curves of the maximum values of the second and third harmonic in Fig. 5.4, for which amplitudes are expressed in kPa, are respectively, $p_{f2f} = 0.4859p_0^2 + 0.4724p_0 - 0.1310$ and $p_{f3f} = 0.0281p_0^3 + 0.1829p_0^2 - 0.2231p_0 + 0.0278$.

The study of the convergence of the numerical model developed in Section 5.2.3 is performed in the Appendix in this single-frequency source case.

5.3.2. Two-frequency experiment

We use the dual-frequency continuous pressure source $s(t) = p_0 sin(\omega_1 t) + p_0 sin(\omega_2 t)$ of amplitude $p_0 = 6\ kPa$ and primary frequencies $f_1 = 570\ kHz$ and $f_1 = 770\ kHz$. The total time is $T_t = 50T_d$, where $T_d = 1/f_d$ is the period at the difference frequency defined by $f_d = f_2 - f_1 = 200\ kHz$. The sum frequency is defined as

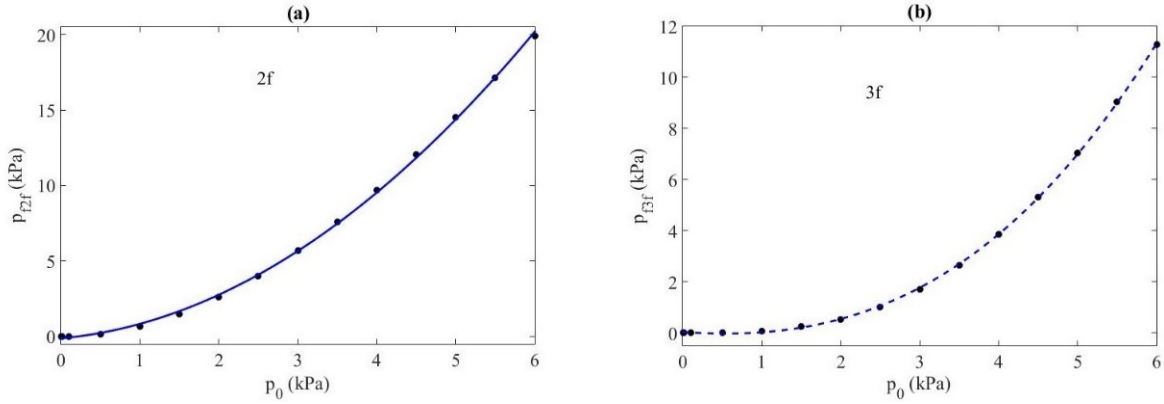

Figure 5.4: Fitting curves of maximum pressure vs. source amplitude in the open domain: (a) 2nd and (b) 3rd harmonics, $2f$ and $3f$. Single-frequency source case.

$f_s = f_2 + f_1 = 1.34\ MHz$. It must be noted that the primary frequencies are around the nonlinear peak of the dispersive medium, 673 kHz [2]. The sound speed in this medium at f_1, f_2, f_d, and f_s is $c = 1185.9\ m/s$, $c = 1141\ m/s$, $c = 1222.8\ m/s$, and $c = 853.9\ m/s$, respectively [2]. We use $Q = 400$ time intervals of length $\tau = 1.25 \times 10^{-8} s$ per period. Figure 5.5 displays the space distribution in the open domain of the primary frequencies, (a) f_1 and (b) f_2, the difference frequency, (c) f_d, and the sum frequency, (d) f_s. Figure 5.6 presents the distribution along the axis of symmetry of the open domain of the primary frequencies, (a) f_1 and f_2, the difference and sum frequencies, (b) f_d and f_s. Figure 5.7 shows the fitting curves of the maximum pressure obtained in the open domain as a function of the amplitude at the source, of the difference and sum frequency components, (a) f_d and (b) f_s.

The maximum pressure amplitude at the difference and sum frequencies obtained in the space domain (Figs. 5.5 and 5.6) are, respectively, $p_{mf_d} = 2.089\ kPa$, which is 34.8% of p_0, and $p_{mf_s} = 4.663\ kPa$, which is 77.7% of p_0. These high relative values reflects the high nonlinearity of the bubbly medium. It can be seen in Fig. 5.6 that the maximum values corresponding to the primary and sum frequencies are situated at the same position as in the case of the single-frequency case, the focus in Section 5.3.1, whereas the maximum value of the difference frequency is slightly shifted toward the source. As it was expected, both the difference and sum frequency components hugely increase when the traveling wave approaches the focus region, i.e.,

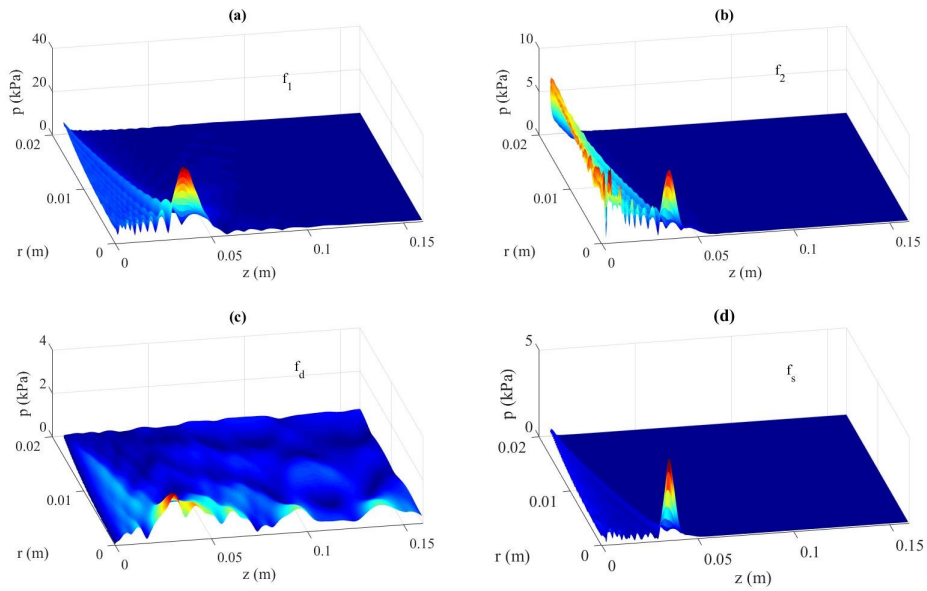

Figure 5.5: Space distribution of frequencies in the open domain: primary frequencies, (a) f_1 and (b) f_2; (c) difference frequency f_d; (d) sum frequency f_s. Dual-frequency source case

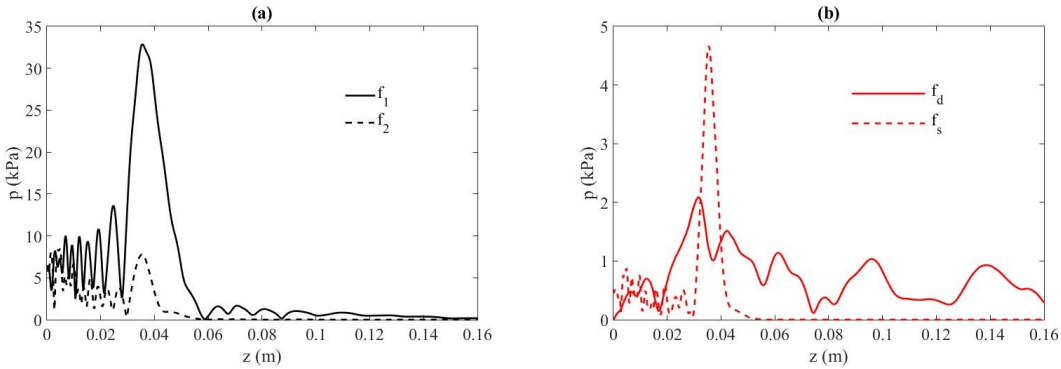

Figure 5.6: Distribution of frequencies along the symmetry axis of the open domain: (a) primary frequencies, f_1 and f_2; (b) difference and sum frequencies, f_d and f_s. Dual-frequency source case.

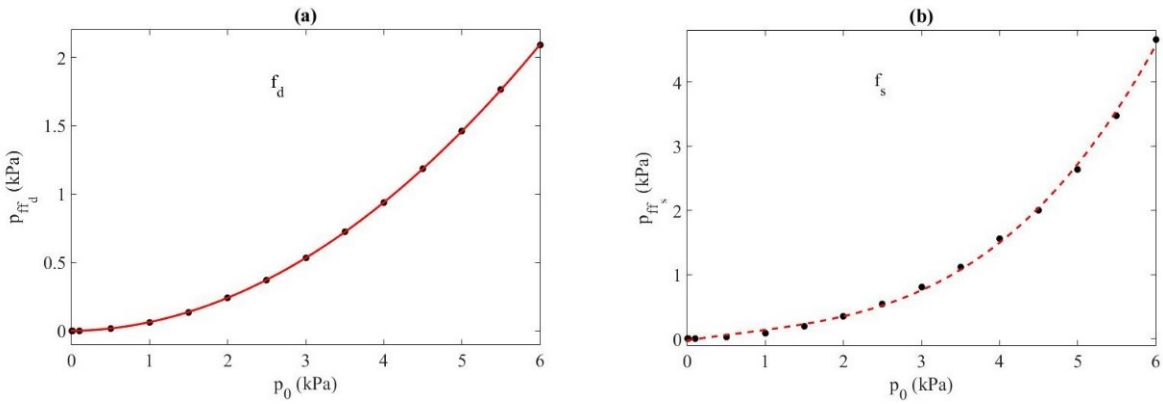

Figure 5.7: Fitting curves of maximum pressure vs. source amplitude in the open domain: (a) difference and (b) sum frequencies, f_d and f_s. Dual-frequency source case.

once the amplitude of the pressure wave is high enough in the high nonlinear medium. Moreover, it is very interesting to observe in Figs. 5.5 and 5.6 that the sum frequency component allows us to clearly localize the place of the focus on the symmetry axis in the bubbly liquid, in a much more precise way than using the difference frequency in this section or the driven and harmonic frequencies in Section 5.3.1. However, the difference frequency signal still have a significant amplitude beyond the focus, whereas the sum frequency vanishes beyond the focus. This result could be useful to detect or characterize the bubble population with a hydrophone situated beyond the focus region. The fitting curves of the maximum values of the difference and sum frequencies in Fig. 5.7 are respectively, $p_{ff_d} = 0.0571p_0^2 + 0.0067p_0 - 0.0012$ and $p_{ff_s} = 0.0241p_0^3 - 0.0481p_0^2 + 0.1881p_0 - 0.0270$, for which amplitudes are expressed in kPa. They indicate, since the sum-frequency response is of higher degree, that the detection or characterization of the bubbly medium through the measurement of the sum-frequency component in a focused ultrasonic field as the source amplitude is raised could be more useful that through the difference-frequency component. It must be also noted that the cubic coefficient of the fitting curve p_{ff_s} is similar to the corresponding coefficient of p_{f3f} (Section 5.3.1).

5.4. Discussion

We have proposed a numerical model to study the nonlinear frequency mixing in the focus region of a three-dimensional bubbly liquid excited by a spherical transducer emitting at two ultrasonic frequencies, by considering an axial symmetry of the problem. The model solves a Rayleigh-Plesset equation coupled to the wave equation that has allowed us to simulate the nonlinear interaction between bubble oscillations and ultrasonic field. The ad-hoc numerical model has been constructed by developing multi-dimensional finite-volume and finite-difference techniques. Our simulations have been performed with one frequency and two frequencies at the source. A convergence study has also been carried out. Results have shown the nonlinear response in terms of fundamental frequency, harmonics components, difference and sum-frequency components. A law has been proposed for the behavior of each one of these components vs. amplitude at the source. The results show the existence of a huge enhancement of the sum frequency in a very restricted volume of bubbly liquid around the focus region and the enhancement of the difference frequency over a much larger distance on the symmetry axis, which could be used to localize the focus and characterize the bubbly medium. This work suggests that the amplitude and space extent of the difference and sum frequencies could be controlled by changing the parameters of the transducer, which can be useful for industrial and medical processes based on nonlinear frequency mixing.

Appendix

The study of the convergence of the numerical model developed in Section 5.2.3 in the single-frequency source case of Section 5.3.1 is performed in this Appendix. To this end, we analyze in both the linear and nonlinear regimes, (i) the stability of the model, and (ii) its convergence.

In both regimes we consider a reference pressure amplitude at the source, p_{0r}, and a perturbed pressure amplitude obtained from this reference value by introducing an error, $p_{0p} = 1.0017 p_{0r}$, and we observe the response of the system, through

the maximal pressure amplitude obtained (at the focus) with both excitations, p_{mr} and p_{mp}, to evaluate the stability of the model. In the linear regime, $p_{0r} = 1Pa$ and $p_{0p} = 1.0017Pa$, whereas $p_{0r} = 6kPa$ and $p_{0p} = 6.010kPa$ in the nonlinear regime. The response obtained is the following: $p_{mp}/p_{mr} = 0.1666\%$ in the linear regime and $p_{mp}/p_{mr} = 0.2853\%$ in the nonlinear regime. These results show that the introduction of a perturbation (an error) into the source data leads to a bounded response of the model after many time steps and calculations, which proves the stability of the numerical model in both the linear and the nonlinear regimes.

Since the discretized equations obtained are consistent with the differential equations, the stability induces the convergence of the model, at least in the linear regime. In the nonlinear regime, this result can be extrapolated locally [25-27].

In this sense, a von Neumann stability analysis for Eq. (5.2) is performed to determine the discretization parameters that guarantee the stable behavior of our model [27]. To this end, we assume a perturbation of the system in the form of a finite Fourier expansion $\epsilon(r,z,t) = \sum_{m=-q}^{+q} v_m(r,z)e^{\underline{i}\alpha_m t}$, where $\underline{i}^2 = -1$, v_m is the amplitude and α_m is the time frequency of the m-component of the series, introduced into the discretized equation. For each m-component we have $\epsilon_{k,m}(r,z,t) = v_m(r,z)e^{\underline{i}\alpha_m(k-1)\tau}$. This analysis considers that the solution is stable if the absolute value of the amplification factor verifies $|\xi| = |e^{\underline{i}\alpha_m\tau}| \leq 1$. Following the comment in the previous paragraph, we simplify our model by considering that both differential equations are not coupled, i.e., $p = 0$ for Eq. (5.2), and that we work in the linear regime, i.e., both constants a and b null. After introducing the perturbation, the following relation is obtained:

$$(\xi - 2 + \xi^{-1}) + \tau\delta\omega_{0g}(1 - \xi^{-1}) + \omega_{0g}^2\tau^2 = 0. \tag{5.10}$$

which, after multiplying by ξ and reorganizing the equation, leads to

$$\xi^2 + \xi(-2 + \tau\delta w_{0g} + w_{0g}^2\tau^2) + (1 - \tau\delta w_{0g}) = 0, \tag{5.11}$$

The solutions of the latter are

$$\xi_{\pm} = \frac{(2 - \tau\delta w_{0g} - w_{0g}^2\tau^2) \pm \sqrt{(-2 + \tau\delta w_{0g} + w_{0g}^2\tau^2)^2 - 4(1 - \tau\delta w_{0g})}}{2}. \tag{5.12}$$

Fig. 5.8a represents the absolute value of $\xi_{\pm}$ as a function of τ, in which the continuous line indicates the unit value and the red, respectively blue, dashed line represents $|\xi_{+}|$, respectively $|\xi_{-}|$. Whereas $|\xi_{+}| \leq 1$ is verified for any τ, $|\xi_{-}| \leq 1$ only for $\tau \leq \tau_{ma} = 2.2395 \times 10^{-7} s$. Thus, from this analytical study, we assume that the system is stable, $|\xi_{\pm}| \leq 1$, for $\tau \leq \tau_{ma}$. About Eq. (5.1), written in cylindrical coordinates, we chose to obtain a stability condition through numerical experiments, in the linear regime. We consider several values of the time step τ. For each one of them, the length of the control volumes h is varying over a range from large to small values and we observe the limit value from which the model is stable. The overall relation between h and τ gives us the actual stability condition, i.e., the stability domain which is the semi-infinite space in the $h - \tau$ plane situated below the limit-value curve, as shown in Fig. 5.8b. Note that the system is never stable for time-step values $\tau \geq \tau_{mn} = 1.786 \times 10^{-7}$ s. This value, calculated numerically, is different from the one evaluated analytically above, although both have the same order of magnitude. Since many simplifications are introduced, the von Neumann analysis only gives an approximation of the actual stability of our model. For time-step values $\tau < 1.2 \times 10^{-7} < \tau_{mn}$ both domains are separated by a straight line that fits the relation $h_n(\tau) = 2298.9\tau - 3.383 \times 10^{-6} m$, shown in brown color in Fig. 5.8b. Thus, the use of $\tau < 1.2 \times 10^{-7}$ and $h > h_n$ ensures the stability, and convergence, of our model. Note that the discretization steps used in Section 5.3, $\tau = 1.25 \times 10^{-8}$ s and $h = 2 \times 10^{-4}$ m , verify the stability conditions described above, $\tau < \tau_{mn} < \tau_{ma}$ and $h_n(1.25 \times 10^{-8}) = 2.5353 \times 10^{-5}$ $m < h$.

The following empirical study of convergence corroborates the consequence given in one of the previous paragraphs, stability induces convergence. The maximum pressure amplitude obtained (at the focus), p_m, is represented in Fig. 5.9 in both regimes, (a) linear and (b) nonlinear, by employing a constant value $\tau = 1.25 \times 10^{-8}$ s and varying the control volume size parameter h , i.e., modifying the control volume number N (top diagrams), and by employing a constant value $h = 2 \times 10^{-4}$ and varying the time step parameter τ, i.e., modifying the time point number per period Q (bottom diagrams). In all the diagrams a rough fitting line is indicated for each phase of the convergence curve, which slope shows the behavior of the convergence. Note that the discretization steps used in this convergence study all verify the stability conditions

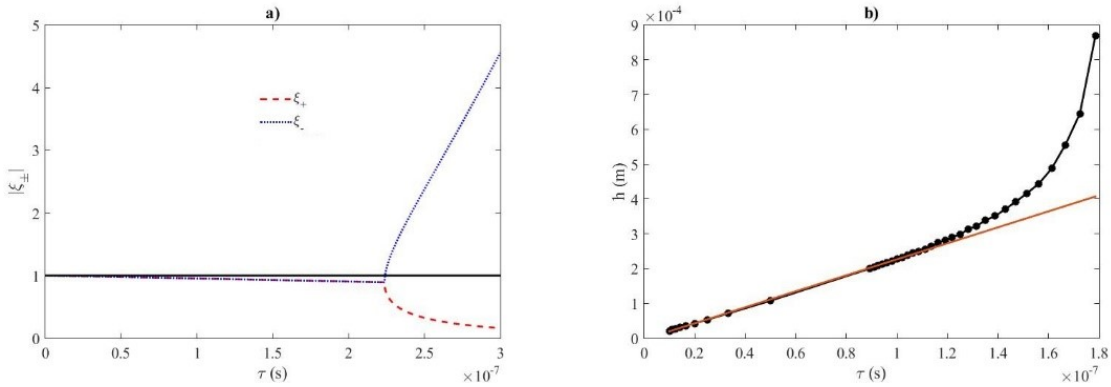

Figure 5.8: Stability curve showing the behavior of the amplification factor vs. time-step length in the linear regime (a) and stability domain in the $h - \tau$ plane (b). Linear regime. Single-frequency source case.

described in the previous paragraph (Fig. 5.8b). In both top diagrams, with large control volumes, i.e., small N values, the curve shows a quasi-vertical asymptote, whereas the slope of the fitting line undergoes a clear drop (in absolute values) for intermediate N values, and the curve finally tends to a constant value (quasi-horizontal asymptote) when the dimension of the control volumes decreases, i.e., for high N values. In both bottom diagrams, a similar behavior, with three different phases, is observed as Q increases. This behavior proves the convergence of the numerical model in both the linear and the nonlinear regimes.

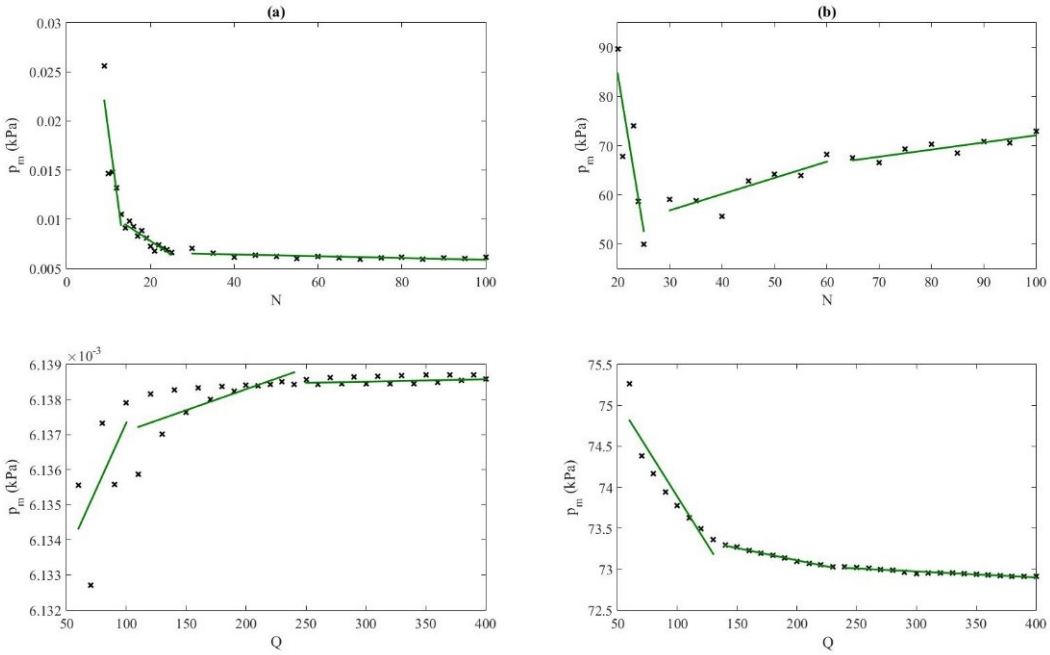

Figure 5.9: Convergence curves, showing the maximum pressure amplitude vs. number of control volumes (top) and time points per period (bottom): (a) linear and (b) nonlinear regimes. Single-frequency source case.

Acknowledgements

The authors acknowledge the support of the National Agency for Research (Agencia Estatal de Investigación, AEI), Ministry of Economy, Industry, and Competitiveness of Spain (Ministerio de Economía, Industria y Competitividad), Ministry of Science, Innovation, and Universities of Spain (Ministerio de Ciencia, Innovación y Universidades), and the European Regional Development Fund (FEDER) [grant numbers DPI2012-34613, BES-2013-064399, and DPI2017-84758].

Christian Vanhille dedicates this work to Dr. Cleofé Campos-Pozuelo.

References

[1] K. Naugolnykh, L. Ostrovsky, Nonlinear Wave Processes in Acoustics, Cambridge University Press, New York, 1998.

[2] M.F. Hamilton, D.T. Blackstock (Eds.), Nonlinear Acoustics, Academic Press, San Diego, 1998.

[3] F. Grieser, P.K. Choi, N. Enomoto, H. Harada, K. Okitsu, K. Yasui (Eds.), Sonochemistry and the Acoustic Bubble, Elsevier, Amsterdam, 2015.

[4] T.S. Desser, R.B. Jeffrey, Tissue harmonic imaging tecniques: physical principles and clinical aplications, Semin. Ultrasound CT MR 22 (2001) 1-10.

[5] M. Cavaro, C. Payan, J. Moysan, F. Baqué, Microbubble cloud characterization by nonlinear frequency mixing, J. Acoust. Soc. Am. 129 (2011) EL179-EL183.

[6] J.C. Buckey, D.A. Knaus, D.L. Alvarenga, M.A. Kenton, P.J. Magari, Dual-frequency ultrasound for detecting and sizing bubbles, Acta Astronaut. 56 (2005) 1041-1047.

[7] V.L. Newhouse, P.M. Shankar, Bubble size measurement using the nonlinear mixing of two frequencies, J. Acoust. Soc. Am. 75 (1984) 1473-1477.

[8] B.N. Kim, S.W. Yoon, Nonlinear parameter estimation in water-satured sandy sediment with difference frequency acoustic wave, Ultrasonics 49 (2009) 438-445.

[9] D.N. Sinha, C. Pantea, Broadband unidirectional ultrasound propagation using sonic crystal and nonlinear medium, Emerg. Mater. Res. 2 (2013) 117-126.

[10] V.V. Krylov, D.F. Parker, Harmonic generation and parametric mixing in wedge acoustic waves, Wave Motion 15 (1992) 185-200.

[11] J.D. Ryder, P.H. Rogers, J. Jarzynski, Radiation of difference-frequency sound generated by nonlinear interaction in a silicone rubber cylinder, J. Acoust. Soc. Am. 59 (1976) 1077-1086.

[12] E.A. Zabolotskaya, S.I. Soluyan, Emission of harmonic and combination-frequency waves by air bubbles, Sov. Phys. Acoust. 18 (1973) 396-398.

[13] Y.A. Kobelev, A.M. Sutin, Difference-frequency sound generation in a liquid containing bubbles of different sizes, Sov. Phys. Acoust. 26 (1980) 485-847.

[14] O.A. Druzhinin, L.A. Ostrovsky, A. Prosperetti, Low-frequency acoustic wave

generation in a resonant bubble layer, J. Acoust. Soc. Am. 100 (1996) 3570-3580.

[15] Q.Y. Ma, Y.Y Qiu, B. Huang, D. Zhang, X.F. Gong, Difference-frequency ultrasound generation from microbubbles under dual-frequency excitation, Chinese Phys. B 19 (2010) 094302.

[16] C. Vanhille, C. Campos-Pozuelo, D.N. Sinha, Nonlinear frequency mixing in a resonant cavity: numerical simulations in a bubbly liquid, Ultrasonics, 54 (2014) 2051-2054.

[17] M.T. Tejedor Sastre, C. Vanhille, A numerical model for the study of the difference frequency generated from nonlinear mixing of standing ultrasonic waves in bubbly liquids, Ultrason. Sonochem. 34 (2017) 881-888.

[18] M.T. Tejedor Sastre, C. Vanhille, Numerical models for the study of the nonlinear frequency mixing in two and three-dimensional resonant cavities filled with a bubbly liquid, Ultrason. Sonochem. 39 (2017) 597-610.

[19] C. Vanhille, Two-dimensional numerical simulations of ultrasound in liquids with gas bubble agglomerates: Examples of bubbly-liquid-type acoustic metamaterials (BLAMMs), Sensors, 17 (2017) 173.

[20] P.Z. He, R.M. Xia, S.M. Duan, W.D. Shou, D.C. Qian, The affection on the tissue lesions of difference frequency in dual-frequency high-intensity focused ultrasound (HIFU), Ultrason. Sonochem. 13 (2006) 339-344.

[21] P.J. Westervelt, Parametric Acoustic Array, J. Acoust. Soc. Am. 35 (1963) 535-537.

[22] G.D. Smith, Numerical Solution of Partial Differential Equations, Finite Difference Methods, Clarendon Press, Oxford, 1985.

[23] C. Vanhille, A. Lavie, C. Campos-Pozuelo, Modélisation numérique en mécanique: introduction et mise en pratique, Hermes Science Publications, Lavoisier, Paris, 2007.

[24] H.K. Versteeg, W. Malalasekera, An introduction to computational fluid dynamics: the finite volume method, John Wiley y Sons Inc., New York, 1995

[25] C. Vanhille, C. Campos-Pozuelo, A high-order finite-difference algorithm for the analysis of standing acoustic waves of finite but moderate amplitude, J. Comput. Phys., 165 (2000) 334-353.

[26] C. Vanhille, C. Campos-Pozuelo, Numerical model for nonlinear standing

waves and weak shocks in thermoviscous fluids, J. Acoust. Soc. Am., 109 (2001) 2660-2667.

[27] K.W. Morton, D.F. Mayers, Numerical Solution of Partial Differential Equations, Cambridge University Press, Cambridge, 1994.

Discusión general

Esta etapa de formación ha dado lugar al desarrollo de varios modelos numéricos en una, dos y tres dimensiones (con simetría axial) basados en el método de volúmenes finitos, en las dimensiones espaciales, y el método de las diferencias finitas, en el dominio temporal, que simulan la propagación del campo ultrasónico en líquidos con burbujas. El sistema de ecuaciones diferenciales formado por la ecuación de ondas y una ecuación de Rayleigh-Plesset, acoplando así la presión acústica y las oscilaciones en el volumen de las burbujas, describe este comportamiento y ha sido resuelto para obtener conclusiones físicas.

En primer lugar se ha desarrollado un nuevo modelo numérico capaz de simular la propagación ultrasónica en líquidos con burbujas en resonadores unidimensionales y que ha sido validado por comparación con resultados publicados en la literatura. Con este modelo se ha estudiado la generación de armónicos, con fuentes mono-frecuenciales, en función de la amplitud de la fuente para así poder proponer leyes que rigen su comportamiento. En particular se ha obtenido que el segundo armónico se ajusta a un polinomio de grado dos mientras que el tercer armónico se ajusta a un polinomio de grado cuatro. Asimismo, el análisis de su formación en función de la cantidad de burbujas presentes en el medio se ha llevado a cabo. En este caso ambas frecuencias se ajustan a polinomios de grado seis, llegando a observar una saturación cuando el número de burbujas aumenta. En este trabajo se ha investigado también las longitudes de resonador que son más eficientes a la hora de potenciar la producción de armónicos, obteniendo así mucho mejores resultados cuando se trabaja con resonadores múltiplos de $\lambda/2$ (se han obtenido resultados para la mejora en la producción del segundo armónico que van del 1 % para múltiplos de $\lambda/4$ al 180 % con múltiplos de $\lambda/2$ respecto a la amplitud de la fuente). De igual modo, se ha estudiado la mezcla de frecuencias cuan-

do se excita el sistema con fuentes bi-frecuenciales y teniendo en cuenta la condición mencionada anteriormente sobre la longitud de los resonadores. Se ha obtenido una amplitud del 110 % para la frecuencia diferencia respecto de la amplitud de la fuente (resultado muy alto comparado con la literatura). Igualmente, se ha propuesto una ley para su comportamiento (en este caso su generación sigue una ley polinómica de grado cuatro) y se ha investigado la eficiencia de su producción en función de las frecuencias fuente obteniendo mejores resultados para frecuencias por debajo de la resonancia de las burbujas (del 154 % por debajo de la frecuencia de resonancia al 27 % por encima respecto a la amplitud de la fuente). Este detallado estudio del comportamiento de los campos ultrasónicos en líquidos con burbujas ha permitido un primer acercamiento al problema físico considerado en esta tesis que ha servido como base fundamental para el entendimiento de los fenómenos y de referencia para todos los estudios en dos y tres dimensiones desarrollados a partir de este estudio unidimensional.

Una vez hecho el profundo estudio unidimensional, se ha aumentado el número de dimensiones para acercarse a la realidad física del problema que se investiga en esta tesis doctoral. Se han desarrollado varios modelos numéricos que simulan la interacción entre el campo ultrasónico y las burbujas con diferentes geometrías en dos y tres dimensiones (con paredes verticales, horizontales, oblicuas o curvas) con diferentes fuentes (de una o dos frecuencias y con diferentes perfiles de crecimiento en su amplitud) y condiciones de contorno (paredes libres o reflectantes). En este estudio se hace un primer cálculo de la frecuencia de resonancia (en régimen lineal) de cada una de las cavidades a partir de un software comercial (COMSOL Multiphysics), y a partir de esa frecuencia obtenida se hace un barrido más fino a fin de conseguir la verdadera frecuencia de resonancia del modelo. Los armónicos, con fuentes mono-frecuenciales, han sido estudiados obteniendo para los trabajos bidimensionales amplitudes para el segundo armónico que oscilan entre el 157 % y el 41 % y para el tercer armónico entre el 94 % y el 12 %. Para los modelos tridimensionales se han obtenido amplitudes que van desde el 29 % al 5 % para el segundo armónico y del 6 % al $0,5$ % para el tercer armónico. La frecuencia diferencia también ha sido estudiada obteniéndose amplitudes que van desde el 33 % al 25 % para el caso bidimensional y entre el 7 % y el 2 % para los casos tridimensionales. La gran diferencia en los porcentajes entre los casos bidimensionales, tridimensionales y el caso

unidimensional se debe principalmente a la relación entre el tamaño de la fuente y el tamaño de la cavidad. Este estudio ha revelado una gran versatilidad de los modelos numéricos desarrollados con cualquier geometría y condición de contorno.

A partir de los modelos en dos y tres dimensiones, en la búsqueda de la frecuencia de resonancia de las cavidades, se ha observado una mejor respuesta (trabajando en régimen no lineal) con frecuencias un poco inferiores a la resonancia en régimen lineal. Este fenómeno ha sido muy poco estudiado en la literatura y por tanto, el modelo unidimensional ha sido retomado a fin de analizarlo. Se ha estudiado la variación de la frecuencia de resonancia de la cavidad unidimensional (y por tanto en la velocidad de propagación de la onda) al aumentar la amplitud de la fuente para varias densidades de burbujas. Se han propuesto leyes que describen este comportamiento obteniendo que la variación en dicha frecuencia se ajusta a polinomios de grado tres para todas las densidades estudiadas. Además, se ha justificado el fenómeno debido a un aumento del volumen efectivo de la burbuja, pues al aumentar la amplitud aumenta el volumen en torno al cual oscila la burbuja, y por tanto, aumenta la fracción de volumen ocupada por el gas y, como consecuencia, disminuye la velocidad de propagación de la onda. La variación en dicha frecuencia sigue una relación lineal con dicho volumen, lo que conlleva dicha disminución en la velocidad de propagación de la onda. Este estudio ha dado paso a su aplicación en la generación de la frecuencia diferencia y, al tener en cuenta este fenómeno, se ha obtenido una amplitud del 174 % respecto a la amplitud de la fuente. Este resultado es muy interesante de cara a la optimización de cavidades resonantes en procesos industriales, pues con sólo una ligera variación de la frecuencia o de la geometría, se puede aumentar en gran medida la generación de las componentes frecuenciales de las señales ultrasónicas.

Por último, se ha desarrollado un modelo numérico tridimensional que simula la propagación ultrasónica en líquidos con burbujas para estudiar los armónicos y mezcla de frecuencias a partir de un transductor esférico que produce campos focalizados. Las condiciones de contorno en este caso son de campo abierto, para que no haya ningún tipo de reflexión. Se ha analizado la producción de armónicos, con fuentes mono-frecuenciales, y la generación de las frecuencias suma y diferencia, con fuentes bi-frecuenciales, en función de la amplitud de la fuente, obteniendo leyes que rigen su

comportamiento. En este caso los armónicos se ajustan a polinomios de grado dos para el segundo armónico, de grado tres para el tercer armónico, y en el caso de la mezcla, polinomios de grado dos para la frecuencia diferencia y de grado tres para la frecuencia suma. Las amplitudes para este caso han sido del 331 % para el segundo armónico, 188 % para el tercer armónico, 35 % para la frecuencia diferencia y 78 % para la suma. Este estudio ha mostrado dos posibles aplicaciones del uso de la mezcla de frecuencias en campos focalizados. Con la frecuencia suma se podría localizar el foco con mucha más precisión que con otras frecuencias debido a que el pico que presenta es muy agudo y más restringido espacialmente, mientras que con la frecuencia diferencia se podrían hacer medidas mucho más allá del foco debido a su menor atenuación, lo que podría ser interesante en el marco de la detección de burbujas.

Todos los modelos numéricos desarrollados en esta tesis doctoral son propios. Desde las ecuaciones que describen el problema físico considerado, se han aplicado técnicas basadas en el método de los volúmenes finitos y de las diferencias finitas, obteniendo así un sistema de ecuaciones discretizadas. Mediante la compleja implementación de los correspondientes códigos en el lenguaje de programación Matlab, se han hecho las simulaciones pertinentes para obtener todos los resultados presentados en esta tesis. Este arduo proceso tiene la gran ventaja de mantener un control total del modelo.

En esta etapa de formación se han desarrollado modelos numéricos propios capaces de simular los fenómenos acústicos no lineales en líquidos con burbujas de gas. Estos modelos permitirán seguir haciendo estudios que nos acercarán cada vez más a la comprensión de este complejo problema y del comportamiento de los efectos asociados. Esta investigación se llevará a cabo en el marco del nuevo proyecto financiado por el Plan Nacional [DPI2017-84758].

Uno de los logros de este trabajo ha sido el conseguir optimizar la generación de armónicos y la mezcla de frecuencias en líquidos con burbujas teniendo en cuenta las dimensiones y las frecuencias idóneas que hacen que su producción sea más eficiente. Como continuación de esta labor, el siguiente paso será hacer un estudio de optimización del medio, es decir, estudiar qué tamaño y cantidad de burbujas, para una frecuencia dada, hacen que la generación no lineal sea más eficaz.

Otra de las líneas que se seguirá a partir de este trabajo es considerar modelos

más realistas intentando acoplar las vibraciones de las paredes de las cavidades con la propagación acústica en el medio con burbujas e incluir términos en las ecuaciones que den cuenta de contribuciones no tenidas en cuenta es esta tesis, como podrían ser la tensión superficial o las fuerzas de Bjerknes.

También se prevé desarrollar modelos donde la distribución y los tamaños de las burbujas no sean uniformes. Además, se desarrollarán modelos que estudien la propagación a través de distintos medios, modelos de capas con presencia/ausencia de burbujas o con distintas densidades.

De igual modo, se intentarán hacer mejoras en los modelos desarrollados usando aproximaciones más finas que den lugar a errores de truncamiento más pequeños.

Por otra parte, podría ser muy interesante intentar acoplar más variables al modelo como por ejemplo ecuaciones que den cuenta de efectos térmicos al producirse los efectos no lineales.

De una manera global, esta etapa de formación predoctoral ha sido un estímulo para seguir estudiando en el futuro fenómenos no lineales en acústica mediante el desarrollo de modelos numéricos propios.

Conclusiones generales

En este trabajo, mediante el desarrollo de nuevos modelos numéricos, se ha conseguido definir leyes físicas que ayudan a comprender el comportamiento muy complejo de campos ultrasónicos en un tipo específico de medio no lineal, a saber, los líquidos con burbujas.

Los modelos numéricos desarrollados en esta tesis han demostrado ser una herramienta muy poderosa para simular la interacción no lineal mutua entre presión acústica de amplitud finita y variaciones de volumen de las burbujas de gas, que viene descrita por un sistema diferencial acoplando la ecuación de ondas y una ecuación de Rayleigh-Plesset. Este sistema es resuelto por los nuevos modelos numéricos que presentan gran versatilidad a la hora de llevar a cabo simulaciones en cualquier geometría con diversos tipos de condiciones de contorno. Han permitido analizar en profundidad los efectos no lineales buscados y proponer leyes físicas que los describen. En particular, se han propuesto leyes para la generación de armónicos y de frecuencias suma y diferencia como función de las principales causas que influyen en su producción, que son la amplitud de la fuente y la cantidad de burbujas presentes en el medio.

Asimismo, nuestros desarrollos numéricos han facilitado el estudio sobre las condiciones a tener en cuenta para potenciar tanto la producción de armónicos como la frecuencia suma y diferencia. Así, condiciones sobre las cavidades y sobre las frecuencias de excitación para que esa generación sea mucho más eficiente han sido obtenidas. Han permitido también observar fenómenos muy poco estudiados anteriormente en este tipo de medios que sugieren un cambio en la velocidad de propagación de la onda (ablandamiento del medio) al aumentar su amplitud. Se han propuesto leyes que cuantifiquen esta variación en función de las amplitudes con las que se trabaje.

General conclusions

In this work, by means of the development of new numerical models, physical laws have been defined to better understand the very complex behavior of ultrasonic fields in a specific type of nonlinear medium, namely bubbly liquids.

The numerical models developed in this thesis are a very powerful tool to simulate the mutual nonlinear interaction between finite-amplitude acoustic pressure and volume variations of gas bubble, described by a differential system that couples the wave equation and a Rayleigh-Plesset equation. This system is solved by the new numerical models that present huge versatility when performing simulations in any geometry with different kinds of boundary conditions. They have made it possible to analyze thoroughly the intended nonlinear effects and to propose physical laws that describe them. In particular, some laws have been proposed for the generation of harmonic components, and sum and difference frequencies, as a function of the main parameters that influence their production, which are the source amplitude and the amount of bubbles in the medium.

Additionally, our numerical developments have provided the study about the conditions that must be taken into account to enhance the production of harmonic components and sum and difference frequencies. In this way, conditions on the cavities and on the driven frequencies that make that generation much more efficient have been obtained. They have also allowed us to observe phenomena insufficiently studied previously in this kind of media that suggest a change in the sound speed (smoothing of the medium) by increasing the source amplitude. Laws that quantify this variation as a function of the wave amplitude have been proposed.

Apéndice A

Análisis del comportamiento numérico

A.1. Convergencia

La convergencia de los modelos numéricos desarrollados en esta tesis doctoral se alcanza si al tomar cada vez más pasos temporales y volúmenes espaciales, los resultados tienden hacia un mismo valor finito [1]. En este apéndice se estudia la convergencia para el caso unidimensional, modelo desarrollado en el Capítulo 2 y con el que también se trabaja en el Capítulo 4. En este caso se trabaja con un resonador de longitud $L = \lambda/2 = 0{,}0031\ m$. Se va variando el número de volúmenes espaciales desde $N = 5$ hasta $N = 100$, que se corresponden con longitudes de volumen de control de $h = 3{,}057 \times 10^{-4}\ m$ a $h = 1{,}529 \times 10^{-5}\ m$. El número de pasos temporales por periodo $T = 1/f$, donde $f = 200kHz$, va desde $M = 25$ hasta $M = 400$, que se corresponde con pasos temporales que van de $\tau = 2 \times 10^{-7}\ s$ a $\tau = 1{,}25 \times 10^{-8}\ s$. Para cada una de las combinaciones de (h, τ) se toma el valor máximo de la presión en el último periodo temporal. Cada experimento numérico dura un tiempo total $T_t = 100\ T$. Este estudio se hace tanto en baja amplitud $p_0 = 1\ Pa$ (Fig. A.1a), cuyo valor máximo de presión está en torno a los 100 Pa, como en alta amplitud $p_0 = 250\ Pa$ (Fig. A.1b), cuyo valor máximo de presión está en torno a los 20 kPa. Como se puede observar, el modelo es convergente ya que, cuanto más pasos temporales y espaciales se toman, el valor del

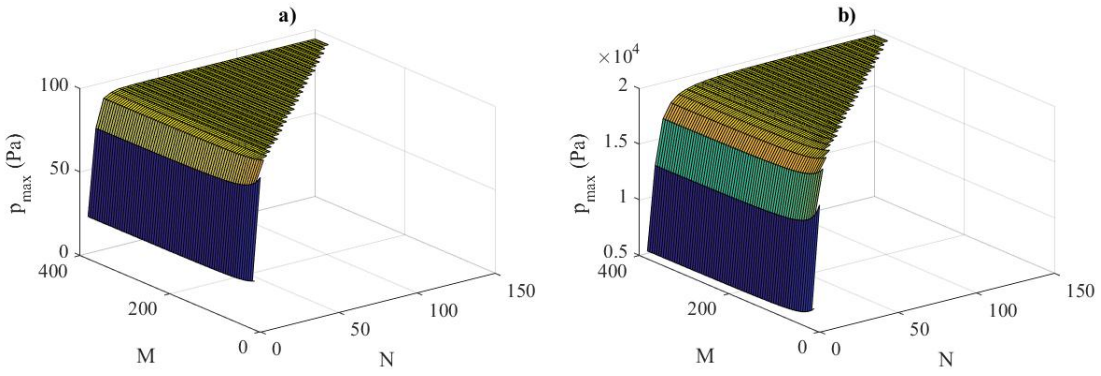

Figura A.1: Presión máxima en función del número de volúmenes N e intervalos temporales M. a) $p_0 = 1\ Pa$. b) $p_0 = 1\ Pa$

máximo de presión tiende a un valor constante. En ambos casos casos la convergencia es rápida como se observa en la Fig. A.1, tanto en baja como en alta amplitud, el valor de la presión se aproxima a un plano cuando el número de pasos e intervalos aumenta. También cabe destacar que el modelo tiene un comportamiento correcto para ciertos valores (h, τ) y para otros no (donde no se obtiene solución). Este estudio se hace a continuación, pero a simple vista se observa que estos valores (h, τ) son los mismos independientemente de la amplitud.

A.2. Estabilidad

Los modelos numéricos desarrollados en esta tesis doctoral se consideran estables si la solución obtenida al introducir una perturbación en los datos iniciales sigue siendo acotada. El método de von Neumann es una herramienta para analizar la estabilidad de un método numérico [1]. Si se supone un error o perturbación del sistema escrito a través de una serie de Fourier finita y se introduce en la ecuación discretizada, se podrá evaluar cómo evoluciona el error dando unas condiciones sobre la estabilidad del sistema. Para el sistema considerado en esta tesis el método consiste en suponer una perturbación del sistema de la forma

$$p(x,t) = \sum_{m=-q}^{+q} p_{0m} e^{i\beta x} e^{i\alpha t}, \tag{A.1}$$

$$v(x,t) = \sum_{m=-q}^{+q} v_{0m} e^{i\beta x} e^{i\alpha t}, \tag{A.2}$$

donde p es la perturbación en la presión (siendo p_{0m} su amplitud), v es la perturbación en el volumen (siendo v_{0m} su amplitud), $i = \sqrt{-1}$, β y α son las frecuencias espacial y temporal respectivamente. Estas perturbaciones escritas de un modo discretizado para un término de la serie evolucionando separadamente de los otros son de la forma $p_{m(n,j)} = p_{0m} e^{i\beta nh} e^{i\alpha j\tau}$ y $v_{m(n,j)} = v_{0m} e^{i\beta nh} e^{i\alpha j\tau}$, donde $x = nh$ y $t = j\tau$, y verificarán las ecuaciones formadas por Eq. (1.29) y Eq. (1.50) ya discretizadas. Para ver qué condiciones aseguran la estabilidad del sistema discretizado, se impone que el valor absoluto del factor de amplificación ξ sea menor o igual a 1, $|\xi| = |e^{i\alpha\tau}| \leq 1$, así el error inducido por la perturbación estará acotado. Esto permite obtener condiciones sobre el paso temporal τ y sobre la longitud del volumen espacial h que garantizan la estabilidad del sistema. La estrategia para usar el método con este sistema de ecuaciones es tomar la ecuaciones como desacopladas para obtener una relación en cada una de ellas.

La ecuación discretizada mediante el método de los volúmenes finitos en la dimensión espacial y el método de las diferencias finitas en la dimensión temporal para la ecuación de ondas no lineal, Eq. (1.29), es

$$\tau^2(p_{n+1,j} - 2p_{n,j} + p_{n-1,j}) - \frac{h^2}{c_{0l}^2}(p_{n,j+1} - 2p_{n,j} + p_{n,j-1}) \\ = -\rho_0 N_g h^2(v_{n,j+1} - 2v_{n,j} + v_{n,j-1}). \tag{A.3}$$

Si se toman como independientes una de la otra entonces $v = 0$. La Eq. A.3 queda entonces

$$\frac{c_{0l}^2\tau^2}{h^2}(p_{n+1,j} - 2p_{n,j} + p_{n-1,j}) = p_{n,j+1} - 2p_{n,j} + p_{n,j-1}. \tag{A.4}$$

Si se denomina $A = c_{0l}^2\tau^2/h^2$ y se sustituye la perturbación $p_{m(n,j)} = p_{0m}e^{i\beta nh}e^{i\alpha j\tau}$ en la Eq. (A.4) se tiene

$$Ap_{0m}e^{i\alpha j\tau}(e^{i\beta(n+1)h} - 2e^{i\beta nh} + e^{i\beta(n-1)h}) \\ = p_{0m}e^{i\beta nh}(e^{i\alpha(j+1)\tau} - 2e^{i\alpha j\tau} + e^{i\alpha(j-1)\tau}). \tag{A.5}$$

Si ahora se divide todo por $p_{0m}e^{i\beta nh}e^{i\alpha j\tau}$ se obtiene

$$(Ae^{i\beta h} - 2 + e^{-i\beta h}) = (e^{i\alpha\tau} - 2 + e^{-i\alpha\tau}). \tag{A.6}$$

Usando la relación $cos(\beta h) = (e^{i\beta h} + e^{-i\beta h})/2$ y si se sustituye $\xi = e^{i\alpha\tau}$ se obtiene

$$2A(cos(\beta h) - 1) = e^{i\alpha\tau} - 2 + e^{-i\alpha\tau}, \tag{A.7}$$

$$2A(cos(\beta h) - 1) = \xi - 2 + \xi^{-1}. \tag{A.8}$$

Haciendo uso de la relación trigonométrica $(cos(\beta h) - 1) = -2sen^2(\beta h/2)$ y multiplicando por ξ y reorganizando la ecuación se obtiene

$$-4Asen^2\left(\frac{\beta h}{2})\right) = \xi - 2 + \xi^{-1}, \tag{A.9}$$

$$\xi^2 - 2\left(1 - 2Asen^2\left(\frac{\beta h}{2}\right)\right)\xi - 1 = 0. \tag{A.10}$$

Cuyas soluciones son de la forma

$$\xi_\pm = \left(1 - 2Asen^2\left(\frac{\beta h}{2}\right)\right) \pm \sqrt{\left(1 - 2Asen^2\left(\frac{\beta h}{2}\right)\right)^2 - 1}. \tag{A.11}$$

El seno cuadrado está acotado por 1 y como A es positivo, entonces se verifica que $1 - 2Asen^2\left(\frac{\beta h}{2}\right) \leq 1$. Se pueden tener dos opciones:
$i)$ $1 - 2Asen^2\left(\frac{\beta h}{2}\right) < -1$.
$ii)$ $-1 \leq 1 - 2Asen^2\left(\frac{\beta h}{2}\right) \leq 1$.

Si se da $i)$ las raíces son reales con $\xi_- < -1$ y por tanto $|\xi_-| > 1$ luego en este caso habría inestabilidad. Si se da $ii)$ las raíces son complejas conjugadas y $|\xi_{+,-}| \leq 1$ luego habría estabilidad. La condición $ii)$ es equivalente a poner $0 \leq Asen^2\left(\beta h/2\right) \leq 1$, entonces $0 < A \leq 1$. La condición de estabilidad es $0 < c_{0l}^2\tau^2/h^2 \leq 1$ o $0 < c_{0l}\tau/h \leq 1$ [1].

Para la ecuación de la burbuja, Eq. (1.50), se sigue un proceso análogo suponiendo ahora $p = 0$ para que sean independientes. Además, se considera que las constantes a y b de la ecuación son nulas ya que se trabaja en régimen lineal. Entonces la ecuación discretizada usando el método de los volúmenes finitos en la dimensión espacial y el método de las diferencias finitas en la dimensión temporal es

$$(v_{n,j+1} - 2v_{n,j} + v_{n,j-1}) + \tau\delta\omega_{0g}(v_{n,j} - v_{n,j-1}) + \omega_{0g}^2\tau^2 v_{n,j} = 0. \tag{A.12}$$

Ahora se supone que la perturbación $v_{m(n,j)} = v_{0m}e^{i\beta nh}e^{i\alpha j\tau}$ es solución de la ecuación,

$$\begin{aligned} v_{0m}e^{i\beta nh}(e^{i\alpha(j+1)\tau} - 2e^{i\alpha j\tau} + e^{i\alpha(j-1)\tau}) + \tau\delta\omega_{0g}v_{0m}e^{i\beta nh}(e^{i\alpha j\tau} - e^{i\alpha(j-1)\tau}) \\ +\omega_{0g}^2\tau^2 v_{0m}e^{i\beta nh}e^{i\alpha j\tau} = 0. \end{aligned} \tag{A.13}$$

Si ahora se divide toda la ecuación por $v_{0m}e^{i\beta nh}e^{i\alpha j\tau}$ y se sustituye $\xi = e^{i\alpha\tau}$ se obtiene:

$$(e^{i\alpha\tau} - 2 + e^{-i\alpha\tau}) + \tau\delta\omega_{0g}(1 - e^{-i\alpha\tau}) + \omega_{0g}^2\tau^2 = 0, \tag{A.14}$$

$$(\xi - 2 + \xi^{-1}) + \tau\delta\omega_{0g}(1 - \xi^{-1}) + \omega_{0g}^2\tau^2 = 0. \tag{A.15}$$

Multiplicando por ξ y reorganizando la ecuación se tiene

$$\xi^2 + \xi(-2 + \tau\delta w_{0g} + w_{0g}^2\tau^2) + (1 - \tau\delta w_{0g}) = 0, \tag{A.16}$$

cuyas soluciones serán de la forma:

$$\xi_\pm = \frac{(2 - \tau\delta w_{0g} - w_{0g}^2\tau^2) \pm \sqrt{(-2 + \tau\delta w_{0g} + w_{0g}^2\tau^2)^2 - 4(1 - \tau\delta w_{0g})}}{2}. \tag{A.17}$$

Ahora habría que ver para que valor de τ se cumple $|\xi_\pm| \leq 1$. Dado que esta ecuación sólo es dependiente del tiempo entonces sólo da información sobre las restricciones en τ . Como no son funciones que a priori se puedan acotar, se procede a ver un ejemplo concreto y a representar las soluciones en función de τ para ver qué valores de τ cumplen tal condición. Una vez hecho esto, se puede usar la condición obtenida en la ecuación anterior a fin de dar las condiciones de convergencia.

A.2.1. Ejemplo

Se supone que se trabaja con un líquido, agua, con burbujas de gas, aire, de radio $R_{0g} = 2{,}5 \times 10^{-6}\ m$. La frecuencia de resonancia para las burbujas es $\omega_{0g} = \sqrt{3\gamma_g p_{0g}/\rho_{0l}R_{0g}^2} = 8{,}46 \times 10^6\ rad/s$ tomando $\gamma_g = 1{,}4$ y $p_{0g} = \rho_{0g}c_{0g}^2/\gamma_g = 1{,}0652 \times 10^5\ Pa$ donde $\rho_{0g} = 1{,}29\ kg/m^3$, $\rho_{0l} = 1000\ kg/m^3$ son las densidades y $c_{0g} = 340\ m/s$ es la velocidad del sonido en el gas en el estado de equilibrio. $\delta = 4\nu_l/\omega_{0g}R_{0g}^2 = 0{,}1082$ es el coeficiente de viscosidad donde $\nu_l = 1{,}43 \times 10^{-6}\ m^2/s$ es la viscosidad cinemática. En la Fig. A.2 se representa el valor absoluto de $\xi_\pm$ en función de τ. Se observa como ξ_+ en valor absoluto es siempre menor que uno mientras que ξ_- llega un valor para el cual su valor absoluto es mayor que 1 y conduciría por tanto a la inestabilidad. Ese valor se corresponde con $\tau_m = 2{,}2395 \times 10^{-7}\ s$. Entonces la condición para la estabilidad debida a la ecuación de la burbuja en este caso es $\tau \leq \tau_m$. Esta condición sólo depende de los parámetros del medio y es independiente de la ecuación de ondas que se use, es decir, no depende de la geometría ni de las dimensiones del modelo considerado. Si ahora se considera la condición debida a la ecuación de ondas se tiene que los valores que conducen a valores estables de la solución son aquellos que verifican $h \geq c_{0l}\tau$ y además $\tau \leq \tau_m$. Para ilustrar estas condiciones se representan en la Fig. A.3.

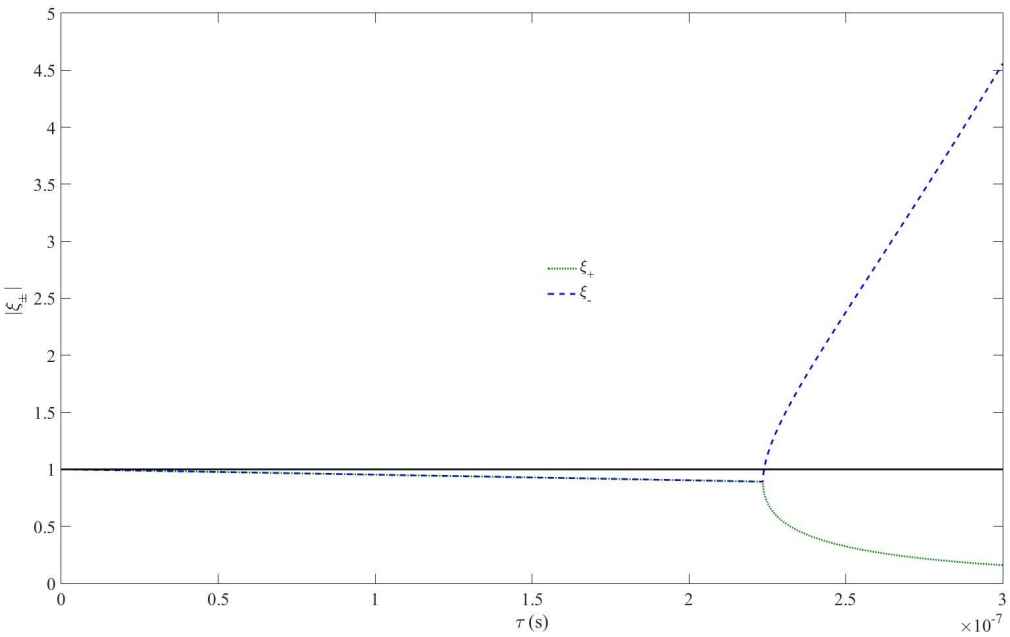

Figura A.2: Valor absoluto de las soluciones de la Eq.(A.17)

.

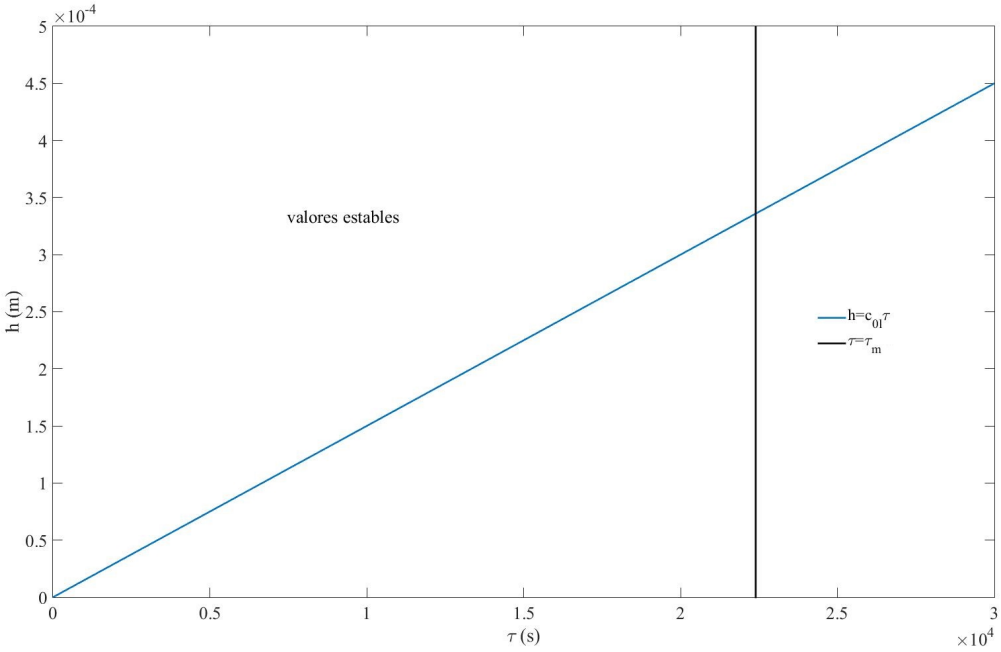

Figura A.3: Relaciones h vs. τ que conducen a soluciones estables.

Estas condiciones de estabilidad son una aproximación de la estabilidad del modelo, ya que se ha supuesto que las ecuaciones están desacopladas y linealizadas ($a = 0$ y $b = 0$). Ahora se estudia cómo se comporta el modelo unidimensional tomando los mismos valores que se ha supuesto en las ecuaciones y se usa un caso análogo al Capítulo 4 con la diferencia que ahora se toma un resonador más largo, $L = 3\lambda$, a fin de poder tener volúmenes más grandes que permitan analizar el modelo. Para ilustrar este comportamiento se representan las condiciones obtenidas con el modelo en la Fig. A.4. Como se observa en la Fig. A.4, el comportamiento es similar al obtenido analíticamente, Fig. A.3, hay un valor máximo de τ para que el sistema sea estable: en este caso $\tau_{mn} = 1{,}78 \times 10^{-7}s$. Además, para valores pequeños de τ se observa que tiene claramente un comportamiento lineal. Si se hace un ajuste para esos valores se obtiene que se aproxima a la ecuación $h = 1532{,}3\tau - 5{,}0825 \times 10^{-7}$. La pendiente de esta recta, 1532,3, es un poco mayor al valor obtenido analíticamente $c_{0l} = 1500$. También cabe destacar que tanto analíticamente como numéricamente, en todos los modelos desarrollados en esta tesis se ha trabajado en condiciones de estabilidad, pues siempre se ha comprobado que se verifiquen dichas condiciones. Por ejemplo, en la sección 3.2 del Capítulo 2, donde se trabaja con el mismo medio considerado en este ejemplo, se hacen simulaciones con pasos temporales $\tau_2 = 3{,}125 \times 10^{-8}\ s$ y longitudes de los volúmenes $h_2 = 4{,}777 \times 10^{-5}\ m$. h_2 está por encima del valor mínimo de estabilidad analítico que sería $h_{2a} = c_{0l}\tau_2 = 4{,}6875 \times 10^{-5}\ m$ y del numérico que sería $h_{2n} = 1532{,}3\tau_2 - 5{,}0825 \times 10^{-7} = 4{,}7376 \times 10^{-5}\ m$. En la sección 3.1 del Capítulo 4, donde se vuelve a tener el mismo medio y modelo, se trabaja con frecuencias que oscilan entre $f_{41} = 198{,}74\ kHz$ y $f_{42} = 202{,}50\ kHz$, lo cual tomando 400 intervalos temporales por periodo nos lleva a pasos temporales entre $\tau_{41} = 1{,}2579 \times 10^{-8}s$ y $\tau_{42} = 1{,}2346 \times 10^{-8}s$. La longitud de los volúmenes en este estudio es siempre $h_4 = 2{,}3883 \times 10^{-5}\ m$. h_4 está muy por encima del mínimo para la estabidad tanto analítica $h_{41a} = c_{0l}\tau_{41} = 1{,}8869 \times 10^{-5}\ m$ como numérica $h_{41n} = 1532{,}3\tau_{41} - 5{,}0825 \times 10^{-7} = 1{,}8767 \times 10^{-5}\ m$ para τ_{41}. h_4 también está por encima del mínimo para la estabidad tanto analítica $h_{42a} = c_{0l}\tau_{42} = 1{,}8519 \times 10^{-5}\ m$ como numérica $h_{42n} = 1532{,}3\tau_{42} - 5{,}0825 \times 10^{-7} = 1{,}8409 \times 10^{-5}\ m$ para τ_{42}.

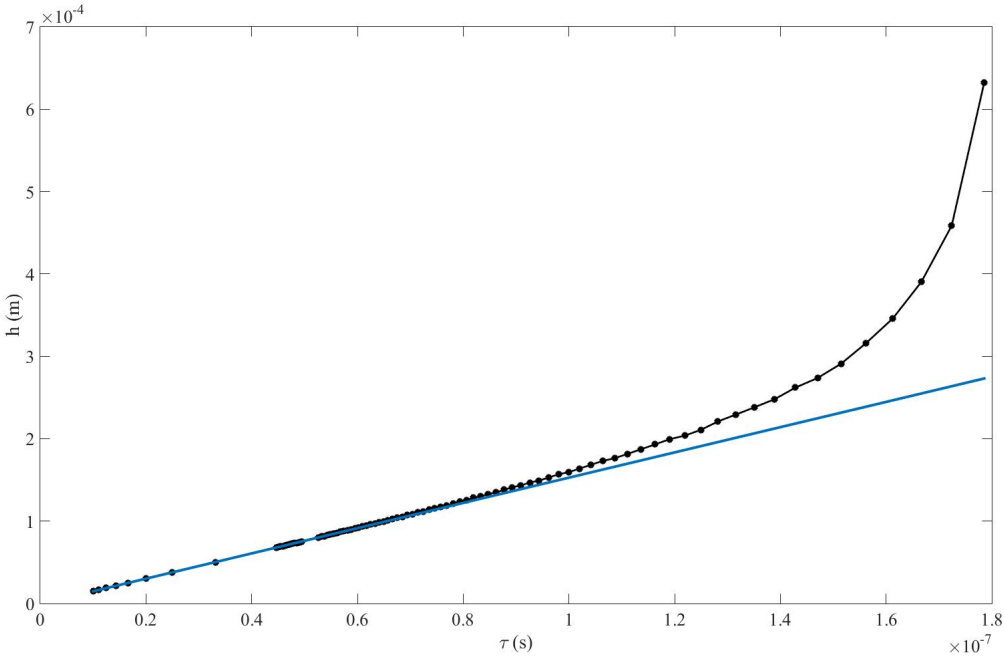

Figura A.4: Relaciones h vs. τ del modelo obtenidas numéricamente.

Referencias

[1] C. Vanhille, A. Lavie, C. Campos-Pozuelo, Modélisation numérique en mécanique: introduction et mise en pratique, Hermes Science Publications, Lavoisier, París, 2007.

Apéndice B

Transformada Rápida de Fourier (FFT)

La transformada discreta de Fourier, o DFT, es un tipo de transformada discreta que permite expresar un conjunto discreto de datos temporales en el dominio de la frecuencia y viceversa [1]. Se define la transformada discreta de Fourier y su inversa como

$$F_k = \sum_{n=0}^{N-1} f_n e^{-ik\omega_0 n},\ k = 0, 1, 2, ..., N-1, \tag{B.1}$$

$$f_n = \frac{1}{N} \sum_{k=0}^{N-1} F_k e^{ik\omega_0 n},\ n = 0, 1, 2, ..., N-1, \tag{B.2}$$

donde N es el número de datos, el subíndice n indica los tiempos discretos donde se toman las muestras y el subíndice k indica las frecuencias discretas. Los valores $f_1, f_2, ..., f_{N-1}$ son las muestras en el dominio temporal, $F_1, F_2, ..., F_{N-1}$ en el dominio frecuencial y $\omega_0 = 2\pi/N$. El cálculo de esta transformada discreta requiere un total de N^2 operaciones complejas por lo que calcularla conlleva un gran tiempo y esfuerzo. Por ello se utilizan métodos que permiten calcularla de un modo más eficiente, como es la Tansformada Rápida de Fourier (FFT). Supongamos que N es una potencia de dos $N = 2^M$, donde M es un número entero. Si se introduce la notación $W = e^{-i\frac{2\pi}{N}}$, la Eq. (B.1) queda

$$F_k = \sum_{n=0}^{N-1} f_n W^{kn},\ k = 0, 1, 2, ..., N-1. \tag{B.3}$$

Si se divide la muestra por la mitad se tiene

$$F_k = \sum_{n=0}^{\frac{N}{2}-1} f_n e^{-ik\frac{2\pi}{N}n} \sum_{n=\frac{N}{2}}^{N-1} f_n e^{-ik\frac{2\pi}{N}n},\ k = 0, 1, 2, ..., N-1. \tag{B.4}$$

Si se crea una variable $m = n - N/2$ se tiene

$$F_k = \sum_{n=0}^{\frac{N}{2}-1} f_n e^{-ik\frac{2\pi}{N}n} \sum_{m=0}^{\frac{N}{2}-1} f_{m+\frac{N}{2}} e^{-ik\frac{2\pi}{N}(m+\frac{N}{2})},\ k = 0, 1, 2, ..., N-1, \tag{B.5}$$

$$F_k = \sum_{n=0}^{\frac{N}{2}-1} (f_n + e^{-i\pi k} f_{n+\frac{N}{2}}) e^{-ikn\frac{2\pi}{N}},\ k = 0, 1, 2, ..., N-1. \tag{B.6}$$

Como $e^{-i\pi k} = (-1)^k$, para los valores pares vale 1 mientras para los impares vale -1, luego se puede separar Eq. (B.6) en dos ecuaciones. Para los valores pares se tiene

$$F_{2k} = \sum_{n=0}^{\frac{N}{2}-1} (f_n + f_{n+\frac{N}{2}}) e^{-i\frac{2\pi(2k)n}{N}} = \sum_{n=0}^{\frac{N}{2}-1} (f_n + f_{n+\frac{N}{2}}) e^{-\frac{i2\pi kn}{N/2}}, \tag{B.7}$$

y para los valores impares

$$F_{2k+1} = \sum_{n=0}^{\frac{N}{2}-1} (f_n - f_{n+\frac{N}{2}}) e^{-i\frac{2\pi(2k+1)n}{N}} = \sum_{n=0}^{\frac{N}{2}-1} (f_n - f_{n+\frac{N}{2}}) e^{-i\frac{2\pi n}{N}} e^{-\frac{i2\pi kn}{N/2}}. \tag{B.8}$$

con $k = 0, 1, 2, ..., N/2 - 1$.

Estas ecuaciones se pueden poner en también, haciendo uso de la notación $W = e^{-i\frac{2\pi}{N}}$, para los valores pares,

$$F_{2k} = \sum_{n=0}^{\frac{N}{2}-1} (f_n + f_{n+\frac{N}{2}}) W^{2kn} \tag{B.9}$$

y para lo valores impares,

$$F_{2k+1} = \sum_{n=0}^{\frac{N}{2}-1} (f_n - f_{n+\frac{N}{2}}) W^n W^{2kn} \tag{B.10}$$

Estas expresiones se pueden interpretar como si fueran las transformadas discretas con N/2 valores $g_n = f_n + f_{n+\frac{N}{2}}$ y $h_n = (f_n + f_{n-\frac{N}{2}}) W^n$ con $n = 0, 1, 2, ..., N/2 - 1$. De este modo se pasa a $F_{2k} = G_k$ y $F_{2k+1} = H_k$ con $k = 0, 1, 2, ..., N/2 - 1$.

Se ha transformado el cálculo de N^2 ecuaciones en $2(N/2)^2$, es decir, se ha logrado dividir entre dos el número de operaciones. Si se aplica lo anterior una vez más se lograría pasar de N^2 a $4(N/4)^2$, es decir, se habría logrado dividir entre cuatro el número de operaciones. Si se continua este proceso de ir dividiendo los puntos hasta que $N/2$ Transformadas Discretas de Fourier de dos puntos se hayan calculado, lo que se logra es el paso de N^2 a $N \log_2 N$ operaciones. En una muestra de 1000 datos, la diferencia entre número de cálculos sería del orden de 100 veces mayor para la DFT que para la FFT.

Referencias

[1] S.C. Chapra, R.P. Canale, Métodos numéricos para Ingenieros , McGraw-Hill, Mexico, 1999.